ACCURATE DETERMINATION OF DISSIPATED CREEP STRAIN ENERGY AND ITS EFFECT ON LOAD- AND TEMPERATURE-INDUCED CRACKING OF ASPHALT PAVEMENT

By

JAESEUNG KIM

A DISSERTATION PRESENTED TO THE GRADUATE SCHOOL
OF THE UNIVERSITY OF FLORIDA IN PARTIAL FULFILLMENT
OF THE REQUIREMENTS FOR THE DEGREE OF
DOCTOR OF PHILOSOPHY

UNIVERSITY OF FLORIDA

2005

ACKNOWLEDGMENTS

I would like to thank my adviser and chairman of my supervisory committee, Dr. Reynaldo Roque. He always listened and respected my opinion. All tasks were accomplished under his support and guidance. I would like to offer heartfelt gratefulness and respect to him. I will never forget his help. I also thank Dr. Bjorn Birgisson, my cochair, for the generous contribution of his discussion, his support, encouragement, and precious guidance. Special thanks go to the other members of my advisory committee (Dr. Mang Tia, Dr. Dennis R. Hiltunen, and Dr. Bhavani V. Sankar).

Special thanks go to Mr. George Lopp and Miss. Tanya Riedhammer for their support in the laboratory and their valuable advice. I would like to thank the former graduate student, Adam P. Jajliardo, for generous help. I also would like to thank Sungho Kim, Dr. Booil Kim, Dr. Christos A. Drakos, and Byungil Kim for their friendship and encouragement. I appreciate the friendship of all the students in the materials group of the Department of Civil and Coastal Engineering at University of Florida.

Lastly, I would like to thank my father, Yangjin Kim, my mother, Sinja Min, my sister, Lee-Eun Kim, my wife, Soojung Lee, and my son, Bryan Kim, for their endless trust, encouragement, and support. I would also like to thank all my family and friends who have also supported me.

TABLE OF CONTENTS

page

LIST OF TABLES

LIST OF FIGURES

Abstract of Dissertation Presented to the Graduate School
of the University of Florida in Partial Fulfillment of the
Requirements for the Degree of Doctor of Philosophy

ACCURATE DETERMINATION OF DISSIPATED CREEP STRAIN ENERGY AND ITS EFFECT ON LOAD- AND TEMPERATURE-INDUCED CRACKING OF ASPHALT PAVEMENT

By

Jaeseung Kim

December 2005

Chair: Reynaldo Roque
Cochair: Bjorn Birgisson
Department: Civil and Costal Engineering

An asphalt mixture's ability to dissipate energy without fracturing is directly related to cracking performance of asphalt pavement. Therefore, it is critical to accurately determine the rate of dissipated creep strain energy (DCSE) accumulation in asphalt mixture subjected to load- and/or temperature-induced stresses. In the laboratory, the dissipated energy per load cycle is commonly determined as the area of the hysteresis loop developed during cyclic loading of asphalt mixture. However, it is unclear whether all dissipated energy determined in this manner is irreversible and associated with damage, or whether it is at least partially reversible and not fully associated with damage. For a range of asphalt mixtures, the area of the hysteresis loop appeared to be strongly affected by the delayed elastic behavior of the mixture, even when cyclic response had reached steady-state conditions. Furthermore, it is generally not possible to reliably separate reversible from irreversible dissipated energy in the hysteresis loop using

conventional complex modulus data. Consequently, it is recommended that irreversible dissipated energy be determined using rheological parameters obtained from static creep test data.

Field observations indicate that both traffic and thermal stress affect top-down cracking performance of pavement. Further evaluation of these observations will require the development and use of cracking models that can consider the combined effects of load and temperature. A rigorous analytical model was developed to assess the effect of thermal loading condition and mixture properties on DCSE and cracking. Accumulation of DCSE in mixture subjected to thermal stresses is much less straightforward than for load-induced stresses, and performance may be affected by rheological aspects of the mixture other than creep (e.g., delayed elasticity). Appropriate equations were developed to calculate thermal stress development and DCSE accumulation for pavement subjected to thermal loading cycles. Calculations performed with the resulting model verified that thermal effects can affect top-down cracking performance. It was also found that delayed elasticity plays an important role in thermal stress development and cracking. Therefore, mixtures where rheological behavior exhibits lower rate of creep and higher levels of delayed elasticity would help mitigate the development of top-down cracking.

CHAPTER 1
INTRODUCTION

1.1 Background

It is generally recognized that a mixture's ability to dissipate energy without fracturing is directly related to cracking performance of asphalt pavement. Zhang et al. (2001) identified the presence of a dissipated energy threshold, which defines a mixture's energy tolerance prior to fracturing. They also determined that mixture viscosity was identified as a key property that determines the rate of damage accumulation in mixtures. Currently, the rate of dissipated energy accumulation can be determined experimentally for specified loading conditions from either cyclic or static creep test data. For static creep tests, the dissipated energy is simply the product of the applied stress and the amount of viscous strain developed at any given time. For cyclic test, the dissipated energy per load cycle is commonly determined as the area of the hysteresis loop developed during cyclic loading. However, it is unclear whether all dissipated energy determined in this manner is irreversible and associated with damage, or whether it is at least partially reversible and not fully associated with damage. Understanding the nature of the energy associated with the hysteresis loop during cyclic loading is of critical importance, because misinterpretation would lead to significant errors in the predicted cracking performance of mixtures.

Temperature-induced cracking is a major distress mode in asphalt pavement. Daily or seasonal temperature change leads to development of tensile stresses in the restrained asphalt surface layer. Currently, several different thermal cracking models with empirical

and/or analytical approaches have been developed, but none of them appears to incorporate a fundamental crack growth model associated with damage accumulation and the dissipated energy threshold in asphalt mixture. In fact, the fracture of viscoelastic materials may be well explained by the energy-based HMA fracture mechanics model developed by Zhang et al. (2001), but their framework has not been used to predict temperature-induced crack development, and it is currently limited to only the evaluation of load-induced crack performance. Therefore, it is expected that a proper thermal cracking model, which is able to incorporate the HMA fracture model, may provide a reasonable and reliable basis to assess for the thermal cracking performance of asphalt pavement, as well as the combined effect of load and thermal stress that may lead to top-down cracking.

Top-down cracking or surface-initiated longitudinal wheel path cracking is considered a common distress mode in flexible pavement. Top-down cracking research at University of Florida, recently led to the introduction of the concept of Energy Ratio, which integrated the HMA fracture model and the structural characteristics of asphalt pavement, to accurately distinguish between pavements that exhibited top-down cracking and those that did not (Roque et al, 2004). However, this work was limited to evaluation of the effect of traffic loads alone. Thermal stresses may have a significant effect on the development of top-down cracking in asphalt pavement. Consequently, it may be expected that load-induced crack performance combined with the effect of temperature may provide a more accurate and reliable estimation of pavement performance associated with top-down cracking.

1.2 Hypothesis

Two hypotheses were investigated:

1. DCSE accumulation in asphalt mixture cannot be reliably determined from conventional complex modulus data
2. DCSE induced by thermal stresses affects top-down cracking performance of pavements.

1.3 Objectives

Evaluation these hypotheses involved investigation in three primary subject area: experimental determination of DCSE accumulation in asphalt mixture, determination of DCSE induced by temperature change in pavement, and evaluation of the effect of temperature-induced DCSE on top-down cracking performance. Detailed objectives related to these subjects are as follows:

- Evaluate static and dynamic test methods to determine the most accurate method to obtain the rate of creep strain of mixtures, which affects prediction of damage and fracture.
- Develop a reliable and accurate thermal cracking prediction model that can incorporate the energy-based HMA fracture mechanics model.
- Understand the nature of thermal cracking, and identify the effect of temperature on top-down cracking performance.
- Extend HMA fracture mechanics to include the combined effects of load and thermal stresses.
- Provide key parameters that can effectively mitigate the development of temperature-induced cracking in hot mix asphalt.

1.4 Scope

The analytical work involved in this study is to provide an accurate determination of dissipated creep strain energy in asphalt mixture, a framework to effectively evaluate the development of temperature-induced top-down cracking in asphalt pavement, and a combined system that can integrate top-down cracking performance. In all analytical

work, the theory of linear viscoelasticity and HMA fracture mechanics are central to the approach used.

The experimental portion of this study involved eleven dense graded mixtures obtained from pavements throughout the state of Florida. The eleven pavement sections involved were evaluated as part of a larger study to investigate top down cracking performance. The mixtures were composed of a variety of aggregates, including limestones and granites typically used in the state. The work has involved a comprehensive set of measurements obtained both in the field and in the laboratory. Multiple cores were obtained from each section and brought back to the laboratory for testing. A complete set of laboratory tests was performed to determine volumetric properties, binder properties, and mechanical properties of the mixtures using the Superpave IDT.

CHAPTER 2
LITERATURE REVIEW

The primary purpose of this section is to summarize the current understanding of cracking mechanisms and damage criteria in the area of design and evaluation of flexible pavement. From the literature review, it is generally agreed that the primary causes of pavement cracking can be divided into two categories: material failure and structural failure. Several types of evaluation approaches have been developed on the basis of different types of mechanisms to evaluate cracking caused by material properties. The following sections provide an explanation of the basic mechanisms and approaches used to evaluate the performance of asphalt pavement.

2.1 Cracking Mechanisms within Asphalt Mixtures

2.1.1 Fatigue Cracking Models

Earlier work to predict fatigue cracking of asphalt mixtures was primarily performed using fatigue tests. The allowable number of load repetition determined at failure of the test specimen was considered the life of the asphalt mixture. A more advanced approach, able to account for the effect of pavement structure was developed by calibrating on the basis of tensile strain in the asphalt pavement. Different types of equations proposed by many researchers have been widely used as damage criteria. A typical predictive equation for fatigue cracking is given as

$$N_f = f_1(\varepsilon_t)^{f_2} E_1^{f_3} \quad (2\text{-}1)$$

where E_1 = HMA modulus
ε_t = tensile strain at the bottom of HMA
f1,f2,f3 = transfer coefficients
N_f = allowable number of load repetitions

where transfer coefficients, which relate HMA tensile strain or modulus to the allowable number of load repetitions, vary between investigators. However, due to lack of a fundamental mechanism, the approach is somewhat limited, and more mechanistic approaches are being employed.

2.1.2 Dissipated Energy in Fatigue

When a load is applied to a material there will be a stress that induces a strain. The area under the stress strain curve represents the energy being input to the material. When the load is removed from the material, the stress is removed and strain is recovered. If the loading and unloading curves coincide, all the energy put into the material is recovered after the load is removed. If the two curves do not coincide, then some energy was lost or dissipated in the material.

Current applications of dissipated energy to describe fatigue behavior assume that all dissipated energy represents damage done to the material. In actuality this may be not true. Only a portion of the total energy that is dissipated may be used in damaging the material. Ghuzlan and Carpenter (2000) indicate that use of the cumulative dissipated energy only indirectly recognizes the fact that not all dissipated energy is inducing damage, without directly determining the value of the damage being done to the material. The failure criteria proposed by these authors was defined as the change in dissipated energy between cycles divided by the total dissipated energy at the prior load cycle. Plotting the values of this ratio versus load cycles results in a decreasing trend during early cycles, then a constant trend for quite a long time, and then increases rapidly. The plateau value of the ratio was recommend as the failure of mixtures.

This energy ratio approaches proposed by Ghuzlan and Carpenter (2000), which evaluates what is going on during cyclic loading by looking at the relative change in dissipated energy between load cycles, appears to adequately identify when failure occurs in the asphalt mixture. However, the approach does not provide for the determination of fundamental energy failure limits. In addition, it does not provide fundamental parameters that allow for the prediction of accumulated dissipated creep strain energy and fracture.

2.1.3 Continuum Damage Mechanics Model

The behavior of asphalt concrete is not yet fully understood. The reason is that asphalt concrete, which is mainly asphalt binder combined with aggregates, exhibits significantly different and more complex material behavior than other common construction materials (e.g., steel, concrete, and wood). The theory of viscoelasticity is important in helping to explain the time-dependent nature of vicoelastic materials like asphalt mixture. One widely used viscoelastic fracture mechanism was developed based on Schapery's work (Schapery, 1984) where pseudo elastic strain (Equation 2-2) derived from hereditary integrals is a fundamental to the evaluation of damage in mixtures. The advantage of introducing pseudo strain is that it can be related to stresses through Hooke's law. Thus, if a linear elastic solution is known for a particular geometry, it is possible to determine the corresponding linear viscoelastic solution through the hereditary integral.

$$\varepsilon^R = \frac{1}{E^R}\int_0^t E(t-\tau)\frac{d\varepsilon}{d\tau}d\tau \qquad (2\text{-}2)$$

where ε = uniaxial strain
ε^R = pseudo elastic strain
E^R = reference modulus that is an arbitrary constant
$E(t)$ = uniaxial relaxation modulus

T = elapsed time from specimen fabrication and the time of interest
τ = time when loading began

Kim et al. (1995), Kim et al. (1997), and Lee et al. (2000) have applied Schapery's theory to predict mixture behavior and failure using continuum damage mechanics. A fifty percent reduction in initial pseudo stiffness is generally used as a failure criterion for asphalt mixtures. Damage functions developed under a cyclic stress or strain controlled loading test of asphalt mixture are used as input parameters to evaluate cracking performance. Based on experimental data of asphalt concrete subjected to continuous and uniaxial cyclic loading in tension, Kim et al. (1997) proposed a constitutive model that describes the mechanical behavior of the material under these conditions:

$$\sigma = I(\varepsilon_e^R)[F + G] \tag{2-3}$$

where I = initial pseudo stiffness
ε = effective pseudo strain
F = damage function
G = hysteresis function

The effective pseudo strain accounts for the accumulating pseudo strain in a controlled stress mode. A mode factor is also applied to the damage function, F, to allow a single expression for both modes of loading. The parameter, I is used to account for sample-to-sample variability in the asphalt specimens. The damage function, F represents the change in slope of the stress-pseudo strain loop as damage accumulates in the specimen. The hysteresis function, G describes the difference in the loading and unloading paths. More details of this model can be found in Kim et al. (1995), Kim et al. (1997), and Lee et al. (2000).

To determine the fatigue life for a controlled-strain testing mode, Kim et al. (1997) found that the hysteresis function, G need not be considered and that stress and pseudo strain values (ε^R_m) at peak loads alone are sufficient.

$$\sigma_m = I(\varepsilon_m^R)[CS] \tag{2-4}$$

where I = initial pseudo stiffness
C = coefficient of secant pseudo stiffness reduction
S = internal state variable

Except for the use of pseudo strain, this approach appears similar to the classic forms based on fatigue damage approaches. As mentioned earlier, the evaluation of cracking performance is more fundamentally related to fracture parameters such as tensile strength, tensile strain, and fracture energy, which can only be reliably obtained from fracture test in tension. Critical stress redistribution occurring after crack initiation is also an important factor affecting cracking performance of mixture. Therefore, a more fundamental approach, which takes these effects into account, is necessary.

2.1.4 HMA Fracture Mechanics

Cracking mechanisms in asphalt mixtures may be more fundamentally understood by way of fracture mechanics. An HMA fracture model developed by Zhang et al. (2001) at University of Florida has provided a fundamental mechanism for evaluating the performance of asphalt mixtures and understanding the physical behavior of composite viscoelastic material. HMA fracture mechanics primarily consists of two principal theories: theory of linear viscoelasticity and energy-based fracture mechanics. From each theory, specialized theories associated with asphalt mixtures were developed and verified experimentally. The following explanations may aid to understand the basic principles of HMA fracture mechanics.

2.1.4.1 Observation of threshold

The concept of the existence of a fundamental crack growth threshold is central to the HMA fracture mechanics framework presented by Zhang, et al. (2001). The concept is based on the observation that micro-damage (i.e., damage not associated with crack

initiation or crack growth) appears to be fully healable, while macro-damage (i.e., damage associated with crack initiation or growth) does not appear to be healable. This indicates that a damage threshold exists below which damage is fully healable. Therefore, A crack will develop or propagate in any region where the induced energy exceeds the threshold as shown in Figure 2-1.

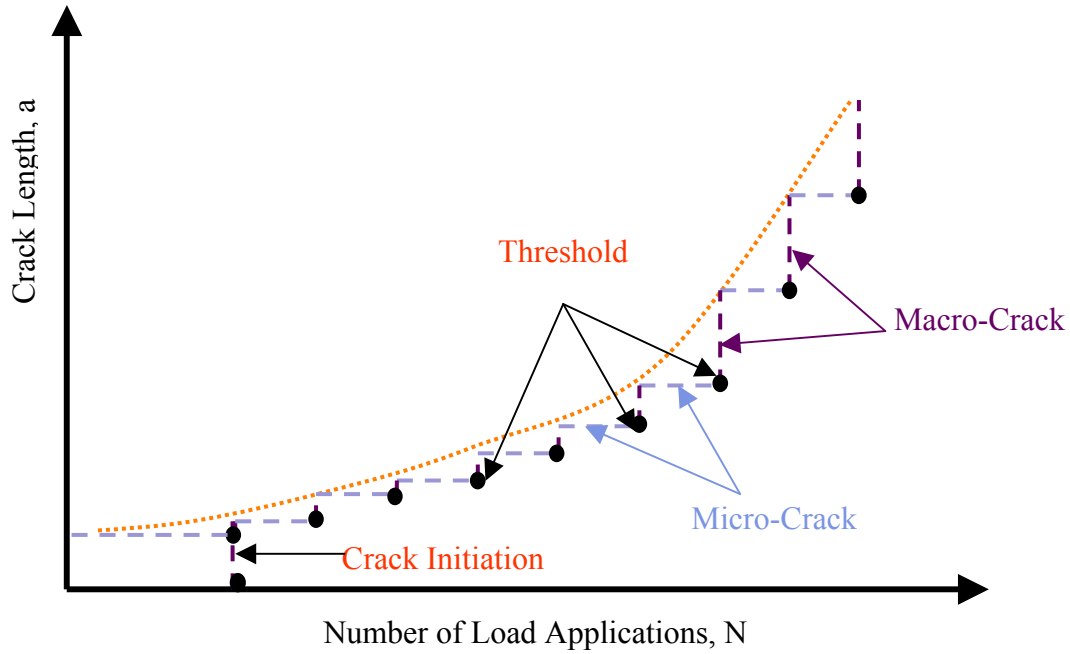

Figure 2-1. Crack Propagation in Asphalt Mixture

2.1.4.2 Determination of DCSE and DCSE limit (threshold)

The time-dependent viscoelastic material's fracture may be well described by a creep test. If a constant stress is applied at zero time, then the strain output will be expressed as shown in Figure 2-2, where $\dot{\varepsilon}_{cr}$ is a rate of creep strain, and ε_{cr} is a amount of creep strain. In general, three stages: primary, secondary, and tertiary are observed during the creep test. The sate of the tertiary stage coincides with the development of a local, which then propagate throughout the system (asphalt mixture), and eventually leads to complete rupture. Kim (2003) reported that the dissipated creep strain energy up to the

macro crack initiation from the creep test (Equation 2-5) is approximately the same as the area of DCSE at failure obtained from the strength test (Figure 2-3).

$$DCSE = \int_0^{t_c} \sigma_0 \cdot \dot{\varepsilon}_{cr} \, dt \tag{2-5}$$

This indicates that the dissipated creep strain energy (DCSE) at failure is independent of mode of loading or loading history. Consequently, a macro crack initiates, once the total dissipated energy of asphalt mixture reaches DCSE limit. The mechanism of crack propagation subjected to different types of loads in asphalt mixture will be explained by adopting energy-based fracture mechanics.

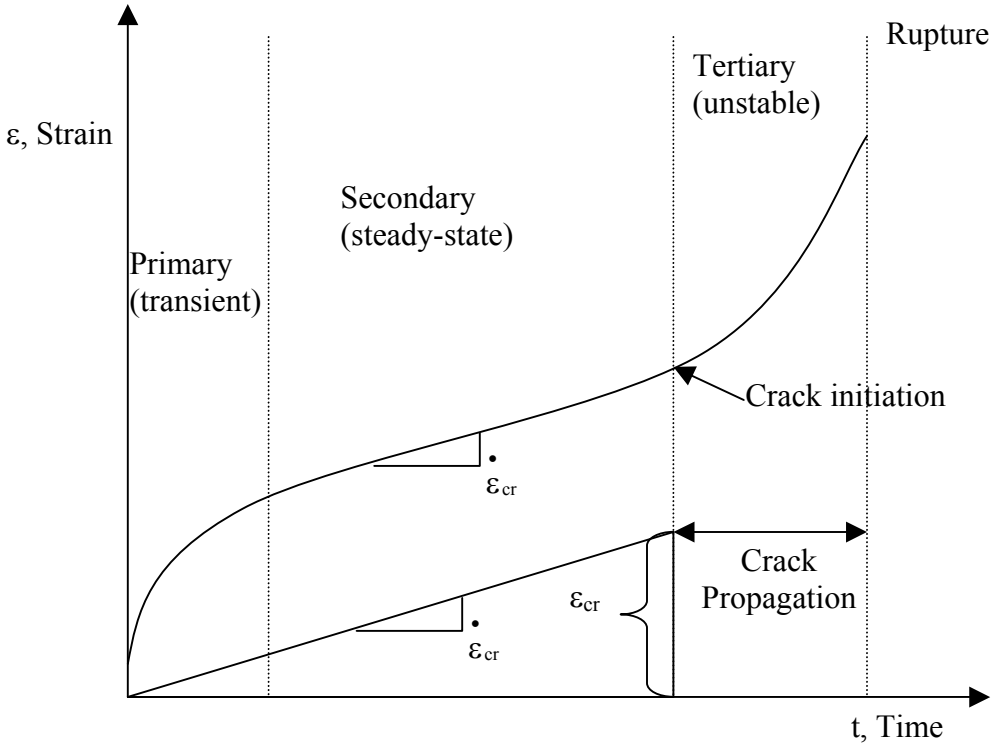

Figure 2-2. Typical Strain-Time Behavior during Static Creep

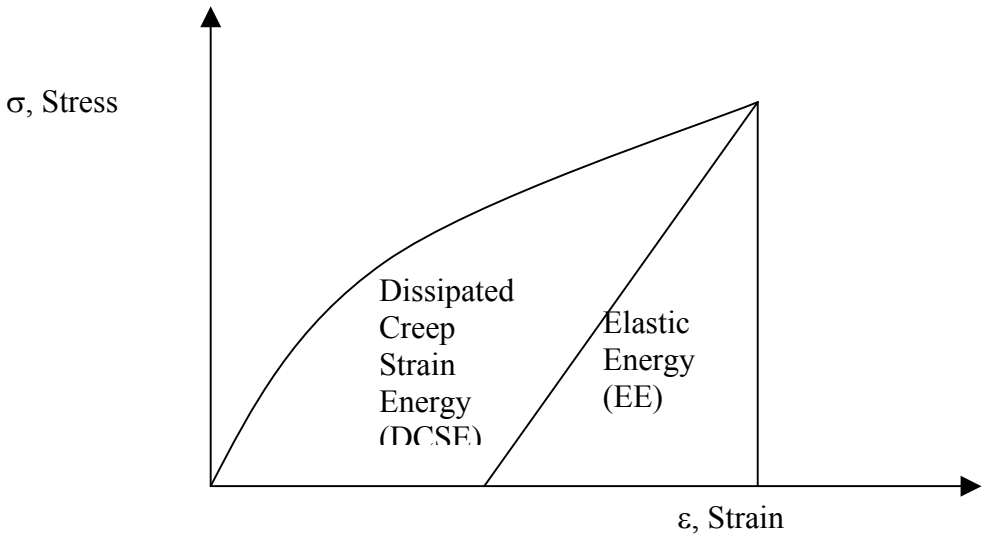

Figure 2-3. Determination of DCSE Limit

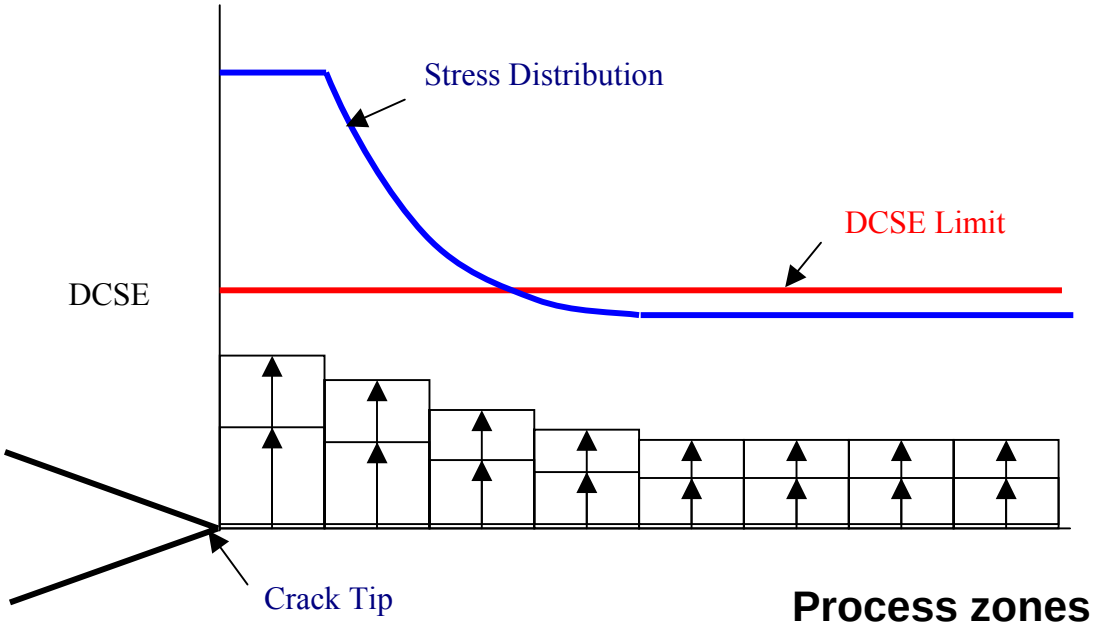

Figure 2-4. Stress Distribution near the Crack Tip

2.1.4.3 Energy-based fracture mechanics

In Linear Elastic Fracture Mechanics (LEFM), stress distribution near the crack tip depends on stress intensity factor K. Myers et al. (2001) reported that the crack

propagation of flexible pavement was primarily a tensile failure, which is driven by the mode I stress intensity factor K_I. Zhang et al. (2001) successfully applied the LEFM, combining the threshold concept and limits presented above to asphalt mixtures. In their study, crack propagation induced by applying repeated haversine loading in the indirect tensile test was successfully predicted with their energy-based crack model.

The basic elements of the crack growth law used are illustrated in Figure 2-4, which shows a generalized stress distribution in the vicinity of a crack subjected to uniform tension. The specific stress distribution for a given loading condition will depend on specific loading condition and the failure limits of the specific mixture. The HMA fracture mechanics framework separated the area in front of the crack tip into a series of "process zones." The crack will propagate by the length of one of the process zones when strain energy representing damage in that zone exceeds the appropriate energy threshold. More detailed procedures in calculating crack propagation are specified in Zhang et al. (2001).

2.1.4.4 Energy Ratio

From the engineering point of view, it is obvious that any theoretical model not correlated to field performance data may not be reliable or even applicable. Roque et al. (2004) have presented Energy Ratio (ER), which integrated the HMA Fracture Model and effects of pavement structural characteristics to predict top-down cracking performance of mixtures. Mixtures gathered from cracked and uncracked sections were used to evaluate the reliability of ER. FWD tests were performed to define the structural characteristics of all the sections. Standard Superpave IDT tests were conducted on cores from twenty-two field sections, and each material property was analyzed with the HMA fracture model to obtain the ER. Energy Ratio (ER) is defined as DCSE limit of the

mixture over DCSE minimum, which is the minimum DCSE required for good cracking performance that serve as a single criterion for cracking performance considers both asphalt mixture properties and pavement characteristics. The Energy Ratio is calculated as follows:

$$ER = \frac{DCSE_{Limit} \cdot \left[0.00299\sigma^{-3.1}(6.36 - St) + 2.46 \cdot 10^{-8}\right]}{m^{2.98} \cdot D_1} \quad (2\text{-}6)$$

where all parameters: applied stress σ, failure strength S_t, D_1 and *m* values should be properly obtained from structural analysis and Superpave IDT. The Energy Ratio must be greater than 1.0 for the mixture to be acceptable.

2.1.5 Thermal Cracking

The primary mechanism generally associated with temperature-induced thermal cracking is a "top-down" initiation and propagation. Contraction strains induced by pavement cooling lead to thermal tensile stress development in the restrained surface layer where thermal stress is greatest at the surface of the pavement because pavement temperature is lowest at the surface and temperature changes are highest there. Even though the major distress of the thermal stress is known as transverse cracking, the effect of daily temperature cooling cycles may have a significant influence on the development of top-down cracking. Dauzats and Rampal (1987) surveyed several pavement sections located in the south of France where pavements are subjected to extreme thermal stresses. Top-down cracks in these sections were observed 3 to 5 years after construction of the road. Therefore, thermal stress may significantly contribute to the development of top-down cracking.

Several different thermal cracking models have been developed using empirical and/or analytical approaches. TC model (Hiltunen and Roque, 1994) developed based on

the theory of linear viscoelasticity appears to be more comprehensive than other models in the literature. However, their approach essentially did not incorporate a fundamental damage development of asphalt mixtures. Conversely, the HMA Fracture Model (Zhang et al., 2001), which was developed based on energy-based fracture mechanism, has not been used to predict thermal cracking of asphalt pavements. Consequently, it appears desirable to develop a proper thermal cracking model, which is able to incorporate the HMA fracture model.

In addition, Lytton et al. (1983) and Roque and Ruth (1990) have noted that thermal cracking is significantly affected by the material properties of asphalt concrete and environmental conditions. Although it is known that pavement thickness may have some effects on thermal cracking, the significance of pavement structure is not yet clear. Therefore, in development of a thermal crack model, which will be introduced in Chapter 6, the effect of pavement structure was not considered.

2.2 Cracking Mechanisms Associated with Pavement Structure

2.2.1 Classic Fatigue Cracking

Fatigue cracking or load-induced cracking of flexible pavement is caused by repeated traffic loading. The cracks initiate at the bottom of the asphalt concrete layer, and then propagate to the surface due to the highest tensile stress or strain at the bottom of AC layer. It is well known that the asphalt pavement structure can be represented as a layered system (e.g. asphalt concrete, base, subbase, and subgrade), which can be analyzed using either linear elastic or nonlinear layer analysis. Due to its convenience, linear elastic layer analysis is widely used and appears to be a reasonably accurate to predict surface lager response. However, unbound layers may be more accurately represented by use of nonlinear analysis. Currently, the systems available for nonlinear

analysis have several deficiencies (Huang, 1993), so pavement system response predicted by the nonlinear analysis may not be reliable. Furthermore, several studies (Roque and Ruth, 1987 and Roque et al, 1992) have reported that the linear elastic analysis provided reasonably accurate results, which agreed favorably with measured pavement response. Therefore, linear elastic layer analysis was selected to evaluate the asphalt pavements involved in this study.

2.2.2 Load-Induced Top-Down Cracking

Top-down cracking initiates from the surface of asphalt concrete layer and propagates downward. Myers et al. (1999) showed that a contact stress between tire and asphalt layer may result in surface tensile stresses that may help initiate longitudinal cracks. They measured contact stress on several types of tires (i.e., trucking companies have shifted from operation on bias ply tires to the exclusive use of radial tires). Their work showed that the structure of the radial tire had a significant influence on development of the contact stresses at the surface of AC layer. Lateral stresses under ribs of the radial tires induced tensile stresses on the pavement's surface. In the same test performed on bias ply tires, the tensile stresses were negligible. Finite element analysis conducted on pre-selected pavement structures has shown that once a crack initiated at the surface of asphalt concrete layer, crack propagation was primarily caused by tensile stresses (Myers et al., 2001 and Myers and Roque, 2002). Their work also showed that the Mode I stress intensity factor was primarily related to the bending characteristic of the pavement structure. In other words, pavements with higher surface-to-base layer modulus ratios result in higher Mode I stress intensity factor at the crack tip of the pavement when appropriate conditions are present for the stress to develop. Extensive work (Roque et al., 2004) investigating the top-down cracking performance of in-service pavements has

shown that a tensile stress obtained from the bottom of AC layer could serve as a substitute of estimation of relative tensile stresses present at the surface of AC layer. As a result, the tensile stress at the bottom of AC appears to be a suitable parameter to describe the structural characteristics of asphalt pavement.

CHAPTER 3
TEST SECTIONS, MATERIALS, AND METHODS

Multi-year study involved multiple sets of test section has been conducted in Florida to investigate top-down performance of the in-service asphalt pavements. Two sets of top-down cracking projects were chosen for this study from among the available sections. This chapter will provide locations and condition, field evaluation, and binder and mixture properties of the pavement sections that were used in this study.

3.1 Locations and Condition

Eleven pavement sections were evaluated as part of this study. These sections were divided into two groups (Group I and II). A general description of these sections is presented below.

Table 3-1. Location and Condition of Group I

Section Name	Condition	Code	County	Section Limits
Interstate 75 Section 1	U	I75-1U	Charlotte	MP 149.3 - MP 161.1
Interstate 75 Section 1	C	I75-1C	Charlotte	MP 161.1 - MP 171.3
Interstate 75 Section 2	U	I75-2U	Lee	MP 115.1 - MP 131.5
Interstate 75 Section 3	C	I75-3C	Lee	MP 131.5 - MP 149.3
State Road 80 Section 1	C	SR 80-2C	Lee	From East of CR 80A To West of Hickey Creek Bridge
State Road 80 Section 2	U	SR 80-1U	Lee	From Hickey Creek Bridge To East of Joel Blvd.

3.1.1 Group I

This group consists of six pavement sections (Table 3-1) evaluated by Jajliardo (2003), (Table 3-1), which exhibited good and poor top-down cracking performance. A thorough description of the six sections, including experiment results and evaluation appears in Jajliardo (2003).

3.1.2 Group II

An additional five test sections (Table 3-2) were cored from four different locations (Figure 3-1) were selected for study. General descriptions of these sections are presented below.

Table 3-2. Location and Condition of Group II

Section Name	Condition	Code	Country	Section Limits
Interstate 10 Section 8	C	I10-8C	Suwannee	The west side of US-129: MP 15.144 - MP 18.000
Interstate 10 Section 9	U	I10-9U	Suwannee	The west side of US-129: MP 18.000 - MP 21.474
State Road 471	C	SR 471C	Sumter	The northbound lane three miles north of the Withlacoochee River
State Road 19	C	SR 19C	Lake	The southbound lane five miles south of S.R. 40
State Road 997	U	SR 997U	Dade	The northbound lane 7.6 miles south of US-27

- First, two adjacent sections, section 8 and section 9 located in I-10 in Suwannee Country, North Florida were selected, where section 8 had exhibited significant top-down cracking, but section 9 was not cracked. Since those sections were connected, they had similar external conditions such as traffic volume and environment. In addition the age since construction was identical (about 7 to 8 years).

- Second, state road 471 and state road 19 located in Sumter County and Lake County, Central Florida respectively were selected to evaluate the top-down cracking performance. Both sections were constructed using hot-in-place recycling, and both exhibited significant top-down cracking after only 2 to 3 years of sevice.

- Last, state road 997 is one of the most excellent performing sections. State road 997 located in Dade County, South Florida has shown good performance without any visual cracks during 40 years of service, making it one of the most interesting sections in this project.

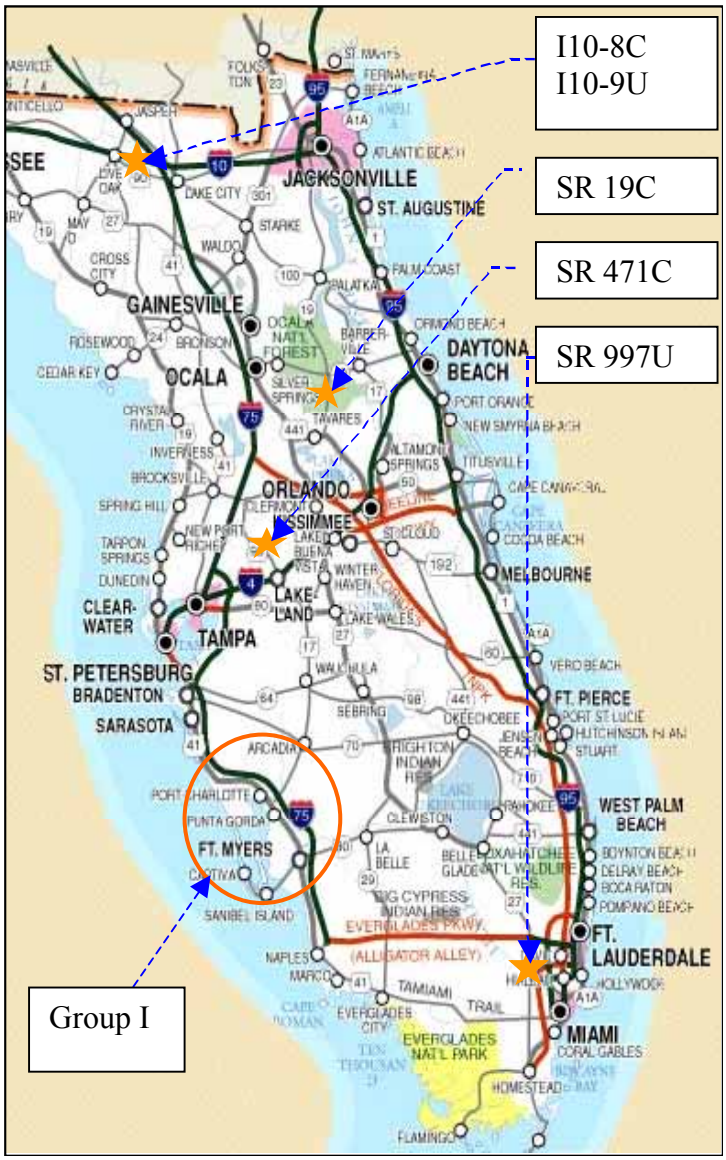

Figure 3-1. Location of Sections (Group II)

3.2 Traffic Volume

The traffic volumes obtained from each section are shown in Table 3-3. These values are expressed in thousands of ESALS.

Table 3-3. Traffic Volumes of Group II

Sections	ESAL/year×1000
I10-1C	392
I10-1U	392
SR 471	26
SR 19	51
SR 997	89

3.3 General Observation

A field trip was taken to each section to observe and take pictures. The cracked sections exhibit a moderate amount of cracking as well as wheel rim markings (Figure 3-2), while the uncracked sections appear to be in an acceptable condition. An inspection of core samples from the cracked sections clearly indicated the presence of top-down cracking (Figure 3-3). The cracks initiated from the surface and moved downward.

Figure 3-2. Cracked Section

Figure 3-3. Cored Mixture in Cracked Section

3.4 Pavement Structure

Flexible pavements are layered systems that may be better understood by conducting layered analysis. In the case of cracking, tensile stress occurring at the bottom of asphalt concrete layer may be used to characterize the pavement is property cracking. Description of the system used to evaluate the tensile stress is presented below.

3.4.1 Falling Weight Deflectometer Testing

Falling Weight Deflectometer Testing (FWD) was performed. FWD procedure used the standard SHRP configuration for the sensors (i.e. 0”, 8”, 12”, 18”, 24”, 36”, and 60”). For each section, the tests were conducted in the travel lane in the wheel path at relatively undamaged locations, on both sides of the coring area. A 9-kips seating load was applied followed by tests involving loads between 8 to 10 kips loads. Deflections at each of the measurement sensors were recorded.

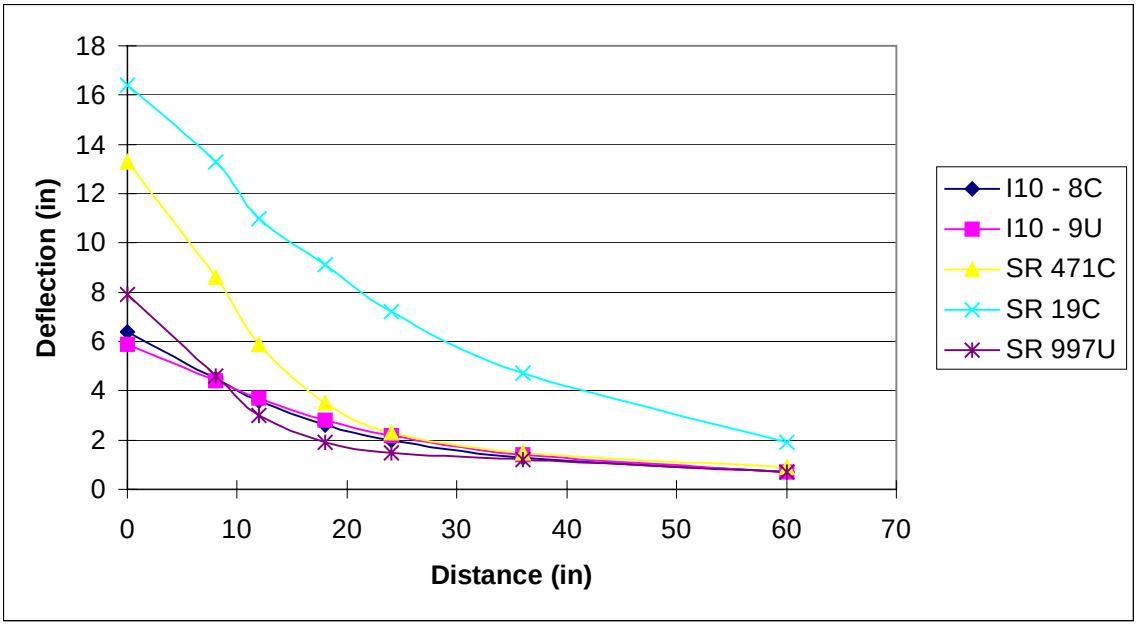

Figure 3-4. Deflections from FWD Results

Deflections from FWD tests are good indicators in understanding the structural behavior of in-situ asphalt pavements. In general, the deflections near the loading center include the effects of moduli from all layers, whereas deflections far away from the loading center include subgrade effect only. Absolute deflections and slope changes between deflections provide important information to estimate the condition of asphalt pavement systems. For example, a sudden increase in slope represents a significant drop of modulus of a certain layer. Figure 3-4 shows deflections of FWD tests obtained from standard SHRP configuration for the sensors.

3.4.2 Layer Moduli

Backcalculation is the ‘‘inverse’’ problem of determining material properties of pavement layers from its response to surface loading. The deflections of a pavement surface are usually determined with the Falling Weight Deflectometer (FWD). Based on the measured deflections, it is currently necessary to employ iteration or optimization

schemes to calculate theoretical deflections by varying the material properties until a ‘‘tolerable’’ match of measured deflection is obtained.

In the process of back calculation, elastic layer analysis program (BISDEF) was used to assess the modulus value of each layer. A measured thickness of cored asphalt mixture was used as for an asphalt layer thickness, which typical thickness of 12 inches was assumed for the base and subbase layers (Table 3-4). The backcalculated moduli of AC, base, subbase, and subgrade were then obtained. Moduli of five sections obtained in this way are given in Table 3-5. More details of the calculated versus measured deflections are given in Appendix A.

Table 3-4. Thickness of Layers

Layers	I10 - 8C	I10 - 9U	SR 471C	SR 19C	SR 997U
AC (psi)	7.20	7.40	2.58	2.39	2.17
Base (psi)	12	12	12	12	12
Subbase (psi)	12	12	12	12	12
Subgrade (psi)	240	240	240	240	240

Table 3-5. Backcalculated Moduli

Layers	I10 - 8C	I10 - 9U	SR 471C	SR 19C	SR 997U
AC (psi)	1428138	1481319	1112923	1348368	1703227
Base (psi)	55724	65179	27408	77971	75413
SubBase (psi)	54532	41414	136649	2644	315397
Subgrade (psi)	38868	46606	36107	27179	52389

3.4.3 Stress Analysis

To obtain stress at the bottom of the AC layer, classic elastic mulilayer analysis was performed. All the modulus values given in Table 3-5 and the thickness values given in Table 3-4 were used as inputs to the BISAR program (elastic multilayer analysis program). Figure 3-5 shows the tensile stresses calculated at the bottom of AC layers of the five pavement sections evaluated.

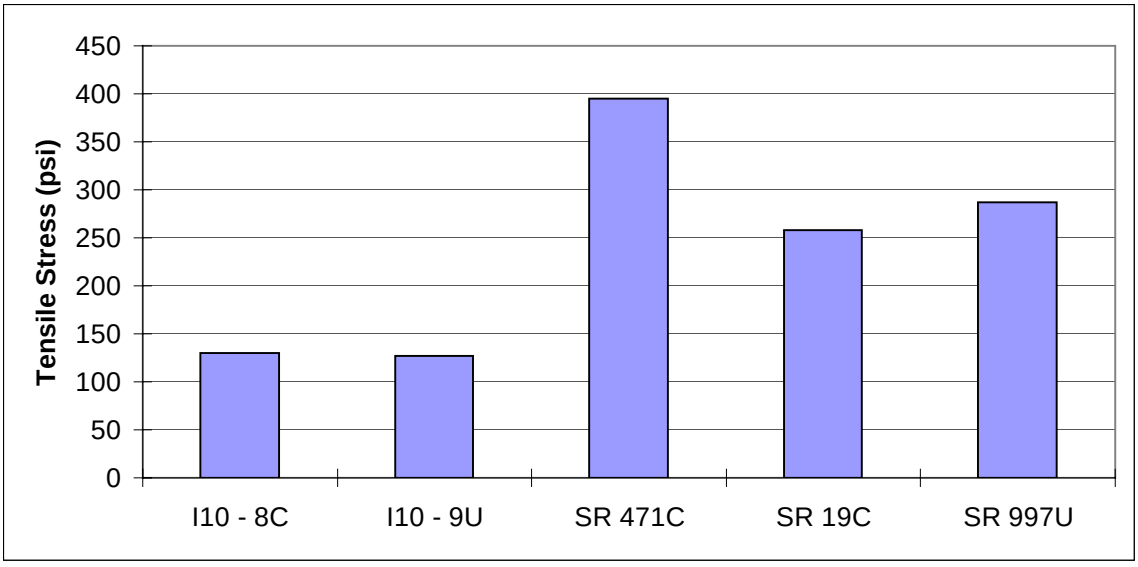

Figure 3-5. Tensile Stresses Calculated at the Bottom of AC of Four-Layer System

The ratio of the asphalt concrete modulus to the base modulus (E1/E2) is a good indicator of the bending stresses in the AC layer. In general, a larger E1/E2 ratio indicates higher bending stress (Huang, 1993). The tensile stresses (Figure 3-5) clearly showed higher values where the slopes of deflections corresponding to the AC modulus and the base modulus were changed significantly (Figure 3-4). That indicates the tensile stresses obtained are reasonably correlated with the deflections of FWD tests.

3.5 Materials and Methods

This section provides the procedure of materials preparation and types of tests used for the five sections (Group II). The results from each type of test then follow. All the test results will be used for the analytical studies presented in Chapter 5 and 6. In addition, for the six sections (Group I), the same types of tests were performed and analyzed by Jajliardo (2003), so details of the test results of Group I appear in Jajliardo (2003).

3.5.1 Materials Preparation

Eighteen 6 in. diameter cores were obtained from between wheel paths, and eighteen cores were obtained in the outer wheel path of the traffic lane of each test section. The coring location was carefully selected through field inspection as being representative in terms of the overall performance of the section. In cracked areas, great care was taken to assure that wheel path cores were not taken through cracks in the pavement. All cores were carefully marked the direction of traffic loading. Upon inspection in the laboratory, the thickness of each lift was measured and recorded.

Approximately 1.5 in. thick slices of the surface mixture were taken for testing. The bulk specific gravity of all the sliced specimens was measured and then dried. A number of slices were used for extraction and recovery of binder, and determination of maximum theoretical density of the mixture. The remaining cores were used to mixture tests using standard Superpave IDT: resilient modulus, creep compliance, and strength tests.

3.5.2 Measurement of Volumetric and Binder Properties

Bulk specific gravity tests (AASHTO T-166) and maximum specific gravity tests (AASHTO T-209) were performed to determine in-place air voids. Binders were extracted and recovered binders obtained through extraction and recovery tests (SHRP B-006) and viscosity was determined using the rotational viscometer (ASTM D 4402). More details with respect to the testing procedures are specified in the references.

3.5.3 Measurement of Mixture Properties

Although several types of tests (e.g., uniaxial and triaxial compression, beam flexure, hollow cylinder, etc.) are being used to test of asphalt mixtures, cracking is essentially associated with tensile properties of mixtures. From that standpoint, the

Superpave indirect tensile test (IDT) developed as part of the Strategic Highway Research Program (SHRP) was used to determine tensile properties from field cores. Superpave IDT was used to perform three types of tests: resilient modulus, creep compliance, and tensile strength. General descriptions associated with the testing and data analysis system are presented below.

3.5.3.1 Experimental design of Superpave IDT

The testing system used included a servo hydraulic testing machine and extensometers mounted on the specimen for measuring displacement (Figure 3-6). The measurement system is attached close to the center of specimen, but 1.5 in. gage length is commonly used for properly assessing aggregate effects. Three specimens (6 in. diameter by about 1.5 in. thick) cut from the asphalt mixture are required to perform one set of Superpave IDT tests at one temperature. Three test temperatures, 0, 10, and 20°C, which are typical low in-service temperatures in Florida, were used. More detail procedures are specified in Roque et al. (1997).

Figure 3-6. Superpave Indirect Tensile Test (IDT)

3.5.3.2 Description of testing types

Three types of tests, resilient modulus, creep compliance, and tensile strength, were performed for each set of three specimens. The resilient modulus test is performed in a load-controlled mode by applying a repeated haversine waveform load to the specimen for a period of 0.1 second followed by a rest period of 0.9 seconds. The load is selected to keep the repeated horizontal strain between 100 and 300 micro-strain during the resilient modulus test (Roque and Buttlar, 1992). The creep compliance test is also performed in the load-controlled mode by applying a monotonic static load to the specimen for a period of 1000 seconds. The load is selected to maintain the accumulative horizontal strain below 1000 micro-strain (Buttlar and Roque, 1994). The strength test is performed in a displacement-controlled mode. A rate of load ram displacement of 50m/min was used.

3.5.3.3 Data analysis

The data analysis procedures developed by Roque et al (1997) were used ot determine resilient modulus, creep compliance, tensile strength, failure strain, fracture energy, and dissipated creep strain energy to failure.

Table 3-6. Binder's Viscosity

Name	Viscosity (cP)
I10-8C	5689298
I10-9U	6158008
SR 471C	682359
SR 19C	442163
SR 997U	13512860

Table 3-7. Mixture's Air void Content

Name	Air Void (%)
I10-8C	8.74189558
I10-9U	9.92712825
SR 471C	5.70411847
SR 19C	4.84338282
SR 997U	7.63542571

3.6 Experimental Results

3.6.1 Volumetric and Binder Properties

Extraction and recovery tests, and viscometer tests performed on binders from the five test sections (Group II). The absolute viscosity of binders presented in Table 3-6 and Figure 3-7). Air voids obtained from bulk specific gravity and maximum specific gravity tests are presented in Table 3-7 and Figure 3-8.

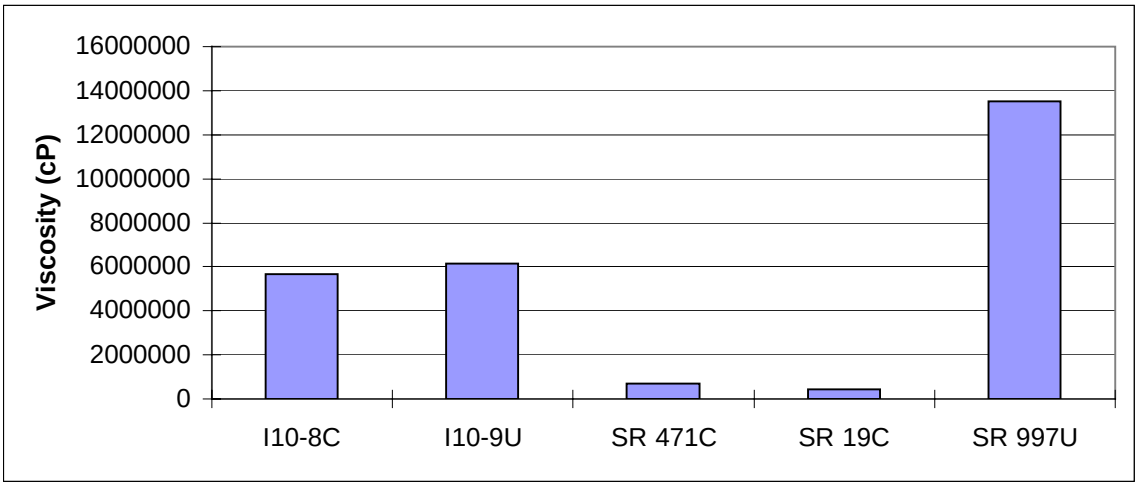

Figure 3-7. Plot of Binder's Viscosity

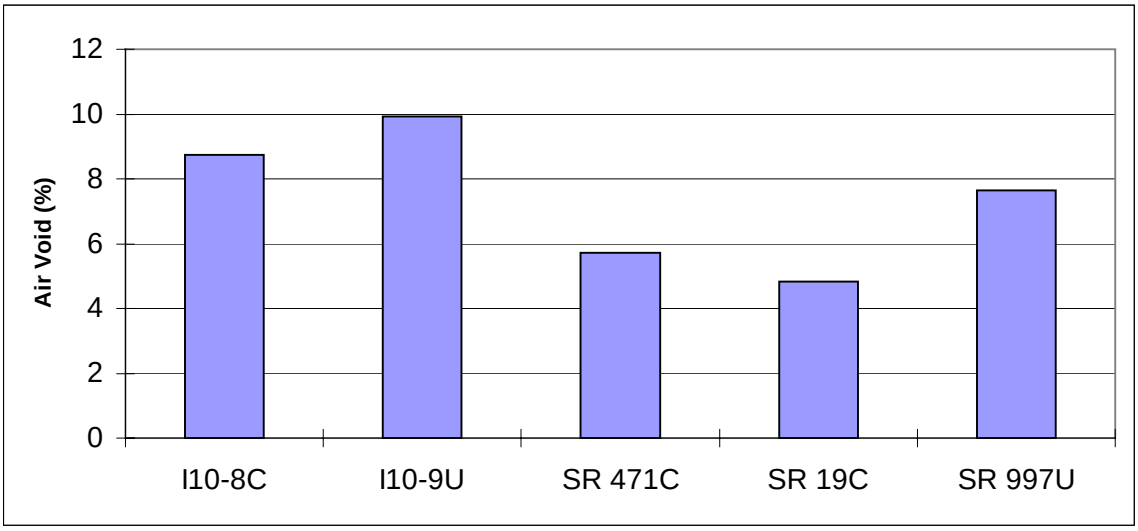

Figure 3-8. Plot of Mixture's Air Void Content

3.6.2 Mixture Test Results

The mixture tests performed were resilient modulus, creep compliance, and tensile strength. These tests were performed at 0° C, 10° C, and 20° C. The mixture properties that were obtained from these tests were the resilient modulus, creep compliance, m-value, tensile strength, fracture energy, failure strain, and the dissipated creep strain energy limit. Test results in terms of value are presented in Appendix B.

3.6.2.1 Resilient modulus test

The resilient modulus (MR) is a measure of a material's elastic stiffness. It can be used to separate elastic energy from the fracture energy of the mixture. Figure 3-9 shows the values of MR for the five sections at three temperatures.

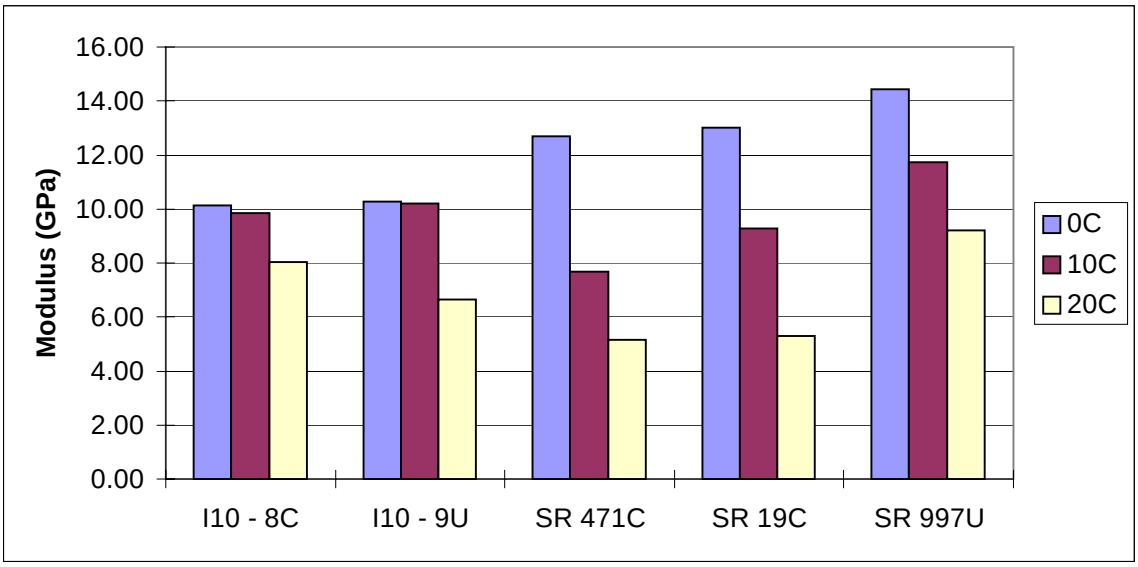

Figure 3-9. Resilient Modulus

3.6.2.2 Creep compliance test

A power function, ($D(t) = D_0 + D_1 t^m$) has been used successfully to represent mixture creep compliance. shown a great agreement between measured and fitted data. However, a real creep test cannot achieve accurate ramp loading at the start of the test, so

Kim et al. (2005) recommended using a fixed D_0 value of 3.33×10-7 psi, to obtain more consistent D_1 and m values. Figure 3-10 and 3-11 show the regression coefficients (D_1 and m), while Figure 3-12 shows the rate of creep strain compliance determined at 1000 sec, which corresponds to the reciprocal of mixture viscosity.

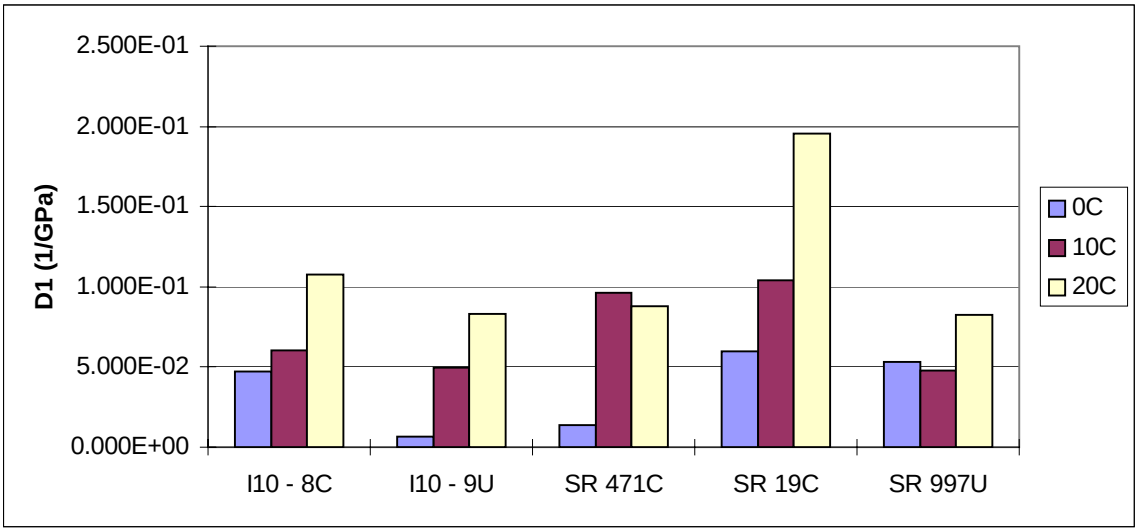

Figure 3-10. D_1 value

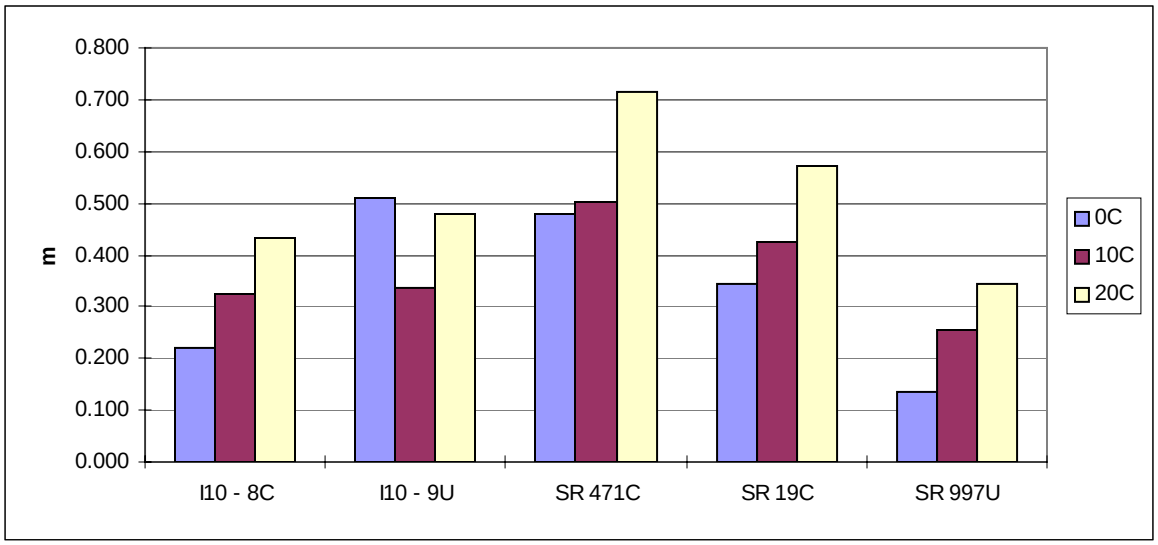

Figure 3-11. m-value

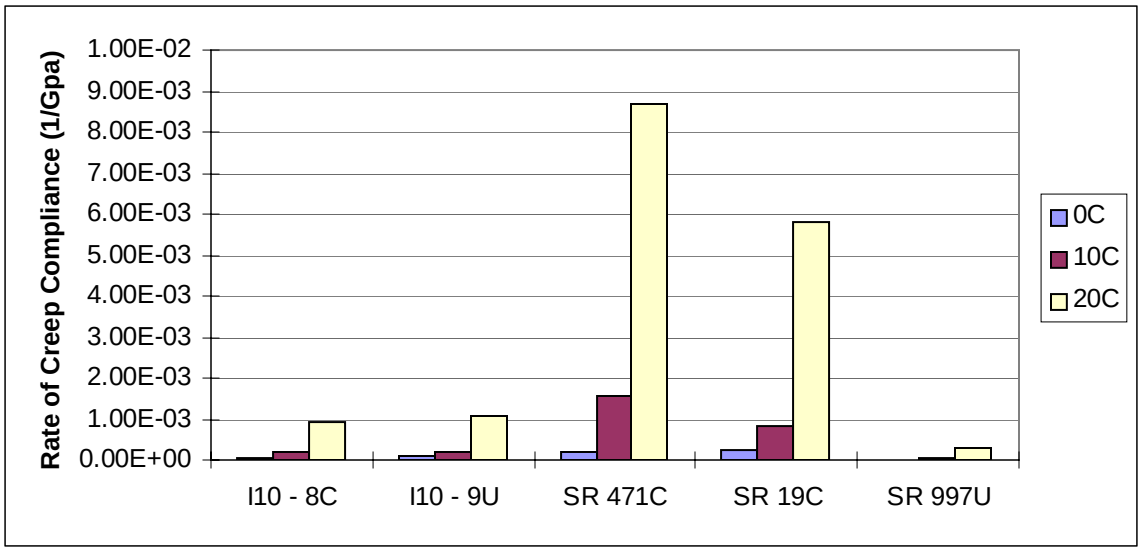

Figure 3-12. Rate of Creep Strain Compliance

3.6.2.3 Tensile strength test

Fracture parameters such as tensile strength, failure strain, and fracture energy can be determined from the tensile strength test using the Superpave IDT. These properties are used for estimating the cracking resistance of asphalt mixtures. In general, from the strength test and the resilient modulus test, fracture energy and dissipated creep strain energy can be determined. The fracture energy is defined as the total energy applied to the specimen through the specimen fracture. Fracture energy can be determined from the area of the stress-strain curve. The dissipated creep strain energy limit defined as the fundamental energy limit of asphalt mixture, can be simply determined as fracture energy minus the elastic energy. The tensile strength, failure strain, fracture energy, and DCSE limit are shown in Figures 3-13 through 3-16.

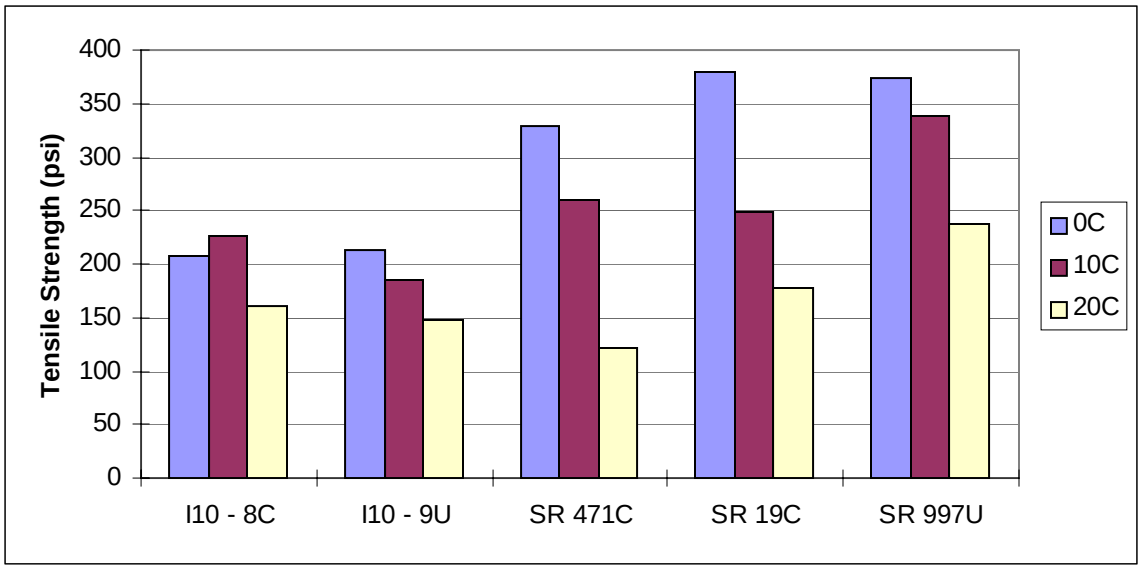

Figure 3-13. Tensile Strength

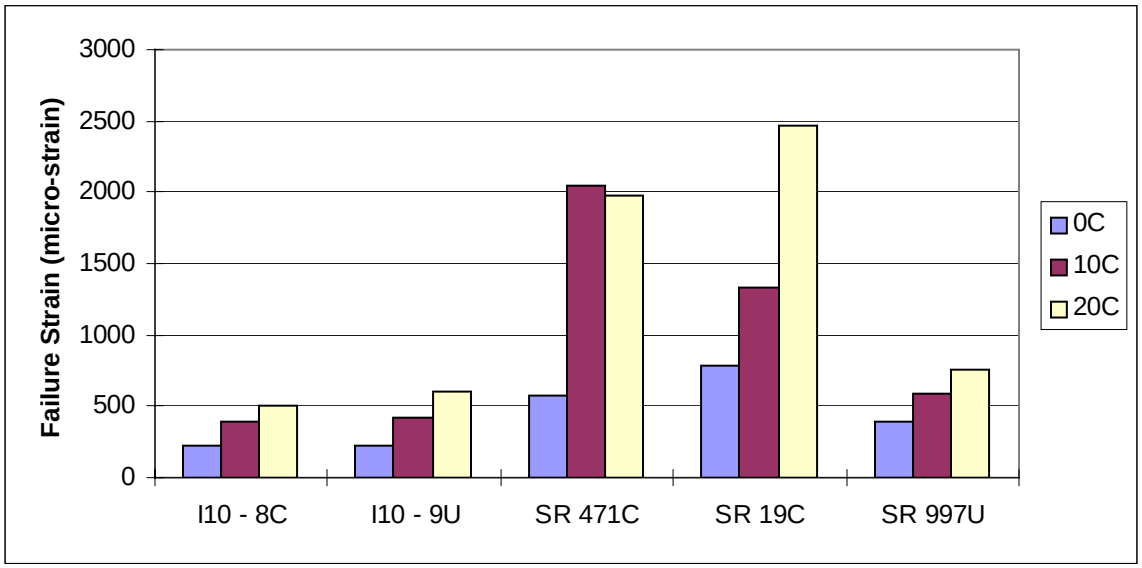

Figure 3-14. Failure Strain

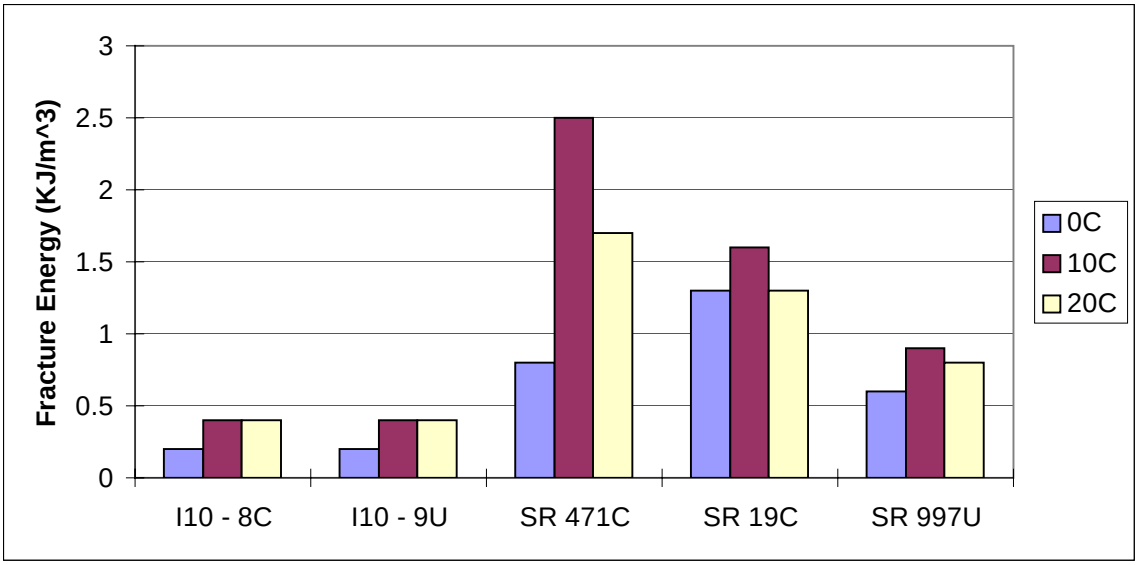

Figure 3-15. Fracture Energy

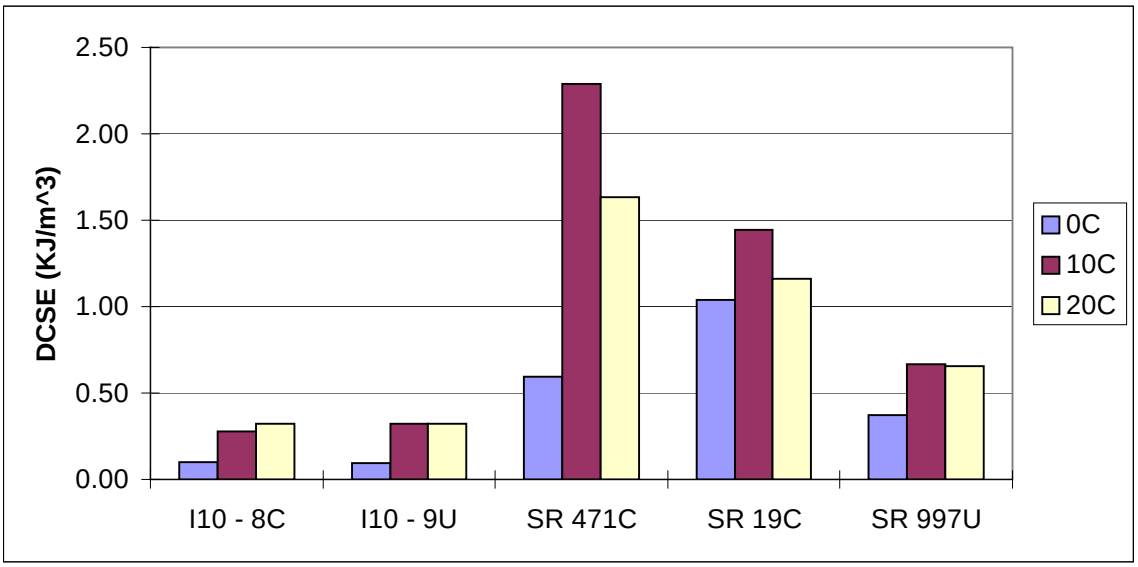

Figure 3-16. Dissipated Creep Strain Energy

CHAPTER 4
DETERMINATION OF ENERGY DISSIPATION

The relationship between dissipated energy and fracture can be clearly illustrated by using the HMA fracture mechanics model developed at the University of Florida. This model, which has been verified with extensive laboratory and field testing, is based on the principle that both crack initiation and crack growth are controlled by a mixture's tolerance to dissipated creep strain energy induced by applied loads. Specifically, a crack will initiate and/or grow when the energy dissipated by the asphalt mixture exceeds the dissipated creep strain energy limit of the mixture at any point in the material.

It is of interest to determine whether other test methods can be used to obtain the rate of dissipated energy accumulation in asphalt mixtures. Of particular interest, is the determination of dissipated energy from cyclic test data, since complex modulus testing has become more common for asphalt mixture, and offers the promise of shorter testing times and/or improved accuracy in determination of properties. Dissipated energy is commonly determined from cyclic test data. The basic approach to determining rate of dissipated energy accumulation for either static or cyclic creep tests is covered in the following sections.

4.1 Materials and Methods

4.1.1 Materials

Mixtures obtained from six dense-graded sections were tested (Group I). Four sections were from I-75: two in Charlotte County and two in Lee County, FL. The other two test sections were from SR 80 in Lee County, Florida. Six-inch diameter cores taken

from each section were sliced to a thickness of approximately 1.5 inches. Three test specimens were obtained for each mixture from field cores taken from test sections associated with the evaluation of top-down cracking in Florida. A total fifty-four specimens were prepared for the complex modulus test using Superave IDT at three temperatures: 0, 10, and 20°C.

4.1.2 Complex Modulus Test

4.1.2.1 Overviews

Dynamic modulus or complex modulus tests are typically performed using unconfined uniaxial compression tests. The standard test procedure is described in ASTM D 3497, which recommends three test temperatures (41°, 77°, and 104°F) and three loading frequencies (1, 4, and 16 Hz). Sinusoidal loading without rest periods for a period of 30 to 45 seconds starting at the lowest temperature and highest frequency, and proceeding to the highest temperature and the lowest frequency.

Birgisson et al. (2004) has used Superpave IDT system to measure complex modulus of asphalt mixtures in tension. They properly modified and extended the test methods and data reduction procedures that are currently used in the Superpave IDT (Buttlar and Roque, 1994 and Roque et al., 1997) resulted in accurately determining dynamic modulus and phase angle from the Superpave IDT system.

4.1.2.2 Testing procedure

The complex modulus tests performed in this study were conducted using the Superpave IDT at the low in-service temperature ranges (0, 10, and 20°C) typically used to evaluate field-cracking performance. Three frequencies were used: 0.333, 0.5, and 1hz. The mixtures were subjected to 100 sec of cyclic loading time, which allowed for determination of both dynamic and static strain response at steady state. Also, the

continuous sinusoidal load applied to the specimen was selected to maintain the horizontal strain amplitude between 35 and 65 micro strain, which was decided from the results of tens of preliminary tests. Additional details on the testing procedure used are as follows:

- After cutting, all specimens were allowed to dry in a constant humidity chamber for a period of two days.
- Four brass gage points (5/16-inch diameter by 1/8-inch thick) were affixed with epoxy to each specimen face.
- Extensometers were mounted on the specimen. Horizontal and vertical deformations were measured on each side of the specimen.
- The test specimen was placed into the load frame. A seating load of 8 to 15 pounds was applied to the test specimen to ensure proper contact of the loading heads.
- The specimen was loaded by applying a repeated and continuous sinusoidal load, where strain level by one cyclic load was adjusted between 35 and 65 micro-strain.
- When the applied load was determined, a total of 100 sec loading time were applied to the specimen, and the computer software began recording the test data.

4.1.3 Static Creep Test

Although linear viscoelastic superposition principle indicates that creep response from the average stress of complex modulus test should be identical to that from the static creep test, to increase comparative purpose, static creep tests were performed after complex modulus tests were done. The static creep tests were performed in the load-controlled mode by applying a monotonic static load to the specimen for a period of 100 seconds, which is identical to the loading period of the complex modulus test used, and the same temperature range (0, 10, and 20°C) was also identically used in the creep test. In addition, the load is selected below a total accumulative horizontal strain of 500 micro-strain. Details of testing procedure are described in Buttlar and Roque (1994).

4.2 Determination of Dissipated Energy

4.2.1 Experimental Determination of Dissipated Energy Based on Hysteresis Loop

Continuous sinusoidal loading is commonly used to perform complex modulus tests on asphalt mixture. The dissipated energy from cyclic load tests can be determined by calculating the energy losses associated with the phase angle δ. Within a limited strain range, the behavior of viscoelastic material can be explained using linear viscoelastic theory (Findley et al., 1976). If an external source $\sigma = \sigma_0 \sin\varpi t$ applies a constant amplitude of stress σ_0 to a viscoelastic material, then the strain response ε will be an oscillation at the same frequency as the stress but lagging behind by a phase angle δ (Figure 4-1(a).) where ε_0 is the amplitude of the stress, ϖ is the angular frequency ($f = \varpi/2\pi$ is the cyclic frequency) and $T=2\pi/\varpi$ is the period of the oscillation.

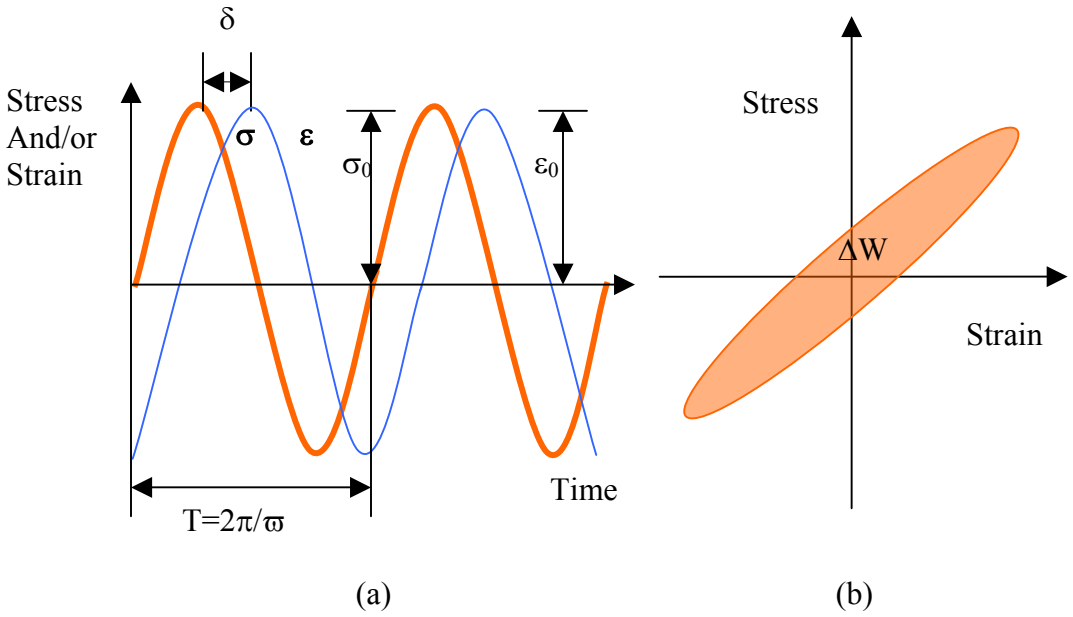

Figure 4-1. Oscillating Stress, Strain and Phase lag

Dissipated energy is denoted as ΔW where ΔW is the energy loss per cycle of vibration of the given amplitude (Figure 4-1(b).). There will be no energy loss in one

cycle if the stress and the strain are in phase, and hence $\delta = 0$. The amount of energy loss during one complete cycle can be calculated by integrating the increment of work done $\sigma d\varepsilon$ over complete cycle of period T, as follows

$$\Delta W = \int_0^T \sigma \frac{d\varepsilon}{dt} dt \tag{4-1}$$

Inserting $\sigma = \sigma_0 \sin\varpi t$ and $d\varepsilon/dt = \varpi\varepsilon_0 \cos(\varpi t - \delta)$ into Equation 4-1, Equation 4-2 is obtained.

$$\Delta W = \int_0^T \varepsilon_0 \sigma_0 \omega \sin \omega t \cdot \cos(\omega t - \delta) dt \tag{4-2}$$

Integration of Equation 4-2 yields the following expression for energy loss per cycle.

$$\Delta W = \pi \sigma_0 \varepsilon_0 \sin\delta \tag{4-3}$$

Equation 4-3 represents the internal loop area shown in Figure 4-1(b), which is the dissipated energy per cycle.

4.2.2 Dissipated Energy from Static Creep Test Data

Figure 2-2 shows typical strain response during a constant load static creep test. As shown in the Figure 2-2, the creep response can generally be separated into three distinct stages. The first stage is the primary or transient stage where the response is highly nonlinear due to the presence of delayed elasticity. The secondary stage begins once most or all of the delayed elastic response has finished, and only the viscous response remains such that the strain-time relationship becomes linear. The creep strain rate $\dot{\varepsilon}_{cr}$ is determined as the slope of this linear portion of the curve. The total creep strain can be determined as the rate of creep multiplied by the time of loading. An increase in the rate of creep strain signifies the start of the tertiary stage, which coincides with crack

initiation in the mixture. The continual increase in the rate of creep strain in the tertiary stage is caused by continual crack propagation during that stage. Eventually, the mixture will rupture if subjected to loading for a long enough period of time.

The dissipated creep strain energy to failure can be determined knowing the creep strain rate and the time to crack initiation, which is the beginning of the tertiary stage. Equation 4-4 can be used to determine the dissipated creep strain energy to failure.

$$\text{DCSE} = \int_0^{t_c} \sigma_0 \cdot \dot{\varepsilon}_{cr} \, dt = \text{Inelastic Energy} \tag{4-4}$$

where t_c is the time to crack initiation.

Kim (2003) has shown that the dissipated creep strain energy determined in this way from creep tests is the same as the dissipated creep strain energy determined from strength tests.

4.2.3 Dissipated Energy for General Loading Conditions

More generally, the dissipated energy accumulated during any loading condition can be calculated once the rheological properties of the mixture are defined. The key is to have parameters in the rheological model that properly separate the elastic (immediate and delayed) from the viscous response, since only the viscous response is irreversible and contributes to damage.

Roque et al. (1997) have successfully used a power law representation of the creep compliance function to obtain parameters from which the viscous response of the mixture can be estimated fairly accurately. The power law relationship is included as Equation 4-5.

$$D(t) = D_0 + D_1 t^m \tag{4-5}$$

The power law regression parameters D_0, D_1, and m-value are obtained by fitting static creep test data. The dissipated creep strain rate for an applied constant stress can be calculated using Equation 4-6, which represents the product of the constant stress and the slope of the creep compliance function at a point where the behavior of the mixture has reached steady state (t_{steady}).

$$\dot{\varepsilon}_{cr} = \sigma_0 \cdot D_1 \cdot m \cdot t_{steady}^{\,m-1} \tag{4-6}$$

Similar equations can be developed to determine the dissipated creep strain for any loading condition using the parameters D_1 and m-value along with the characteristics of the load function of interest. For example, Sangpetngam (2003) mathematically derived Equations 4-7 and 4-8, which represent the dissipated energy per load cycle for haversine loading and sinusoidal loading conditions, respectively. The parameters D_1 and m-value, and t_{steady} represent the same values used in Equation 4-5, which are obtained from a power law representation of the mixture's creep compliance function. T represents the period of the cyclic loading, and σ_{max} is the maximum amplitude of the cyclic loading. Equations 4-7 and 4-8 can be used to calculate the dissipated energy accumulated during cyclic loading based on parameters obtained from static creep test results. These results can be compared to experimentally determined values of cumulative dissipated creep strain energy obtained using the approaches described.

$$\text{DCSE per cycle} = \frac{\sigma_{max}^{\,2} \cdot D_1 \cdot m \cdot t^{m-1} \cdot T}{2} \quad \text{(haversine)} \tag{4-7}$$

$$\text{DCSE per cycle} = \frac{\sigma_{max}^{\,2} \cdot D_1 \cdot m \cdot t^{m-1} \cdot T}{8} \quad \text{(sinusoidal)} \tag{4-8}$$

4.2.4 Dissipated Energy from Cyclic Creep Test

Within a limited strain range, the linear viscoelastic superposition principle is valid for combining static and cyclic loading (Figure 4-2(a). and 4-2(b): where σ_{avg} is the average of cyclic load, $\varepsilon(t)$ is the resulting average strain, and $\dot{\varepsilon}_{cr}$ is the rate of creep strain induced by the average stress). One can define a stress independent compliance $1/\eta$, as $\dot{\varepsilon}_{cr}$ divided by σ_{avg}. By obtaining $\dot{\varepsilon}_{cr}$ using the power law function presented as Equation 4-5, the stress independent compliance can be determined as shown in Equation 4-9.

$$\frac{1}{\eta} = \frac{\dot{\varepsilon}_{cr}}{\sigma_{avg}} = D_1 \cdot m \cdot t_{steady}^{\,m-1} \tag{4-9}$$

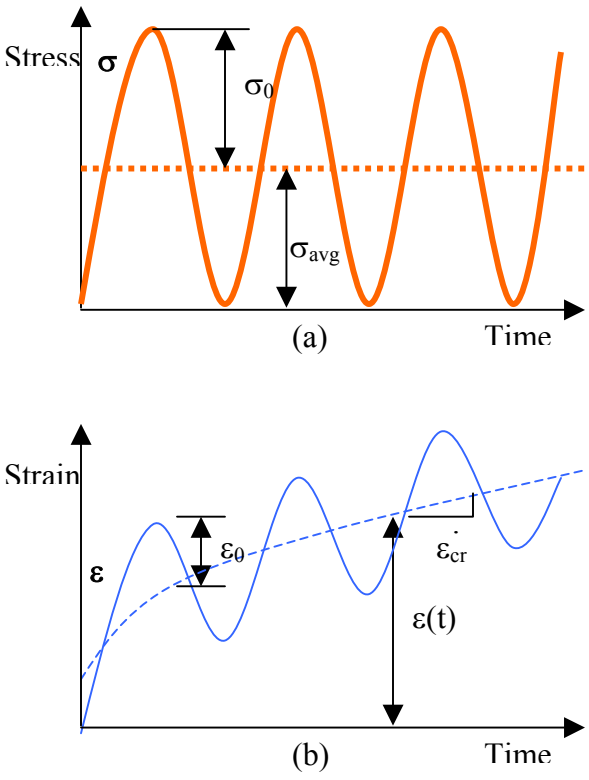

Figure 4-2. Combining Cyclic and Creep Response

Once the rate of the stress-independent compliance 1/η is determined, truly irrecoverable dissipated creep strain energy can be extracted from the area of hysteresis loop (Figure 4-2(b)). During one cycle T, the energy loss dominated by DCSE in the steady state can be computed by integrating the increment of work $\sigma(t)\,\dot{\varepsilon}_{cyc}$ as shown in Equation 4-10.

$$\text{DCSE per cycle} = \int_0^T \sigma(t) \cdot \dot{\varepsilon}_{cyc}\, dt = \int_0^T \sigma(t)^2 \cdot \frac{1}{\eta} dt \tag{4-10}$$

Herein, the stress-independent compliance can be expressed as $\dot{\varepsilon}_{cyc}$, which is the rate of creep for a specified cyclic stress σ(t) (obtained from σ(t)×1/η). T is the period of the oscillation, and ω (=2π*f*) is the angular frequency.

Equation 4-11 is obtained by replacing σ(t) in the sinusoidal loading function $\sigma_0 \sin \omega t$:

$$\text{DCSE per cycle} = \int_0^T \sigma_0 \sin \omega t \cdot \dot{\varepsilon}_{cyc}\, dt = \int_0^T (\sigma_0 \sin \omega t)^2 \cdot \frac{1}{\eta} dt \tag{4-11}$$

Inserting $1/\eta = D_1 m (t_{steady})^{m-1}$ (Equation 4-9) into Equation 4-11, dissipated creep strain energy per cycle becomes

$$\text{DCSE per cycle} = \int_0^T (\sigma_0 \sin \omega t)^2 \cdot D_1 \cdot m \cdot (t_{steady})^{m-1} dt \tag{4-12}$$

Integration of Equation 4-12 yields the following expression for energy loss per cycle.

$$\text{DCSE per cycle} = \frac{\sigma_0{}^2 \cdot D_1 m \cdot t_{steady}{}^{m-1} \cdot T}{2} \tag{4-13}$$

Equation 4-13 may be useful, since the phase angle portion was dropped from Equation 4-3, and only stress and strain are required. Equation 4-13 is analogous to Equation 4-8. Considering that $\sigma_{max} = 2\sigma_0$, Equation 4-13 is essentially the same as Equation 4-8, as long as the stress-independent compliance from the cyclic loading test is

the same as the stress-independent compliance from the static loading test. As a result, all three Equations 4-3, 4-8, and 4-13 finally should provide the same dissipated creep strain energies per cycle.

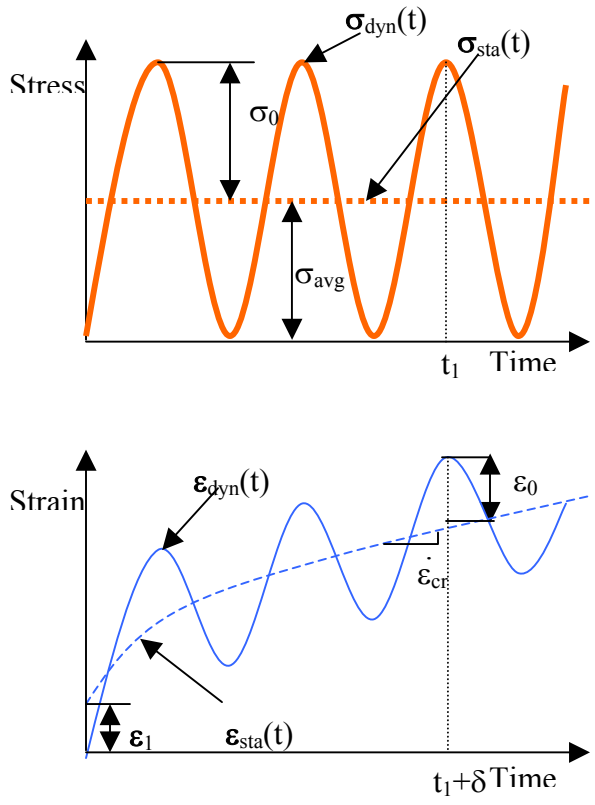

Figure 4-3. Data Fitting of Stress-Strain Response for Cyclic Test

4.3 Data Interpretation

Complex modulus test typically applies a continuous sinusoidal load having constant stress amplitude σ_{avg}, so the strain output is also a sinusoidal curve. Since asphalt mixture is a time-dependant viscoelatic material, the strain outputs include additional time-dependent damping responses. The phase angle δ and the resulting creep curve are shown in Figure 4-3. Within a limited strain range, the linear viscoelastic superposition principle is valid, so strain or stress can be fit using the following

functions: (4-14) through (4-17), Sinusoidal stress, average stress, sinusoidal strain and creep strain is noted as σ_{dyn}, σ_{sta}, ε_{dyn}, and ε_{sta} respectively, and ω is the angular frequency of a given complex modulus test. During the test, complex modulus (dynamic modulus and phase angle) was determined at the average of five loading cycles, which were recorded immediately before the end of the 100-sec loading time.

$$\sigma_{sta}(t) = \sigma_{avg} \tag{4-14}$$

$$\sigma_{dyn}(t) = \sigma_0 \cdot \sin(\omega t) \tag{4-15}$$

$$\varepsilon_{sta}(t) = \varepsilon_1 + \varepsilon_2 \cdot t^m \tag{4-16}$$

$$\varepsilon_{dyn}(t) = \varepsilon_0 \cdot \sin(\omega t - \delta) + \varepsilon_{sta}(t) \tag{4-17}$$

Table 4-1. Energy from Hysteresis Loop and Static Creep Test

Frequencies (hz)		0.333	0.5	1	0.333	0.5	1
Name	Temp. (°C)	Energy from Hysteresis Loop (KJ/m^3)			Energy from Static Creep Test (KJ/m^3)		
I75-1C	0	1.96E-02	1.96E-02	1.81E-02	4.82E-04	3.13E-04	1.41E-04
I75-1U	0	1.79E-02	1.88E-02	1.57E-02	4.14E-04	2.46E-04	1.54E-04
I75-3C	0	1.69E-02	1.83E-02	1.73E-02	4.80E-04	2.85E-04	1.52E-04
I75-2U	0	1.55E-02	1.17E-02	8.62E-03	2.34E-04	1.64E-04	7.43E-05
SR-1C	0	4.28E-02	4.72E-02	4.10E-02	1.15E-03	6.61E-04	3.49E-04
SR-2U	0	8.65E-03	9.59E-03	8.48E-03	2.72E-04	1.76E-04	5.79E-05
I75-1C	10	4.17E-02	4.12E-02	3.35E-02	1.95E-03	1.33E-03	6.33E-04
I75-1U	10	4.22E-02	4.16E-02	3.47E-02	1.33E-03	1.12E-03	5.63E-04
I75-3C	10	3.73E-02	3.30E-02	2.99E-02	1.46E-03	9.84E-04	5.56E-04
I75-2U	10	1.08E-02	1.59E-02	1.30E-02	8.08E-04	5.49E-04	2.68E-04
SR-1C	10	9.39E-02	8.46E-02	7.08E-02	3.28E-03	2.40E-03	1.16E-03
SR-2U	10	2.36E-02	2.09E-02	1.95E-02	5.77E-04	3.55E-04	1.67E-04
I75-1C	20	7.26E-02	5.72E-02	5.23E-02	4.31E-03	2.73E-03	1.52E-03
I75-1U	20	8.11E-02	7.07E-02	5.45E-02	3.66E-03	2.61E-03	1.43E-03
I75-3C	20	7.90E-02	6.90E-02	5.43E-02	5.42E-03	3.80E-03	1.92E-03
I75-2U	20	3.53E-02	2.99E-02	2.35E-02	2.20E-03	1.43E-03	6.94E-04
SR-1C	20	1.81E-01	1.72E-01	1.24E-01	9.22E-03	6.45E-03	2.99E-03
SR-2U	20	4.05E-02	4.19E-02	3.15E-02	1.31E-03	9.16E-04	4.78E-04
Equations		$= \pi \frac{\sigma_0}{\lvert E^* \rvert} \cdot \sin(\delta)$			$= \frac{\sigma_0^{\,2} D_1 m (t_{steady})^{m-1} T}{2}$		

4.4 Analysis and Findings

If only irreversible energy dissipation is present during cyclic loading in the steady state, then the dissipated energy determined from the hysteresis loop should equal the dissipated creep strain energy (DCSE) predicted from viscous response parameters obtained from static creep tests. In order to directly compare the dissipated energy per cycle from the cyclic and the creep test, the same stress level was used.

Table 4-2. Energy from Cyclic and Static Creep Test

Frequencies (hz)		0.333	0.5	1	0.333	0.5	1
Name	Temp. (°C)	Energy Cyclic Test (KJ/m^3)			Energy from Static Creep Test (KJ/m^3)		
I75-1C	0	5.43E-04	3.62E-04	1.81E-04	4.82E-04	3.13E-04	1.41E-04
I75-1U	0	6.10E-04	4.07E-04	2.04E-04	4.14E-04	2.46E-04	1.54E-04
I75-3C	0	5.27E-04	3.52E-04	1.76E-04	4.80E-04	2.85E-04	1.52E-04
I75-2U	0	2.41E-04	1.61E-04	8.04E-05	2.34E-04	1.64E-04	7.43E-05
SR-1C	0	8.55E-04	5.70E-04	2.85E-04	1.15E-03	6.61E-04	3.49E-04
SR-2U	0	1.31E-04	8.75E-05	4.37E-05	2.72E-04	1.76E-04	5.79E-05
I75-1C	10	1.89E-03	1.26E-03	6.31E-04	1.95E-03	1.33E-03	6.33E-04
I75-1U	10	1.74E-03	1.16E-03	5.79E-04	1.33E-03	1.12E-03	5.63E-04
I75-3C	10	1.55E-03	1.03E-03	5.17E-04	1.46E-03	9.84E-04	5.56E-04
I75-2U	10	9.27E-04	6.18E-04	3.09E-04	8.08E-04	5.49E-04	2.68E-04
SR-1C	10	4.06E-03	2.71E-03	1.35E-03	3.28E-03	2.40E-03	1.16E-03
SR-2U	10	6.04E-04	4.03E-04	2.01E-04	5.77E-04	3.55E-04	1.67E-04
I75-1C	20	3.57E-03	2.38E-03	1.19E-03	4.31E-03	2.73E-03	1.52E-03
I75-1U	20	4.44E-03	2.96E-03	1.48E-03	3.66E-03	2.61E-03	1.43E-03
I75-3C	20	5.14E-03	3.43E-03	1.71E-03	5.42E-03	3.80E-03	1.92E-03
I75-2U	20	1.94E-03	1.29E-03	6.46E-04	2.20E-03	1.43E-03	6.94E-04
SR-1C	20	8.76E-03	5.84E-03	2.92E-03	9.22E-03	6.45E-03	2.99E-03
SR-2U	20	1.45E-03	9.67E-04	4.84E-04	1.31E-03	9.16E-04	4.78E-04
Equations		$= \frac{\sigma_0^{\,2} \cdot D_1^{\bullet} m^{\bullet} \cdot t_{steady}^{\,m-1} \cdot T}{2}$			$= \frac{\sigma_0^{\,2} \cdot D_1 m \cdot (t_{steady})^{m-1} \cdot T}{2}$		
		□• : from cyclic response					

Table 4-1 and Table 4-2 show a comparison of energies computed using the different approaches. The equations used, which are stemmed from Equation 4-3, Equation 4-8, and Equation 4-13 are shown in the tables, where σ_0 is the half of the stress applied, |E*| is dynamic modulus, and other parameters have the same meaning as in their original equations.

The dissipated energy per cycle based on the phase angle was much greater than the DCSE per cycle from creep test results, regardless of section, temperature, or frequency of loading. The comparison is shown Figure 4-4. This appears to indicate that the dissipated energy associated with the hysteresis loop includes responses other than just viscous response and is not a good predictor of the DCSE per cycle.

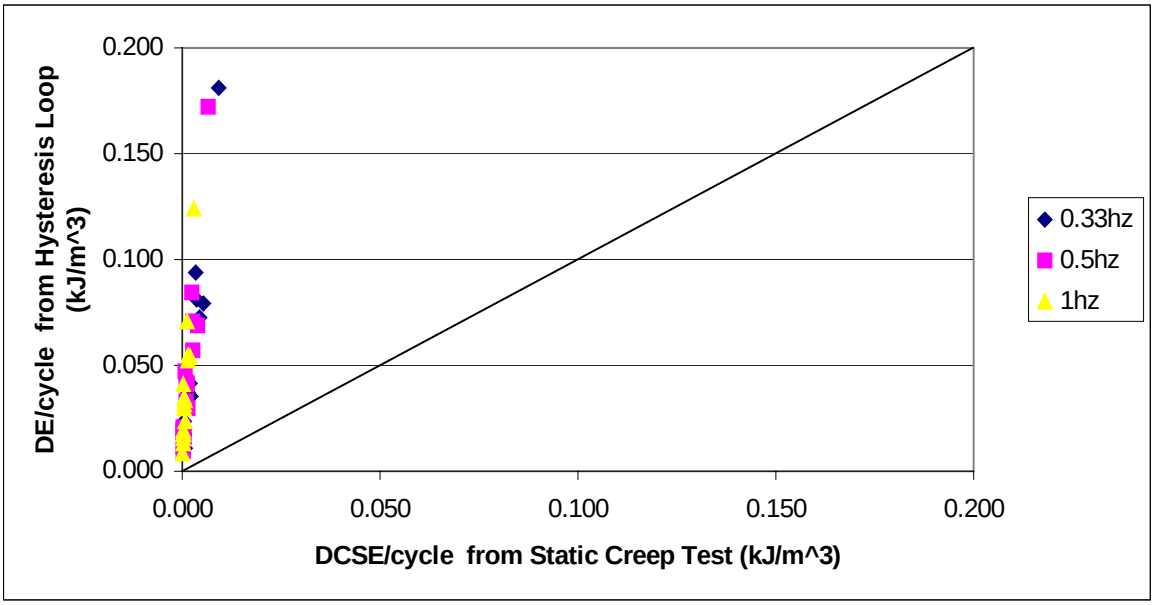

Figure 4-4. Energy from Hysteresis Loop and Static Creep Test

The dissipated energy per cycle was also determined using creep parameters obtained from the creep portion of the cyclic load tests. The results are presented in Table 4-2, and are compared to values determined using static creep test data in Figure 4-5. In all cases, good agreement was observed between the cyclic and static creep tests. This indicates that the stress-independent compliance η determined from cyclic creep tests is essentially the same as the creep compliance determined from static creep.

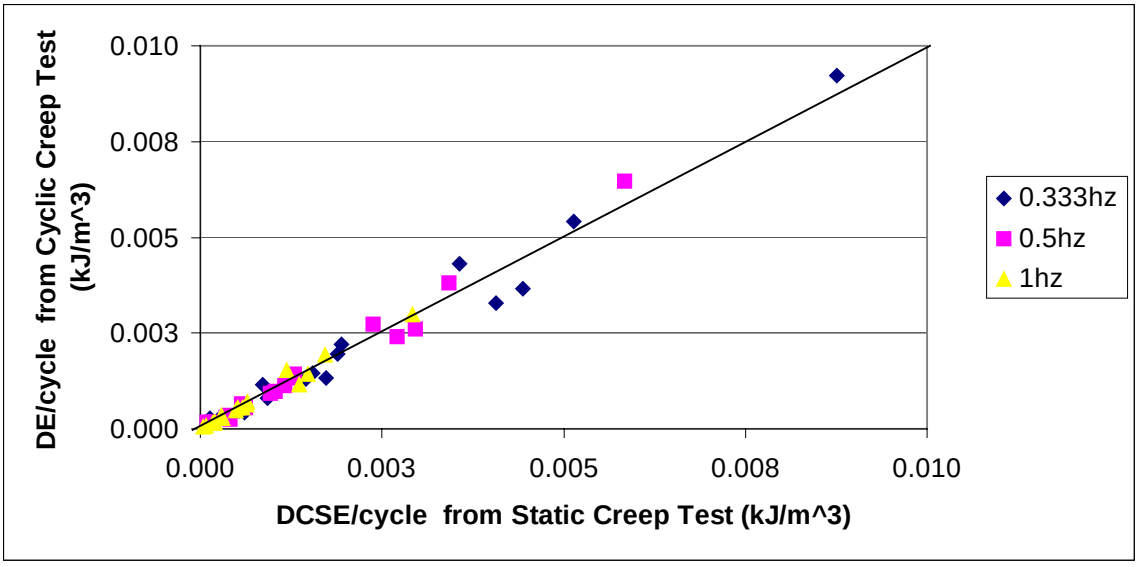

Figure 4-5. Energy from Cyclic and Static Creep Test

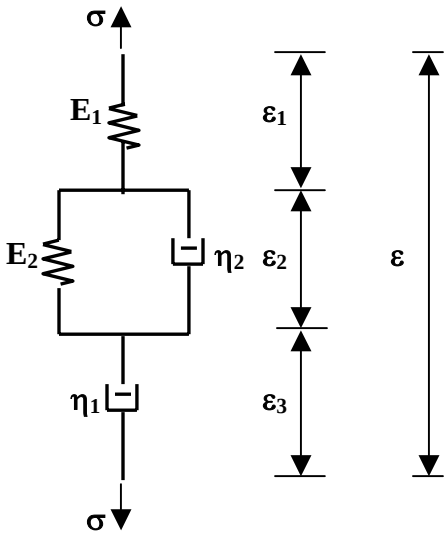

Figure 4-6. Burgers Model

4.5 Analysis by Use of Rheological Model

Conventional energy dissipation theory has indicated that the area enclosed by stress-strain hysteresis loop represents the energy dissipation per cycle. Test results, however, implied the loop area did not represent irrecoverable dissipated creep strain energy. It appears that the loop area included not only irreversible energy but also

reversible energy. Ghuzlan and Carpenter (2000), and Daniel et al. (2004) pointed out that only a portion of the total dissipated energy goes to damaging the material, and the remainder is due to viscoelasticity and other factors such as nonlinear behavior. Consequently, the use of the cumulative dissipated energy only indirectly recognizes the fact that not all dissipated energy is inducing damage. It appears many researchers have recognized that the hysteresis loop does not only include damage (irreversible energy), but there has been no clear explanation of what constitutes the difference. Thus, the meaning of the hysteresis loop is still unclear.

In order to investigate this phenomenon, a simple rheology model (Figure 4-6), which is a well-known Burgers model, was considered. This model can simply approximate time-dependant viscoelastic material response for a given stress history. The Burgers model is a four-element model consisting of a linear spring (E_1), a spring element (E_2) and dashpot element (η_2) connected in parallel, and a linear viscous dashpot (η_1). If constant stress is applied, the creep response in terms of compliance becomes

$$D(t) = \frac{1}{E_1} + \frac{1}{\eta_1} t + \frac{1}{E_2}(1 - \exp(-E_2 t / \eta 2)) \tag{4-18}$$

According to Boltzmann's superposition principle (Findley et al., 1976), if the stress input $\sigma(t)$ is arbitrary (variable with time), this arbitrary stress input can be approximated by Equation 4-19. This equation can be used to describe the creep strains under any given stress history provided the creep compliance D(t) is known, where ξ is dummy variable time corresponding to step-wisely increasing or decreasing stresses.

$$\varepsilon(t) = \int_0^t D(t-\xi) \frac{\partial \sigma(\xi)}{\partial(\xi)} d\xi \tag{4-19}$$

Applying Laplace transform to Equation 4-19 yields an algebraic Equation 4-20 in the transform variable s:

$$\hat{\varepsilon}(s) = s\,\hat{D}(s)\,\hat{\sigma}(s) \tag{4-20}$$

Taking the Laplace transform to both of Equation 4-18 and cyclic stress $\sigma(t) = \sigma_0 \sin(\omega)$ with a constant amplitude of stress σ_0 fixed at a single frequency (ω), and substituting two transformed terms to equation (4-20) respectively, the strain response yields

$$\varepsilon(t) = \frac{\sigma_0}{E_1}\sin(\omega t) + \frac{\sigma_0}{\eta_1 \omega}(1-\cos(\omega t)) + \sigma_0 \omega\left[\frac{-\eta_2 \cos(\omega t)}{(E_2{}^2 + \omega^2 \eta_2{}^2)} + \frac{E_2 \sin(\omega t)}{\omega(E_2{}^2 + \omega^2 \eta_2{}^2)} + \frac{\eta_2}{(E_2{}^2 + \omega^2 \eta_2{}^2)}\exp(-E_2 \frac{t}{\eta_2})\right] \tag{4-21}$$

The last term in Equation 4-21 is negligible at steady state, since it approaches zero. Equation 4-21 can be simplified as follows

$$\varepsilon(t) = \frac{\sigma_0}{E_1}\sin(\omega t) + \frac{\sigma_0}{\eta_1 \omega}(1-\cos(\omega t)) + \sigma_0 \omega\left[\frac{-\eta_2 \cos(\omega t)}{(E_2{}^2 + \omega^2 \eta_2{}^2)} + \frac{E_2 \sin(\omega t)}{\omega(E_2{}^2 + \omega^2 \eta_2{}^2)}\right] \tag{4-22}$$

Inserting Equation 4-22 and the stress function $\sigma(t) = \sigma_0 \sin(\omega)$ into Equation 4-6 finally yields

$$\Delta W = \pi \sigma_0{}^2 \frac{(E_2{}^2 + \omega^2 \eta_2{}^2 + \omega^2 \eta_1 \eta_2)}{\omega \eta_1 (E_2{}^2 + \omega^2 \eta_2{}^2)} \tag{4-23}$$

It is interesting to note that the area of hysteresis loop is affected by not only viscosity (viscous dashpot) but also delayed elasticity (spring element and dashpot element) even in steady state. However, one may ask whether the simple model used in this analysis is different with the response of real material. In reality, the response of

viscoelastic material may be more complex than the simple Burgers model. In cases where the stress history is prescribed, real material response can be closely described as series of delayed elasticity elements, instead of only one delayed elastic element. Even in that case, Equation 4-23 is still valid except for an increasing number of delayed elasticity terms. Consequently, mathematically derived Equation 4-23 proves that unknown or reversible energy dissipation in the area of hysteresis loop is delayed elasticity.

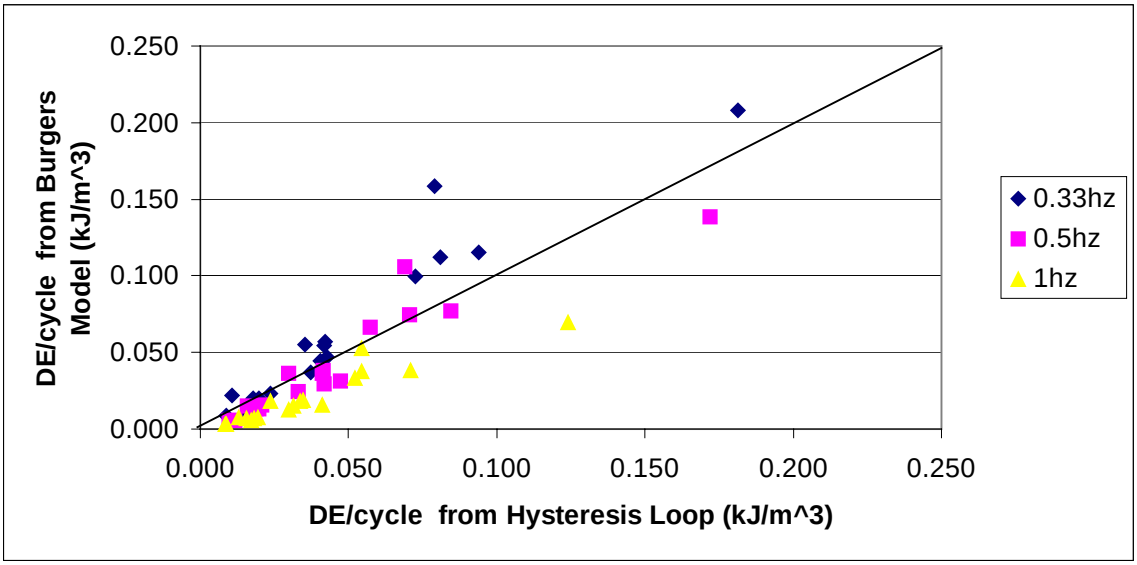

Figure 4-7. Conventional Energy Approach vs. Dissipated Energy from Burgers Model Fit

In order to verify Equation 4-23 experimentally, the Burger model (Equation 4-18) was fitted to creep compliance data obtained from Superpave indirect tension creep tests. The parameters obtained were used along with frequency and stress information to calculate the area of hysteresis loop using Equation 4-23. Figure 4-7 shows a plot comparing the dissipated energy from cyclic test using the measured phase angle to the dissipated energy from the Burgers model fitting. Although some of values were a bit off from the line of equality (probably due to the limitation of the fitting model used), it

clearly showed good agreement. It indicates that the area of hysteresis loop is dominated by both delayed elasticity and viscous response. So, it is emphasized that the delayed elasticity remains even in steady state.

To enhance the comparison, the former assumption that the area of hysteresis loop is only dominated by unrecoverable damage (viscosity) was investigated with the same fitting model. Since the dashpot (η_2) has no effect in steady state in the former assumption, only the first two terms are relevant in Equation 4-22, and the remaining E_2 is combined with E_1. It becomes a well-known Maxwell model as given in Equation 4-24.

$$\varepsilon(t) = \frac{\sigma_0}{E}\sin(\omega t) + \frac{\sigma_0}{\eta_1 \omega}(1 - \cos(\omega t)) \tag{4-24}$$

where

$$E = \frac{1}{1/E_1 + 1/E_2}$$

Likewise, dissipated energy found by inserting Equation 4-24 and stress function into Equation 4-6 yields

$$\Delta W = \sigma_0^{\,2} \frac{\pi}{\omega \eta_1} \tag{4-25}$$

Figure 4-8 shows a plot comparing the dissipated energy from cyclic testing using the phase angle to the dissipated energy obtained from the Maxwell model fit. Once again, the dissipated energies from cyclic test were much higher than the energies from the Maxwell model fitting results, which includes only the effects of viscous or dissipated creep strain energy.

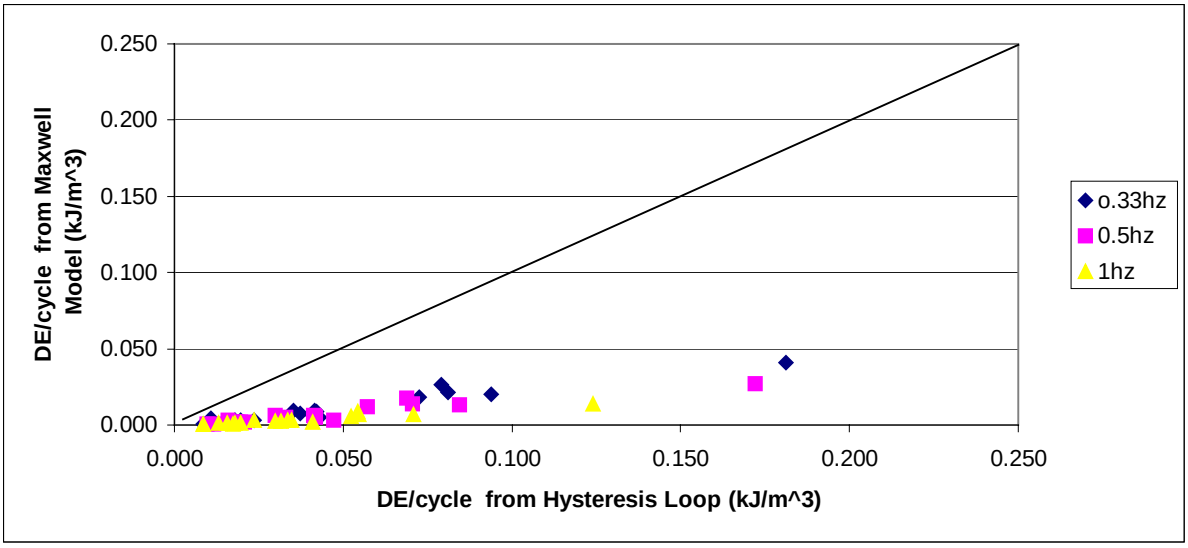

Figure 4-8. Conventional Energy Approach vs. Dissipated Energy from Maxwell Model Fit

CHAPTER 5
INTEGRATION OF THERMAL FRACTURE IN THE HMA FRACTURE MODEL

5.1 Review of the Past Work

5.1.1 TC Model

A mechanics-based thermal cracking performance model (TCMODEL) that was developed as part of the Strategic Highway Research Program (SHRP) consists of two main mechanisms: theory of linear viscoelasticity and linear elastic fracture mechanics. A system to predict thermal stresses in asphalt pavement was developed on the basis of the theory of linear viscoelasticity. The analytical derivations developed from the model that will be incorporated in the system used in this research are explained below.

5.1.2 Conversion of Creep Compliance to Relaxation Modulus

The physical behavior of asphalt mixture can be approximated by theory of linear viscoelasticity. The primary difference between linear elasticity and linear viscoelasticity is time dependency. The time-dependent behavior of linear viscoelastic materials may be studied by means of two types of experiments: creep and stress relaxation. Since creep and stress relaxation phenomena are two aspects of the same viscoelastic behavior of material, they are obviously related. In other words, one can be predicted if the other is known. Therefore, the relaxation modulus is generally converted from a more convenient stress-controlled creep compliance test.

The theoretical derivation for converting creep compliance to relaxation modulus may be easily explained by a simple rheology model (Figure 4-6), which is the well-known Burgers model. The Burgers model is a four-element model consisting of a linear

spring (E_1), a spring element (E_2) and dashpot element (η_2) connected in parallel, and a linear viscous dashpot (η_1). If constant stress is applied, the creep response in terms of compliance becomes

$$D(t) = \frac{1}{E_1} + \frac{1}{\eta_1}t + \frac{1}{E_2}(1 - \exp(-E_2 t / \eta 2)) \tag{5-1}$$

According to Boltzmann's superposition principle (Findley et al., 1976), if the stress input $\sigma(t)$ is arbitrary (variable with time), this arbitrary stress input can be approximated by Equation 5-2. This equation can be used to describe the creep strains under any given stress history provided the creep compliance D(t) is known, where ξ is dummy variable time corresponding to step-wise increasing or decreasing stresses.

$$\varepsilon(t) = \int_0^t D(t-\xi)\frac{\partial \sigma(\xi)}{\partial(\xi)}d\xi \tag{5-2}$$

Applying Laplace transform to Equation 5-2 yields an algebraic Equation 5-3 in the transform variable s:

$$\hat{\varepsilon}(s) = s\,\hat{D}(s)\,\hat{\sigma}(s) \tag{5-3}$$

Taking the Laplace transforms to both the creep compliance (Equation 5-1) and constant input strain ε_0, and substituting two transformed terms to Equation 5-3 respectively, the stress response yields

$$\hat{\sigma}(s) = \frac{\varepsilon_0(\eta_1 + \frac{\eta_1\eta_2}{E_2}s)}{1 + (\frac{\eta_1}{E_1} + \frac{\eta_1}{E_2} + \frac{\eta_2}{E_2})s + (\frac{\eta_1\eta_2}{E_1E_2})s^2} \tag{5-4}$$

Expanding Equation 5-4 by partial fractions and performing inverse Laplace transformation yields

$$\sigma(t) = \varepsilon_0 (C_1 \exp(-\frac{t}{\lambda_1}) + C_2 \exp(-\frac{t}{\lambda_2})) \tag{5-5}$$

The relaxation modulus becomes

$$E(t) = C_1 \exp(-\frac{t}{\lambda_1}) + C_2 \exp(-\frac{t}{\lambda_2}) \tag{5-6}$$

The coefficients C1 and C2, and λ1 and λ1 correspond to E1 and E2, and η1 and η2 of two Maxwell models connected in parallel as shown in Figure 5-1. As a result, a generalized model, which has elastic response (spring), viscous response (dashpot), and delayed elasticity with multiple retardation times can be mathematically converted to multiple Maxwell models connected in parallel.

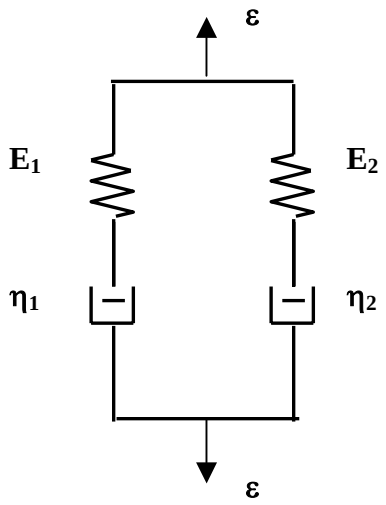

Figure 5-1. Two Maxwell Models Connected in Parallel

5.1.3 Time-Temperature Superposition Principle and Master Curve Fit

Theoretical and experimental results indicate that for linear viscoelastic materials, the effect of time and temperature can be combined into a single parameter through the concept of the time-temperature superposition principle. From a proper set of creep or relaxation tests under different temperature levels the master curve can be generated by

shifting the creep or relaxation curves based on reference temperature. A material exhibiting such a physical behavior is called thermorheologically simple. The relations between real time t, reduced time ξ, and a shifting factor a_T are given in Equation 5-7.

$$\xi = t/a_T \tag{5-7}$$

An automated procedure to generate the master curve was developed as part of the Strategic Highway Research Program (Buttlar et al, 1998). The system uses results of 1000-second creep tests performed at three different temperatures using Superpave IDT. Prony series (generalized model), which have one Maxwell model (a spring and a dashpot) and several Kelvin elements (a spring element (E_2) and dashpot element (η_2) connected in parallel), were used to accurately fit the generated master curve. Buttlar (1996) concluded that Prony series with one Maxwell element and four Kelvin elements (N=4) were generally suitable for fitting the generated master curve. The equation used in the Prony series is as follows

$$D(\xi) = D_0 + \sum_{i=1}^{N} D_i\left(1 - e^{-\xi/\tau_i}\right) + \frac{\xi}{\eta_v} \tag{5-8}$$

5.1.4 Thermal Stress Prediction

Unlike the response of viscoelastic media at single temperature, for transient temperature conditions where temperature varies with time, thermal stress is generally involved and developed due to its thermal contraction. Since under the transient temperatures, two different domains: time and temperature are coincidently involved, the stress or strain constitutive equations are somewhat different. Consequently, the convenient Laplace transform cannot be simply applied to the double domains. Time-temperature constitutive stress and strain equations at time t are given by

$$\sigma(t) = \int_0^t E(\xi(t) - \xi(t')) \cdot \frac{d\varepsilon(t')}{dt'} dt' \tag{5-9}$$

$$\varepsilon(t) = \int_0^t D(\xi(t) - \xi(t')) \cdot \frac{d\sigma(t')}{dt'} dt' \tag{5-10}$$

Morland and Lee (1960) introduced the following reduced time, which is able to take into account both effects of temperature gradients and time variations coincidentally.

$$\xi(t) = \int_0^t \frac{1}{a_T(T(t'))} dt' \tag{5-11}$$

Soules et al. (1987) derived the following equations able to calculate the thermal stress of linear viscoelastic media. In fact, the relaxation modulus can be represented as the generalized Maxwell model, where several Maxwell components are connected in parallel. Mathematically, the multiple Maxwell model consists of a series of exponential functions that facilitate mathematical derivation of the thermal stress from Equation 5-9. The details of the derivation of the thermal stress are as follows:

The partial stress component $E_1 e^{-\xi(t)/\lambda_1}$ substituted into Equation 5-9 yields

$$\sigma(t) = E_1 \int_0^t \exp\frac{-1}{\lambda_1}(\xi(t) - \xi(t')) \cdot \frac{d\varepsilon(t')}{dt'} dt' \tag{5-12}$$

The portions are independent of t' can be taken out from the integral.

$$\sigma(t) = E_1 \exp(\frac{-1}{\lambda_1}\xi(t)) \cdot \int_0^t \exp(\frac{1}{\lambda_1}\xi(t)) \frac{d\varepsilon(t')}{dt'} dt' \tag{5-13}$$

Dividing the above integral into two ranges: from 0 to t-Δt and from t-Δt to t yields

$$\sigma(t) = E_1 \exp(\frac{-1}{\lambda_1}\xi(t)) \cdot \{\int_0^{t-\Delta t} \exp(\frac{1}{\lambda_1}\xi(t)) \frac{d\varepsilon(t')}{dt'} dt' + \int_{t-\Delta t}^t \exp(\frac{1}{\lambda_1}\xi(t)) \frac{d\varepsilon(t')}{dt'} dt'\} \tag{5-14}$$

Meanwhile, the partial stress component $E_1 e^{-\xi(t-\Delta t)/\lambda_1}$ at time t-Δt substituted into Equation 5-9 yields

$$\sigma(t-\Delta t) = E_1 \exp(\frac{-1}{\lambda_1}\xi(t-\Delta t)) \cdot \int_0^{t-\Delta t} \exp(\frac{1}{\lambda_1}\xi(t)) \frac{d\varepsilon(t')}{dt'} dt' \qquad (5\text{-}15)$$

The first term of Equation 5-14 can be replaced by Equation 5-15, which yields

$$\sigma(t) = E_1 \exp(\frac{-1}{\lambda_1}\xi(t)) \cdot \{\frac{\sigma(t-\Delta t)}{E_1 \exp(\frac{-1}{\lambda_1}\xi(t-\Delta t))} + \int_{t-\Delta t}^{t} \exp(\frac{1}{\lambda_1}\xi(t)) \frac{d\varepsilon(t')}{dt'} dt'\} \qquad (5\text{-}16)$$

The last term of Equation 5-16 can be rewritten as follows

$$\left[\frac{\exp(\frac{1}{\lambda_1}\xi(t'))}{\frac{d(\frac{1}{\lambda_1}\xi(t'))}{dt'}} \cdot \frac{d\varepsilon(t')}{dt'} \right]_{t-\Delta t}^{t} = \left[\lambda_1 \exp(\frac{1}{\lambda_1}\xi(t')) \cdot \frac{d\varepsilon(t')}{d\xi(t')} \right]_{t-\Delta t}^{t} \qquad (5\text{-}17)$$

Note that $\int_a^b \exp(f(x))dx = \left[\frac{\exp(f(x))}{\frac{d(f(x))}{dx}} \right]_a^b$

Assuming the dε(t')/dξ(t') is constant between t-Δt and t, Equation 5-17 becomes

$$\lambda_1 \frac{d\varepsilon(t')}{d\xi(t')} \left[\exp(\frac{1}{\lambda_1}\xi(t')) \right]_{t-\Delta t}^{t} = \lambda_1 \frac{\varepsilon(t)-\varepsilon(t-\Delta t)}{\xi(t)-\xi(t-\Delta t)} \left[\exp(\frac{1}{\lambda_1}\xi(t)) - \exp(\frac{1}{\lambda_1}\xi(t-\Delta t)) \right] \qquad (5\text{-}18)$$

Substituting Equation 5-18 into 5-16 finally yields

$$\sigma(t) - \exp\{\frac{-1}{\lambda_1}(\xi(t)-\xi(t-\Delta t))\}\sigma(t-\Delta t) = E_1 \frac{\lambda_1 \Delta\varepsilon}{(\xi(t)-\xi(t-\Delta t))}[1-\exp\{\frac{-1}{\lambda_1}(\xi(t)-\xi(t-\Delta t))\}] \qquad (5\text{-}19)$$

Equation 5-19 deals with only one term of relaxation modulus. The rest of stress components should be added up.

$$\sigma(t) = \sum_{i=1}^{N+1} \sigma_i(t) \qquad (5\text{-}20)$$

Lastly, the final equation of thermal stress prediction (Equation 5-20) can be determined numerically using the finite difference method.

5.2 Development of Basic Algorithm for HMA Thermal Fracture Model

5.2.1 Development of Thermal Creep Strain Prediction

Although the power model has been successfully used as a fitting function of the creep behavior for linear viscoelastic materials, its mathematical deficiency does not allow predicting the thermal stress of viscoelastic materials under multiple temperature ranges that indicates thermal creep strain should be predicted by viscosity η_v (Equation 5-8) obtained from the Prony series rather than the power model. Therefore, the thermal creep strain prediction equations were derived from the time-temperature constitutive strain equation combined with the irreversible creep component, η_v in a similar manner that was used in the thermal stress prediction. Equations to calculate the thermal creep strain prediction are correspondent to the principle of linear viscoelasticity theory. Considering only the viscous component representing the rate of damage of viscoelastic media, Equation 5-8 becomes

$$D(\xi) = \frac{\xi}{\eta} \tag{5-23}$$

Substituting Equation 5-23 into Equation 5-10 yields the following equation representing only irreversible creep strain.

$$\varepsilon_{cr}(t) = \int_0^t \frac{1}{\eta}(\xi(t) - \xi(t')) \cdot \frac{d\sigma(t')}{dt'} dt' \tag{5-24}$$

The portions are independent of t' can be taken out from the integral, which yields Equation 5-26.

$$\varepsilon_{cr}(t) = \frac{1}{\eta}\int_0^t (\xi(t) - \xi(t')) \cdot \frac{d\sigma(t')}{dt'} dt' \tag{5-25}$$

$$\varepsilon_{cr}(t) = \frac{1}{\eta}[\xi(t)\int_0^t \frac{d\sigma(t')}{dt'} dt' - \int_0^t \xi(t') \cdot \frac{d\sigma(t')}{dt'} dt'] \tag{5-26}$$

Since the thermal stress σ(t) at time t was determined from the thermal stress prediction above, the thermal stress σ(t) is independent of t', so it can be taken out from the integral. Equation 5-26 becomes

$$\varepsilon_{cr}(t) = \frac{1}{\eta}[\xi(t)\sigma(t) - \int_0^t \xi(t') \cdot \frac{d\sigma(t')}{dt'} dt'] \tag{5-27}$$

Dividing the above integral into two ranges: from 0 to t-Δt and from t-Δt to t becomes

$$\varepsilon_{cr}(t) = \frac{1}{\eta}[\xi(t)\sigma(t) - \{\int_0^{t-\Delta t} \xi(t') \cdot \frac{d\sigma(t')}{dt'} dt' + \int_{t-\Delta t}^t \xi(t') \cdot \frac{d\sigma(t')}{dt'} dt\}] \tag{5-28}$$

Meanwhile, the creep strain at time t-Δt is obtained from Equation 5-24 as follows

$$\varepsilon_{cr}(t-\Delta t) = \int_0^{t-\Delta t} \frac{1}{\eta}(\xi(t-\Delta t) - \xi(t')) \cdot \frac{d\sigma(t')}{dt'} dt' \tag{5-29}$$

Taking out the portions are independent to t' becomes

$$\varepsilon_{cr}(t-\Delta t) = \frac{1}{\eta}[\xi(t-\Delta t)\int_0^{t-\Delta t} \frac{d\sigma(t')}{dt'} dt' - \int_0^{t-\Delta t} \xi(t') \cdot \frac{d\sigma(t')}{dt'} dt'] \tag{5-30}$$

The stress σ(t-Δt) at t-Δt determined from the thermal stress prediction above can be taken out, so Equation 5-30 becomes

$$\varepsilon_{cr}(t-\Delta t) = \frac{1}{\eta}[\xi(t-\Delta t)\sigma(t-\Delta t) - \int_0^{t-\Delta t} \xi(t') \cdot \frac{d\sigma(t')}{dt'} dt'] \tag{5-31}$$

The integral from 0 to t-Δt in Equation 5-31 is rearranged as follows

$$\int_0^{t-\Delta t} \xi(t') \cdot \frac{d\sigma(t')}{dt'} dt' = \xi(t-\Delta t)\sigma(t-\Delta t) - \eta\varepsilon_{cr}(t-\Delta t) \tag{5-32}$$

The first integral term of Equation 5-28 can be replaced by Equation 5-32 that yields

$$\varepsilon_{cr}(t)=\frac{1}{\eta}[\xi(t)\sigma(t)-\{\xi(t-\Delta t)\sigma(t-\Delta t)-\eta\varepsilon_{cr}(t-\Delta t)+\int_{t-\Delta t}^{t}\xi(t')\cdot\frac{d\sigma(t')}{dt'}dt\}] \tag{5-33}$$

$$\varepsilon_{cr}(t)=\varepsilon_{cr}(t-\Delta t)+\frac{1}{\eta}[\xi(t)\sigma(t)-\xi(t-\Delta t)\sigma(t-\Delta t)-\int_{t-\Delta t}^{t}\xi(t')\cdot\frac{d\sigma(t')}{dt'}dt] \tag{5-34}$$

Assuming the dσ(t')/dt' is constant between t-Δt and t, Equation 5-34 becomes

$$\varepsilon_{cr}(t)=\varepsilon_{cr}(t-\Delta t)+\frac{1}{\eta}[\xi(t)\sigma(t)-\xi(t-\Delta t)\sigma(t-\Delta t)-\frac{d\sigma(t')}{dt'}\int_{t-\Delta t}^{t}\xi(t')\cdot dt] \tag{5-35}$$

$$\varepsilon_{cr}(t)=\varepsilon_{cr}(t-\Delta t)+\frac{1}{\eta}[\xi(t)\sigma(t)-\xi(t-\Delta t)\sigma(t-\Delta t)-\frac{\sigma(t)-\sigma(t-\Delta t)}{\Delta t}\int_{t-\Delta t}^{t}\xi(t')\cdot dt] \tag{5-36}$$

Although the integral function still remains in the last term of Equation 5-36, the function can be calculated numerically as long as the shifting function is known. As shown in the thermal stress prediction, the thermal creep strain prediction (Equation 5-36) can be determined using the finite difference method as well.

5.2.2 Dissipated Creep Strain Energy and Energy Transfer

Dissipated creep strain energy is an irreversible parameter that represents fundamental energy loss in viscoelastic materials. Therefore, the thermal strain should be irreversible and only developed in the case when tensile stress develops. Unfortunately, the thermal creep strain prediction (Equation 5-36) cannot deal with those conditions, so that it should note that these effects must be considered by use of a proper conditional statement before determining the dissipated creep strain energy.

In general, energy can be determined from the stress-strain relationship. Once the thermal stress and thermal creep strain are known, dissipated creep strain energy can be obtained at each time increment. The increment of dissipated creep strain energy at small time increment Δt is as follows

$$DCSE(\Delta t)=\frac{\sigma(t)-\sigma(t-\Delta t)}{2}\cdot\varepsilon_{cr}(t)-\varepsilon_{cr}(t-\Delta t) \tag{5-37}$$

It is noticed that dissipated creep strain energy limit is constant at fixed temperature, while DCSE limits may vary with temperature. Therefore, DCSE obtained from Equation 5-37 may be different depending on temperatures. If the DCSE limits are the same for any temperature, it may be more convenient to detect the failure at the given temperature. It is also of benefit that the energy transfer simplifies mathematical complication and reduces relevant time delay. Therefore, DCSE limits at the given temperature can be transferred to a correspondent DCSE limit at a reference temperature using Equation 5-38, which was developed based on the energy principle.

$$DCSE(\Delta t) = \frac{\sigma(t) - \sigma(t-\Delta t)}{2} \cdot \varepsilon_{cr}(t) - \varepsilon_{cr}(t-\Delta t) \cdot \frac{DCSE \text{ limit at reference temperature}}{DCSE \text{ limit at given temperature}} \tag{5-38}$$

The nature of DCSE is irrecoverable and is accumulated with continued loading. However, DCSE obtained in Equation 5-38 is only for a small time increment Δt. Consequently, total accumulated DCSE can be obtained from the summation of dissipated creep strain energies at each time step up to the applied time t. The accumulated DCSE at any given time t is as follows

$$DCSE(t) = \sum DCSE(\Delta t) \tag{5-39}$$

5.3 HMA Thermal Fracture Model

5.3.1 Physical Model, Temperature Variation, and Assumptions

The physical representation of the actual pavement structure assumed in the HMA thermal fracture model is shown in Figure 5-2. As mentioned in Chapter 2, since the effects of pavement geometry are not clear yet, a preliminary physical model representing thermal crack development of HMA was assumed as an infinite thin plane with a central crack, which allows to limit thermal crack development of HMA to only the level of

material itself. A 10mm initial crack length, followed by 5mm of processing zones, which generally corresponds half the nominal maximum aggregate size, was assumed for the initial physical model. Two simply supported edges to y-axis, which allow stress development in one-dimension only, and so that its boundary conditions satisfy the one-dimensional constitutive stress and strain equation were used in the stress and strain prediction above.

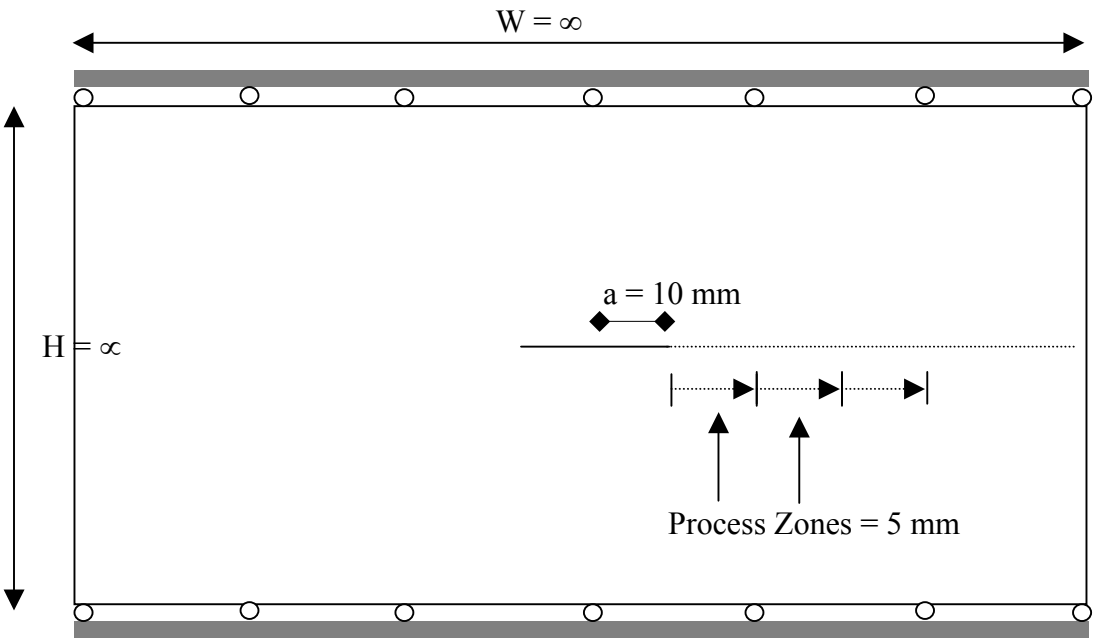

Figure 5-2. Physical Model

It is noticed that the thin plane assumption of the physical model implies that a single and uniform temperature develops over the body of the physical model, and a single stress σ_0 develops near the supports. The theoretical stress distribution along the process zones satisfying the conditions of the physical model is given in Equation 5-40. The equation was theoretically derived from the well-known Westergaard function where stress limit was set as the tensile strength at the reference temperature.

$$\sigma_y = \frac{\sigma_0(r+a)}{\sqrt{r(r+2a)}} \tag{5-40}$$

where σ_0 is stress, a is crack length, and r is distance measured from the crack tip.

From field observations (Roque et al., 1993), a general pattern of the daily or seasonal temperature variation of pavement's surface appears to have a cyclic form, so that the external source of the temperature variation may be reasonably represented as a sinusoidal function. The benefit of the sinusoidal function is to allow the continuous and successive application of fatigue loading to the physical model. It also allows continuous development of crack propagation through the body.

5.3.2 General Concept of HMA Thermal Fracture Model

The general concept of HMA thermal fracture model consists of four steps: defining the process zones, predicting thermal stresses, calculating average stresses within each process zone, and calculating and assigning DCSE within each individual process zone. Average stresses over the process zones calculated by the thermal stress at small time increments are used to get the DCSEs over the process zones. The DCSEs obtained are then assigned to each process zone, which were previously defined. An overall procedure for crack development along the process zones used the time-increment iteration process is shown in Figure 5-3. During the iteration process, a process zone near the crack tip is failed when the total accumulated DCSE reached DCSE limit. At the same time, the stress distribution along the processing zones is changed by the increase of crack length, so the stress redistribution should be assigned and considered in the next step.

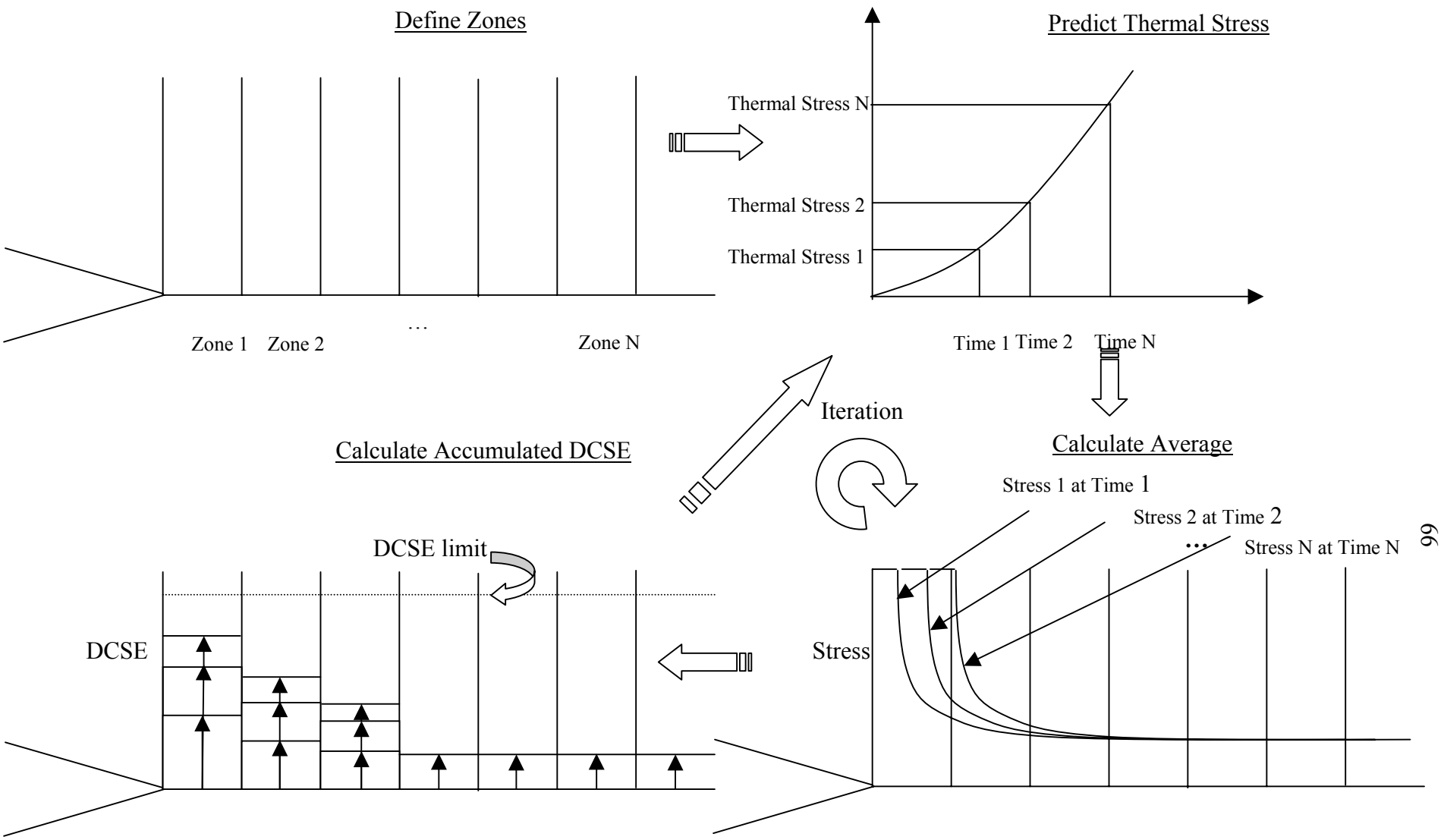

Figure 5-3. General Concept of HMA Thermal Fracture Model

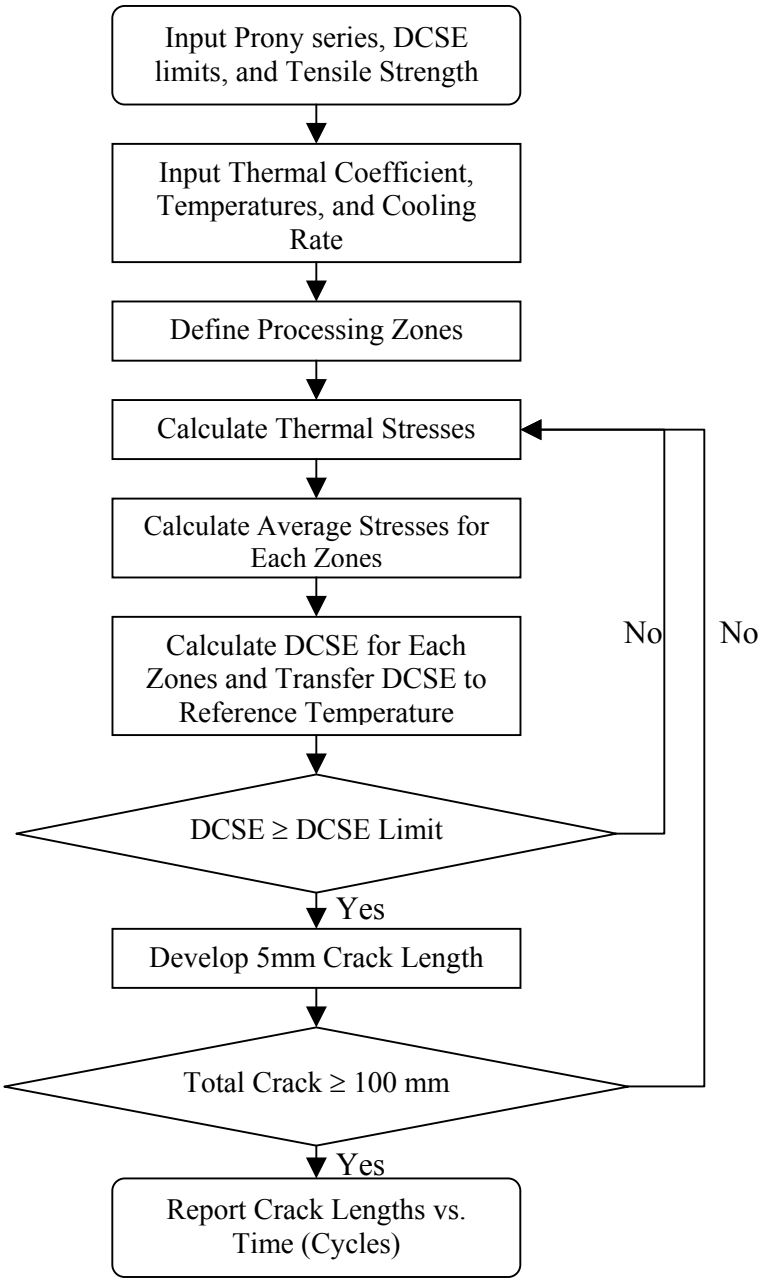

Figure 5-4. General Steps of HMA Thermal Fracture Model

5.3.3 Software Development

Calculation procedures to determine the amount of crack development have been programmed using Mathcad software. The regression coefficients fitted by Prony series, DSCE limits, and tensile strength at the reference temperature were obtained from

Superpave IDT tests. Additional user dependent inputs: thermal coefficient, maximum and minimum temperatures, and cooling rate can be properly controlled by users.

The number of data point of thermal stresses and thermal creep strains appears critical due to the nature of the finite different method. From the hundreds of preliminary tests, 50 data point per cooling cycle appears adequate when considering accuracy of the predicted thermal stresses and computation time. Besides, the number of processing zones contributes as an important factor that affects the computation time. A 100 mm crack limit was set, so the program is automatically stopped when the total length of crack reaches 100 mm. In addition, the lowest temperature (0°C) was consistently set as reference temperature to generate a master curve and transfer accumulated DCSE to other temperatures. General steps used to calculate the amount of crack development of the HMA thermal fracture model are shown in Figure 5-4.

5.4 Evaluation of HMA Thermal Fracture Model

5.4.1 Parametric Study

In evaluation of the HMA thermal fracture model it may be reasonable to check whether or not the model provides clearly expected results. For example, a faster cooling rate, a higher thermal coefficient, and a lower temperature range should accelerate crack development of HMA, and vice versa. Figure 5-5 through 5-7 shows effects of the cooling rates, thermal coefficients, and temperatures, respectively. Based on peselected mixture properties (I75-1C section), three different cooling rates, thermal coefficients, and temperature ranges were applied to evaluate the HMA thermal crack model where each control parameter was varied as fixing the others at the same levels. The results clearly showed that when a faster cooling rate, a higher thermal coefficient, and a lower temperature range were applied, the cracks advanced at a much faster rate than when

other conditions were applied. These results are clearly in accordance with the expected results.

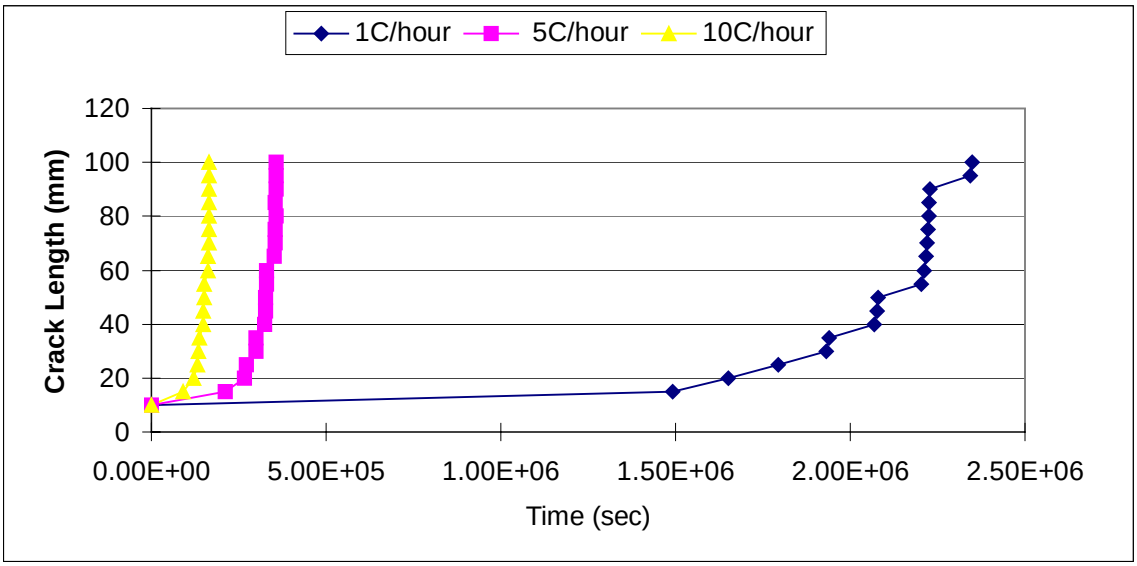

Figure 5-5. Effect of Cooling Rates

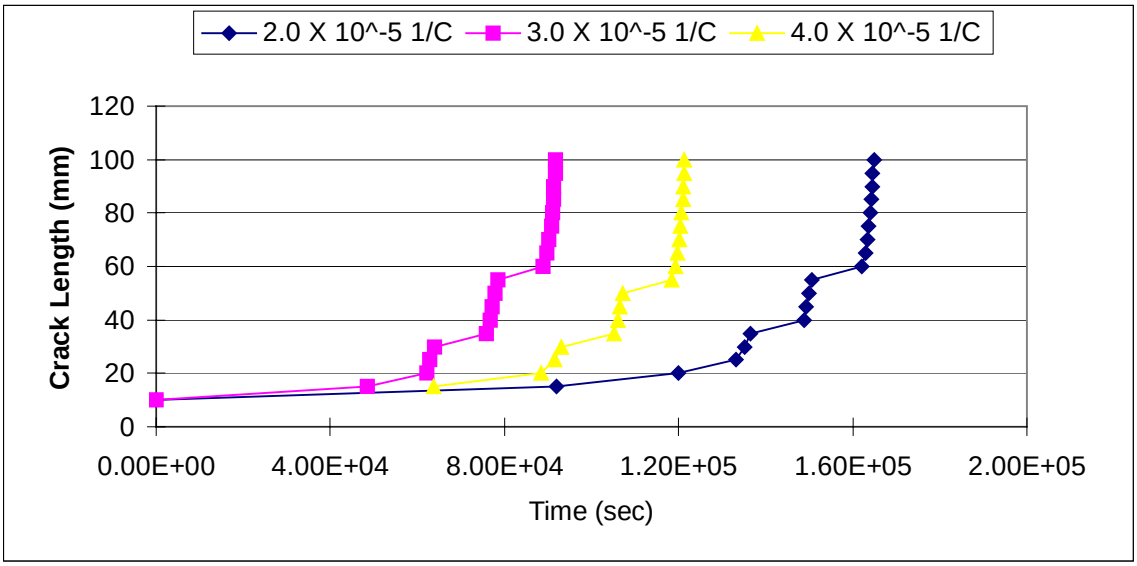

Figure 5-6. Effect of Thermal Coefficients

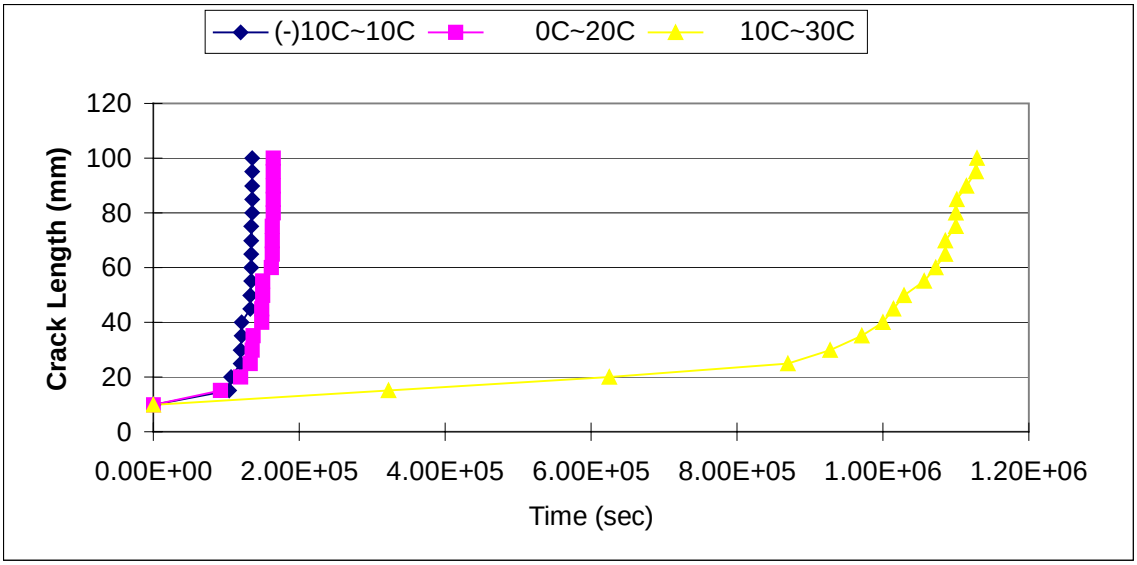

Figure 5-7. Effect of Temperatures

5.4.2 Evaluation of Material Characteristics Related to Thermal Cracking

One of the primary goals of the ongoing study is to evaluate thermally induced top-down cracking related to field performance data. If the same user-dependent inputs apply to all the pavement sections, an amount of crack development obtained can be limited to material effects alone. Asphalt mixtures from the eleven pavement sections (Group I and II) were evaluated in this way. From the one set of standard Superpave IDT tests performed on all the pavement sections at three temperatures: 0, 10, and 20°C, Prony series, DCSE limits, and tensile strength at 0°C were obtained and used as input parameters of HMA thermal fracture model. The same user-dependent input conditions as shown in Table 5-1 were applied to all the pavement sections. Since the HMA thermal fracture model evaluates amount of crack development on the basis of time increments, longer cracking time of mixture presents good resistance of the thermal cracking. In evaluation of the eleven pavement sections, the cracking times were selected at 100 mm crack length and plotted in Figure 5-8. All the sections evaluated in this study generally

indicated that a mixture having lower binder viscosity (soft binder) and higher fracture resistance (high DCSE limit) showed a greater resistance to the thermal crack development. These results are in agreement with the well accepted premise that the asphalt binder that are softer or have lower viscosity will provide better performance in resisting thermal cracking. A higher fracture limit is also important to improve cracking performance. This indicates that the HMA thermal cracking model provides reasonable and reliable predictions for the thermal crack development of HMA.

Table 5-1. User-Dependant Inputs of HMA Thermal Fracture Model

Thermal Coefficient (1/°C)	$2x10^{-5}$
Temperature Range (°C)	0 to 20
Temperature Shape	Sinusoidal
Cooling Rate (°C/hour)	10
Initial Crack Length (mm)	10
Zone Length (mm)	5

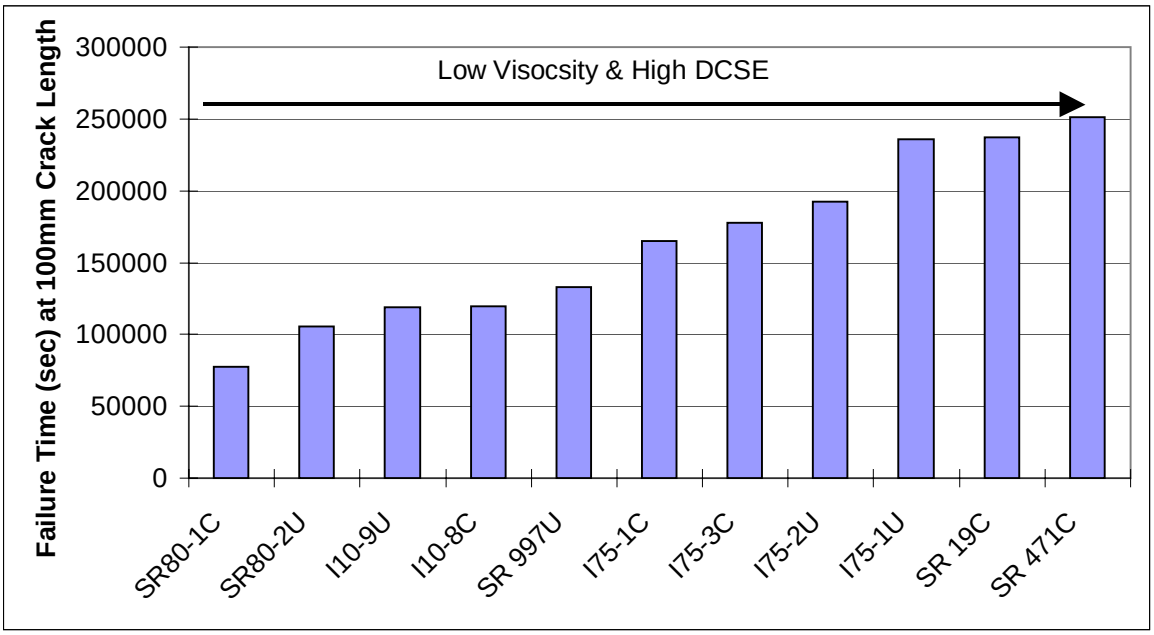

Figure 5-8. Thermal Crack Development Based on Material's Characteristics

5.4.3 Evaluation of Pavement Performance Related to Thermal Cracking

To evaluate the model's performance related to in-service pavement sections, regional temperature of each section is an important input parameter. However, if the input temperature range is out of the temperature range that was used in the tests for asphalt mixtures, it may provide inaccurate prediction, and as mentioned earlier, increasing temperature increases computation time due to the nature of the finite different method. From inspection of the field temperature data, the data consists of two primary factors: mean air temperature and range in air temperature. According to the parametric study, higher temperature increased crack resistance of asphalt pavement while increasing cooling rate reduces pavement performance. Therefore, a simple equation (Equation 5-41) was developed upon the concept that the increase of annual mean air temperature may increase the cracking performance while the broad range in air temperature may decrease the performance.

$$CFT = FT \times AMT / RMT \tag{5-41}$$

where CFT = Calibrated Failure Time
FT = Failure Time
AMT = Annual Mean Air Temperature
RMT = Range in Annual Mean Air Temperature
(Annual Max. Mean Temp. – Annual Min. Mean Temp.)

The annual mean air temperatures and the ranges in air temperature (difference between maximum and minimum mean air temperatures) recorded at each pavement section are given in Table 5-2. The failure time at 100 mm crack length and two regional temperature inputs of each section were used to calculate the calibrated failure times (Figure 5-9).

Table 5-2. Regional Temperature of Individual Sections

Sections	Annual Mean Air Temp.	Range in Annual Mean Air Temperature
SR80-1C	22.92	13.08
I10-8C	21.08	13.25
I75-1C	23.17	11.58
I75-3C	22.92	13.08
SR 19C	21.42	13.08
SR 471C	22.42	12.83
SR80-2U	22.92	13.08
I10-9U	21.08	13.25
SR 997U	23.25	10.17
I75-2U	22.92	13.08
I75-1U	23.17	11.58

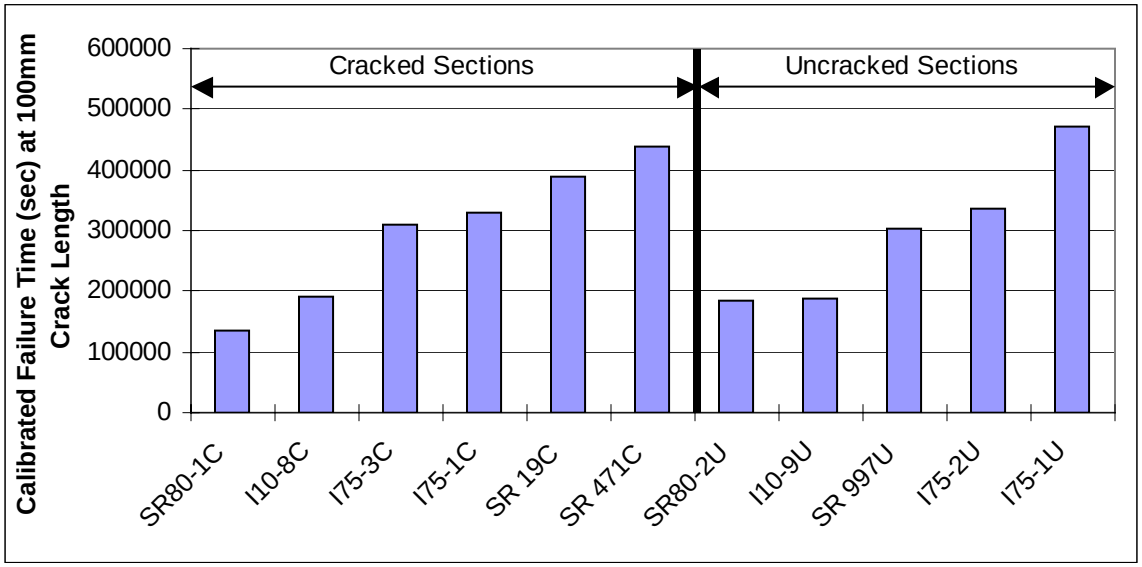

Figure 5-9. Thermal Crack Development Based on Field Performance

As shown in Figure 5-9 two types of pavement sections where the symbol ‘C’ represents a cracked section while the symbol ‘U’ represents a uncracked section indicate that the top-down cracking performance did not uniquely relate to thermal cracking prediction through the model. It appears that load-induced damage is far more significant than that temperature induced damage, which explains the lack of correlation with the performance data in the field. In fact, the annual mean temperature in Florida is much higher than other states. Therefore, only a combined model that integrates top-down

cracking performance associated with loading and thermal effects is needed to provide more accurate predictions related to pavement performance data.

CHAPTER 6
FIELD PERFORMANCE EVALUATION BASED ON COMBINED EFFECT OF TEMPERATURE AND LOAD

It was recognized that thermal cracking alone was not directly related to the top-down cracking performance. It appears that performance data evaluated in this study was gathered from a limited area (the state of Florida), so that the thermal effect may be smaller than for other areas. However, this phenomenon doesn't mean the thermal effect is negligible in this area because the nature of thermal cracking is fundamentally related to the top-down cracking development.

Prior work done by Roque et al. (2004) introduced the concept of Energy Ratio (ER), which integrated HMA fracture model and the structural characteristics of asphalt pavement. ER was determined to accurately distinguish between pavements that exhibited top-down cracking and those that did not. However, this system was limited to the evaluation of load-induced top-down cracking. Consequently, by combining the concept of Energy Ratio with the system developed for the evaluation of thermal cracking performance, it is expected that Energy Ratio may provide a more accurate estimation for the pavements exhibited to top-down cracking.

6.1 Evaluation of Load-Induced Top-Down Cracking Performance

As explained in Chapter 2, the Energy Ratio was developed based on field performance data, where DCSE limit over minimum DCSE requirement is a critical definition. For eleven pavement sections, the Energy Ratios were determined using Equation 6-1 where applied stress σ, and all other input parameters: failure strength S_t,

D_1, *m* value, and DCSE limit were obtained from pavement structure analysis, and mixture tests (Chapter 3), respectively.

$$ER = \frac{DCSE_{Limit} \cdot \left[0.00299\sigma^{-3.1}(6.36 - St) + 2.46 \cdot 10^{-8}\right]}{m^{2.98} \cdot D_1} \quad (6\text{-}1)$$

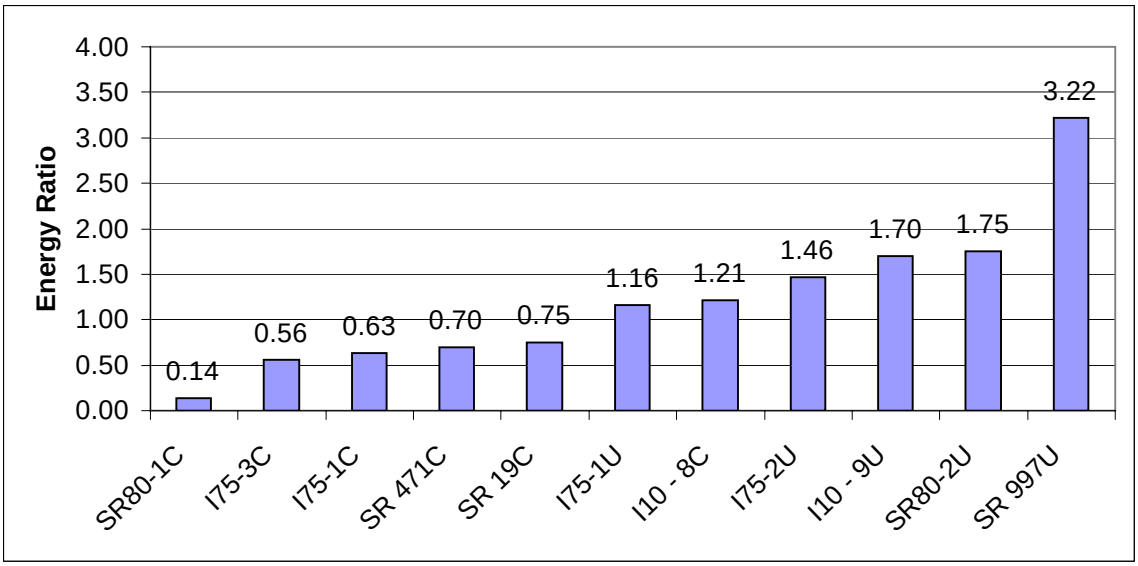

Figure 6-1. Energy Ratio

As shown in Figure 6-1, the eleven sections with different properties of binders and gradation have shown that the Energy Ratios obtained from uncracked sections were higher than 1.0 while those obtained from cracked section were smaller than 1.0, except for one cracked section (I10-8C). It appears that the Energy Ratios are generally acceptable, even though the Energy Ratio of I10-8C was somewhat higher than the energy criterion. Prior work (Roque et al., 2004) has reported that mixture had a DCSE limit that was less than 0.75 KJ/m^3, and a very high DCSE of 2.5 KJ/m^3 did not correlate the principle of Energy Ratio. Considering that I10-8C had a very low DCSE limit, which may explain why the Energy Ratio of the section did not meet the energy requirement.

However, even though the Energy Ratio showed well-matched results on the pavements with cracked and uncraked condition, individual cracked condition of each section was not directly matched with a visual observation for the cracked sections. For example, I10-8C, which had relatively heavy top-down cracks over the surface of asphalt layer, had showed relatively a higher ER value, while SR 471 that recently showed top-down cracks had shown relatively low ER value. Of particular interest, it is noticed that the unmatched performance sections came from the northern area (Figure 3-1). These observations indicate that the top-down cracking performance may be affected by the effect of thermal stress. Consequently, the evaluation of top-down cracking performance with thermal effect may provide an accurate prediction of top-down cracking performance in pavement.

6.2 Consideration of Load Effect to Top-down Cracking Performance

It appears that regional temperature has an influence on development of the top-down cracking. In fact, the annual mean temperature and the temperature-cooling rate in Florida is much higher and lower than other states, which indicates the effect of temperature may be less significant. On the other hand, it can be imagined that in northern area where relatively lower temperature are dominant, top-down cracking performance may be more significantly affected by the thermal effect. In this case, the performance evaluated by the effect of traffic loads alone may not be reliable. Consequently, the only way to reliably estimate the top-down cracking performance appears to assemble two different aspects of mechanisms.

To quantify both loading and thermal effects, it is important to understand the principle of Energy Ratio. The Energy Ratio, which is defined as dissipated creep strain energy threshold of the mixture divided by minimum dissipated creep strain energy

required. It is a single dimensionless parameter that was developed based on performance data. By simply multiplying the ER to the calibrated failure time, the loading effect can be transferred to a form of failure time (Equation 6-2). Consequently overall thermal and loading effects are integrated as the failure time.

Figure 6-2 shows the integrated failure times of the eleven pavement sections. The plot shows that the uncracked sections were clearly discriminated from the sections exhibit top-down cracking. This indicates that when both temperature and load effects were properly combined better correlation resulted with the top-down cracking performance data. As a result, the integrated failure time was able to more effectively distinguish the sections that exhibit top-down cracking.

However, it is noticed that the failure time alone may not be directly related to the top-down cracking performance. A more efficient equation that can directly relate the performance of in-situ pavements was developed in the similar manner that was used in the Energy Ratio.

$$IFT = FT \times AMT / RMT \times ER \quad (6\text{-}2)$$

Where IFT = Integrated Failure Time
FT = Failure Time
AMT = Annual Mean Air Temperature
RMT = Range in Annual Mean Air Temperature
(Annual Max. Mean Temp. – Annual Min. Mean Temp.)
ER = Energy Ratio

6.2 Energy Ratio Correction

As shown in Figure 6-2, the performance of cracked and uncracked sections was clearly discriminated by the single failure time, which is Minimum Time Requirement. The Minimum Time Requirement is a unique parameter that is obtained from the field performance data. As dividing the Integrated Failure Time by the Minimum Time Requirement with the same time dimension, it can be transferred to the same form of the

Energy Ratio. It is a more convenient and even an identical form with the Energy Ratio, but it can now deal with both the loading and thermal effects. As shown Figure 6-3, the Energy Ratio Correction (Equation 6-3) developed based on the mechanistic-empirical approach presented above clearly separated performance, where all the Energy Ratio Correction values were greater than 1.0 for the uncracked sections.

$$\text{Energy Ratio Correction (ERC)} = FT \times AMT / MTV \times ER / MTR \quad (6\text{-}3)$$

where FT = Failure Time
AMT = Annual Mean Temperature
MTV = Range of Mean Temperature Variation
(Annual Max. Mean Temp. – Annual Min. Mean Temp.)
ER = Energy Ratio
MTR = Minimum Time Requirement

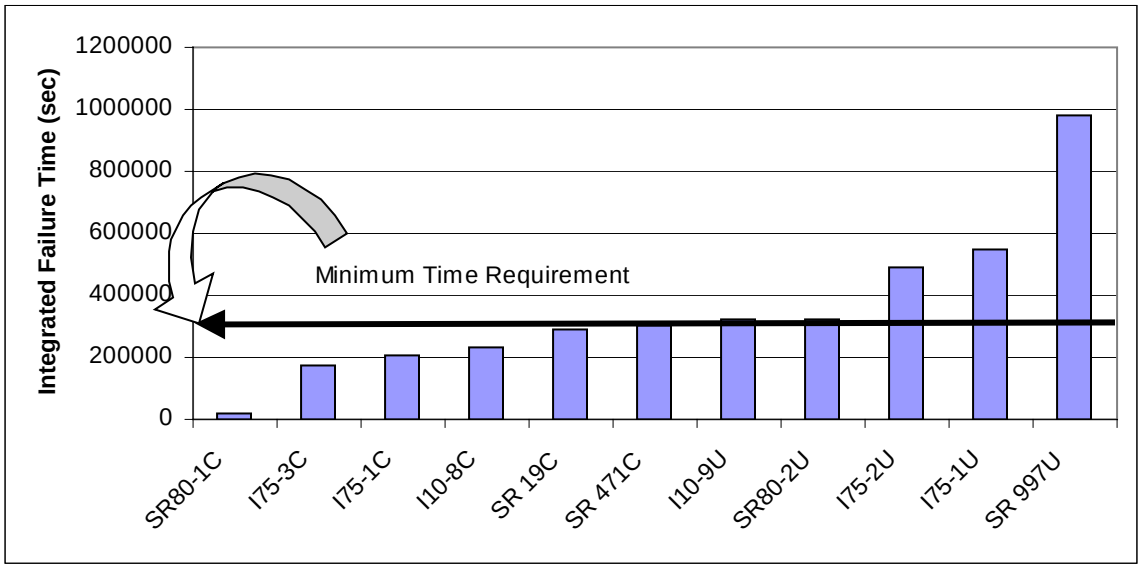

Figure 6-2. Integrated Failure Time

The newly modified Energy Ratio Correction, including thermal effects related to top-down cracking, has shown well-matched performance predictions with the crack conditions of the individual sections (i.e., a section showed a higher ER value that showed relatively heavier top-down cracks than a section has a lower ER value). It appears that thermal effect along with traffic loading plays an important role to contribute

the development of the top-down cracking. Consequently it may be concluded that the Energy Ratio Correction is promising as a simple and reliable predictive tool for evaluating top-down cracking performance.

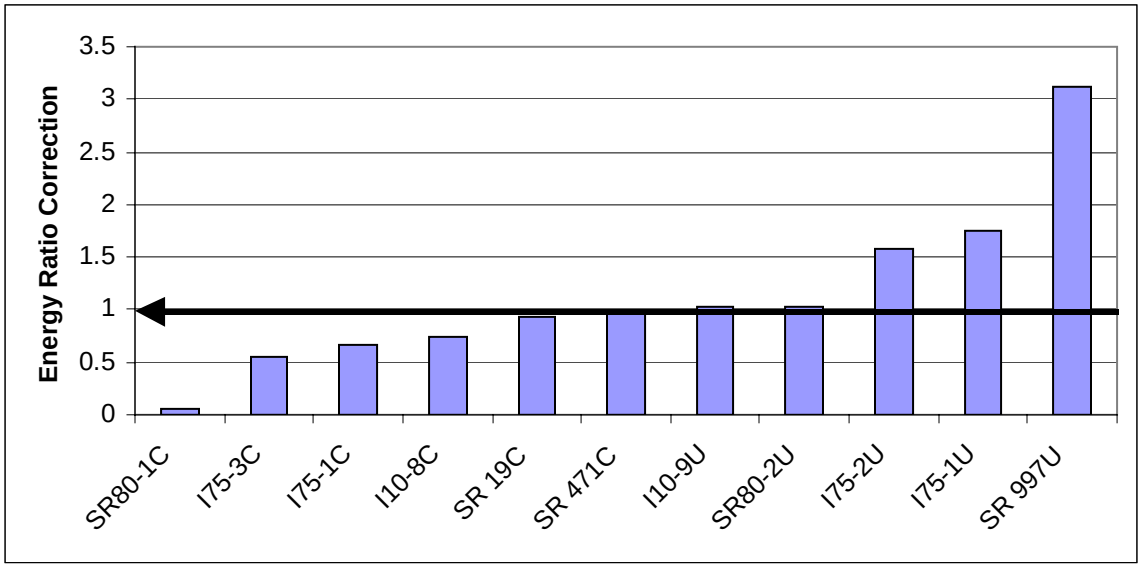

Figure 6-3. Energy Ratio Correction

6.4 Further Analysis

In understanding the nature of thermal cracking, it is important to identify a fundamental parameter that mainly contributes the development of thermal cracking in asphalt pavement. According to HMA fracture model, it was emphasized that dissipated creep strain energy limit (mixture's threshold) is the most important property to preclude the potential crack development of HMA. Also, the rate of creep strain, representing the rate of damage accumulation of mixture is also a fundamental parameter that contributes the development of load-induced damage. Similar to the load-induced cracking, higher DCSE limit appears an important key to effectively mitigate the development of thermal cracking. However, it is unclear whether the rate of creep strain is also a critical parameter that contributes to thermal cracking performance, because the accumulation of

creep strain in mixtures subjected to thermal stresses is much less straightforward and more complex to all other time dependent behavior will affect thermal cracking development in HMA. Therefore, this complementary study is important in understanding the nature of the thermal cracking.

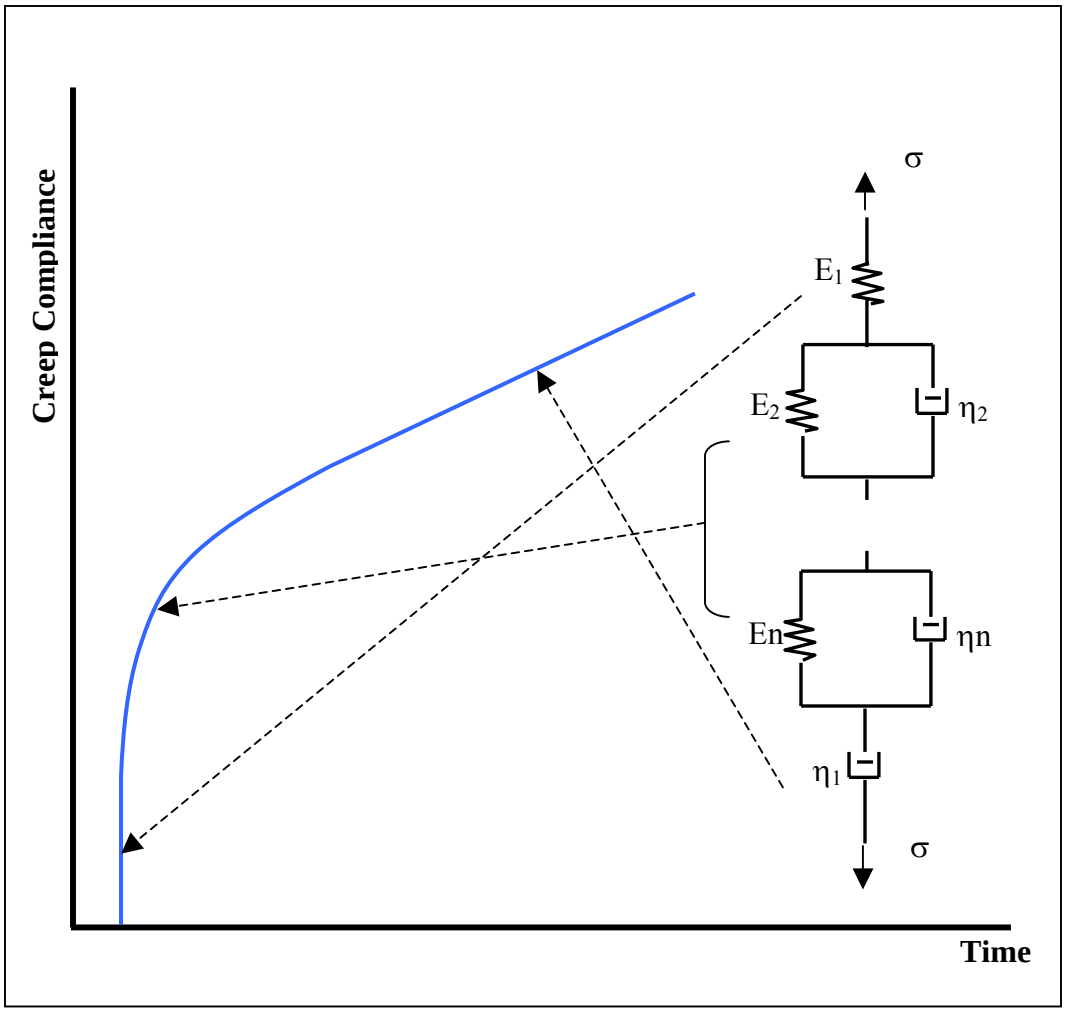

Figure 6-4. Creep Responses Corresponding to Viscoelastic Rheology Model

It is generally known that viscoelastic response can be expressed using a rheology model. In cases where the stress history is prescribed, real material response can be closely described as series of a elastic element, delayed elastic elements, and a viscous element. The combined response under constant static stress is expressed in Figure 6-4

where the purely elastic or time-independent behavior results in an immediate increase in creep compliance when stress is applied, while, and the time-dependent delayed elasticity results in the non-linear portion of the creep compliance curve. Once all time-dependent delayed elasticity response is complete, only viscosity, which represents permanent deformation or damage in mixtures, continues to increase compliance. The viscous response is represented as the linear portion of the creep compliance curve.

Based on HMA fracture mechanics indicates that the load-induced top-down cracking is controlled by two key mixture properties: viscosity and DCSE limit. However, in the case of thermal cracking, the mixture's viscosity may be not the only component that controls the thermal cracking development. One way to quantify the effect of each component is to consider virtual data. Mixture data from the I75-1C section was selected for this purpose. As shown in Equation 6-3, Prony series function, used to get the compliance data has three components: elasticity, delayed elasticity, and viscosity. Conceptually, the effect of individual components on Energy Ratio Correction can be observed by changing coefficients α, β, and γ. All other inputs, such as regional temperature and Energy Ratio were fixed to those of I75-1C. Then the Energy Ratio Correction was monitored by only increasing the value of one coefficient and fixing the other coefficients as 1.0. The plots of three generated data sets (Figure 6-5 to Figure 6-7) and the Energy Ratio Correction (Figure 6-8) calculated from the data are shown in figures below.

$$D(\xi) = \alpha D_0 + \beta \sum_{i=1}^{N} D_i \left(1 - e^{-\xi/\tau_i}\right) + \gamma \frac{\xi}{\eta_v} \tag{6-3}$$

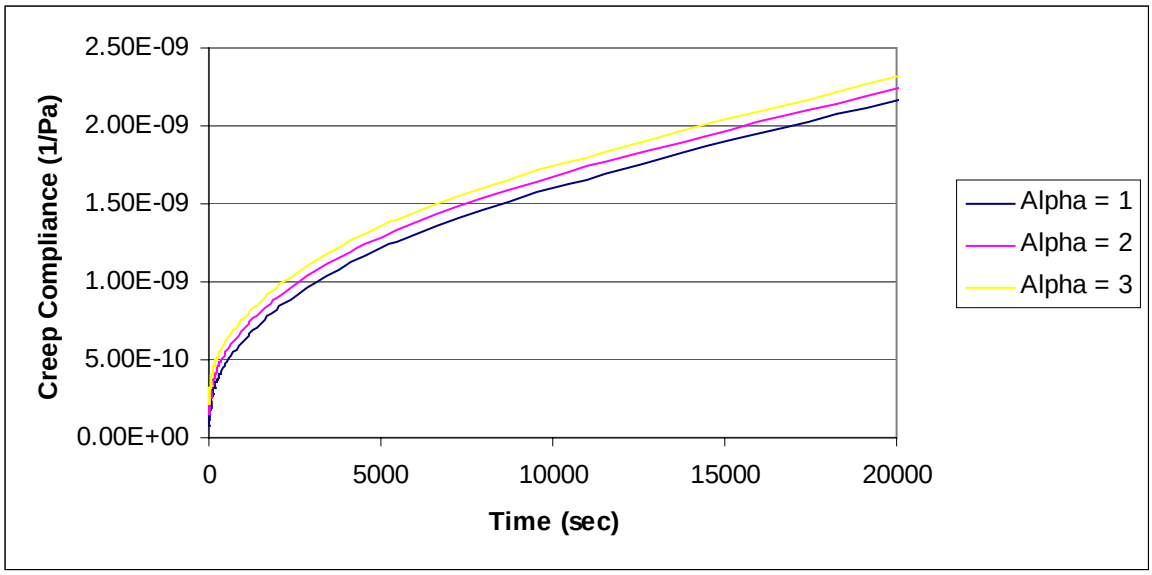

Figure 6-5. Effect of Elasticity

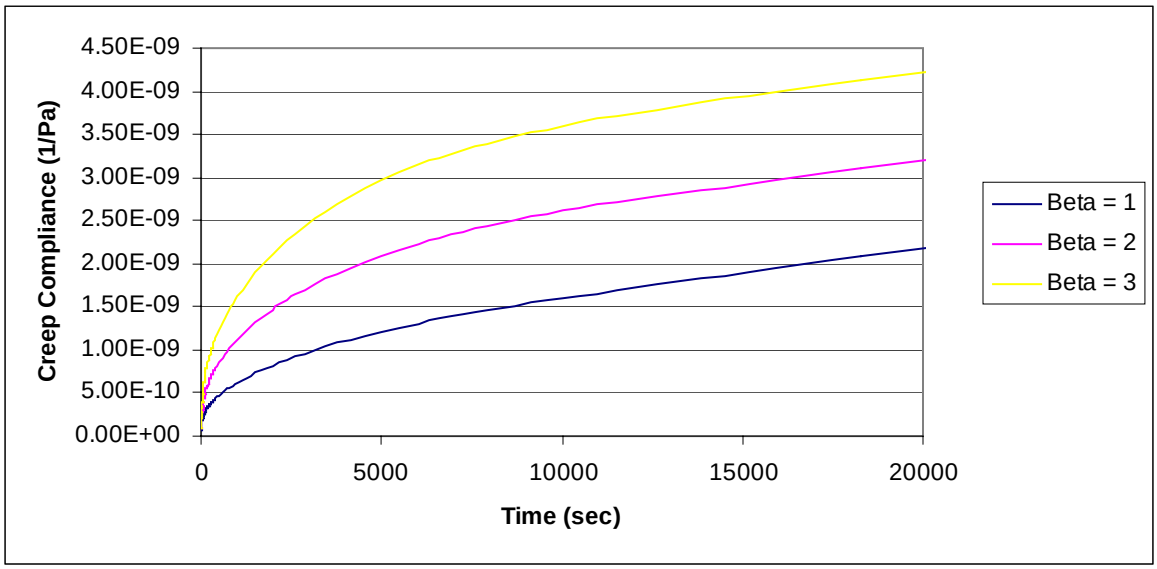

Figure 6-6. Effect of Delayed Elasticity

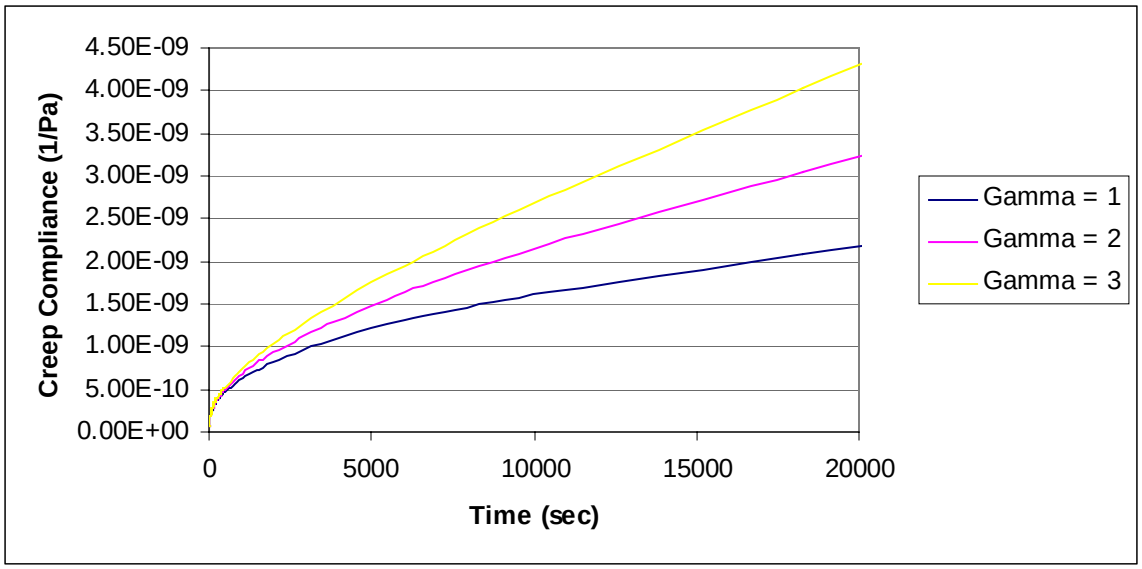

Figure 6-7. Effect of Viscosity

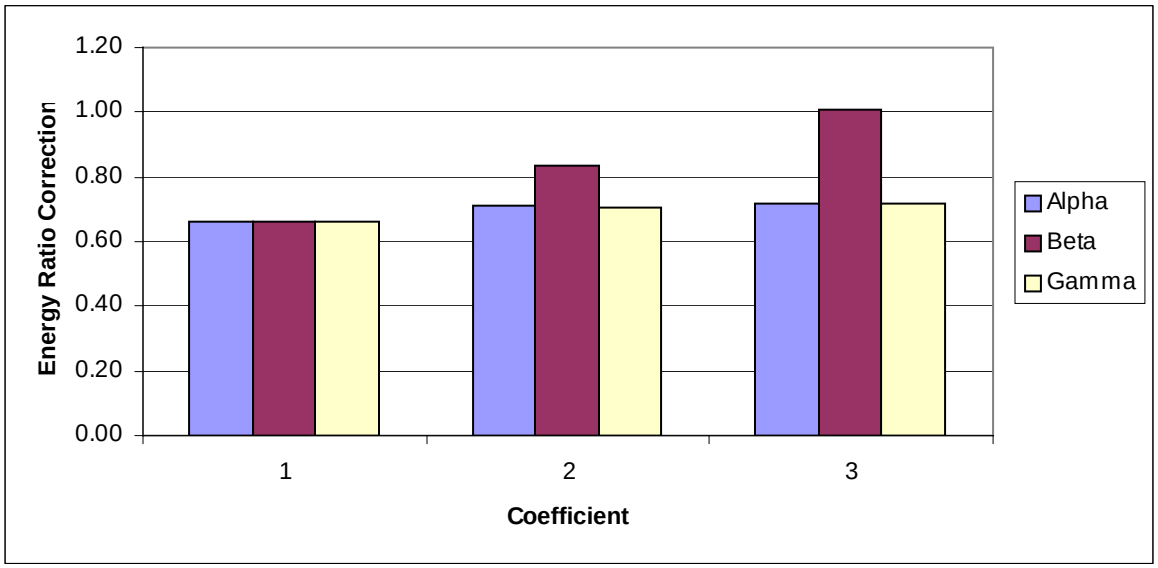

Figure 6-8. Energy Ratio Corrections Corresponding to the Coefficients

As shown in Figure 6-8, even though the initial compliance (elasticity) and viscosity have a little effect, it is interesting that delayed elasticity has a strong effect on ER, which is associated with top-down cracking performance. In contrast to load-induced cracking, short-term creep response (delayed elasticity) is more important than long-term creep response (viscosity) to development of the thermal cracking. It is concluded that

mixture with higher short-term creep response can also help to mitigate top-down cracking.

CHAPTER 7
SUMMARY, CONCLUSIONS AND RECOMMENDATIONS

7.1 Summary

7.1.1 Evaluation of Energy Dissipation

Prior work performed on the fracture behavior of asphalt mixture has indicated that damage in asphalt mixture is directly related to the development of dissipated creep strain energy. This prior work has also shown that a dissipated creep strain energy threshold exists, which defines the development (initiation or propagation) of macro cracks. Consequently, it is of critical importance to be able to predict the rate of dissipated creep strain energy development to evaluate the cracking performance of asphalt mixture.

The work performed in this study indicated that the dissipated energy determined as the area of the hysteresis loop that develops during cyclic loading of asphalt mixture is not a good measure of the dissipated creep strain energy that develops in the mixture, which explains why it is not a good indicator of damage development and cracking resistance of asphalt mixture. Results showed that the dissipated energy determined from the hysteresis loop was far greater than the dissipated creep strain energy predicted from the measured viscous response of the mixture. Further analysis indicated that the difference in energy was clearly explained by the delayed elastic response of the mixture. In fact, for the mixtures tested, the majority of the dissipated energy associated with the hysteresis loop was caused by delayed elastic response.

In summary, it appears that an independent measure of the viscous response of asphalt mixture is required to accurately predict or determine the dissipated creep strain

energy incurred during loading. Although theoretically this can be determined either from static creep tests or from cyclic load tests at multiple frequencies, the results of the study indicate that viscous response of mixtures can be obtained more accurately and reliably from static creep tests. Because of the relatively short loading times involved, the response of cyclic load tests performed at typical loading frequencies is generally dominated by elastic and delayed elastic response, which makes it different and impossible to isolate the viscous response accurately.

The fact that a large portion of the hysteresis loop is composed of delayed elastic energy may result in misinterpretation of dissipated energy results and its relationship to mixture cracking performance. Depending on their rheological characteristics, mixtures exhibiting the same dissipated energy per load cycle may in fact have very different resistance to the development of damage. A mixture whose response is strongly influenced by delayed elasticity may be incurring little or no damage even though a significant amount of dissipated energy is observed. Conversely, a mixture exhibiting the same level of dissipated energy per load cycle may be incurring a significant amount of micro damage if most of its response is associated with viscous behavior, as opposed to delayed elastic behavior.

In conclusion, it appears that the absolute value of the dissipated energy measurements obtained from the area of the hysteresis loop during cyclic load testing should not be used to interpret the cracking performance of asphalt mixture. An independent set of parameters that allows for the prediction of the viscous response of the mixture is required for this purpose.

7.1.2 Evaluation of HMA Thermal Fracture Model

The HMA fracture model was based on theory of viscoelasticity and energy-based fracture mechanics, which uniquely deals with fracture associated with a fundamental dissipated creep strain energy loss in viscoelastic materials. Its damage principle and crack growth law were favorably adapted to the development of HMA thermal fracture model.

An HMA thermal fracture model was developed based on the same principle and failure criteria used in the HMA fracture model. These involved inclusion of algorithms to account for DCSE accumulation induced by temperature changes, which are distinctly different them those associated with load-induced DCSE.

A parametric study was conducted to evaluate the model, and material characteristics were clearly matched with expected results. These results indicated that the HMA thermal fracture model developed has the potential to reliably evaluate the performance of asphalt mixtures subjected to thermally induced damage. The model was further evaluated using pavement performance data from test section in Florida. Predicted performance using the HMA thermal fracture model with regional temperature effect indicated that although the top-down cracking performance in Florida was most strongly affected by traffic loading, thermal effects can also affect performance.

Consequently, it was concluded that a combined model able to deal with both temperature-induced and load-induced crack performance provides a more realistic and reliable estimation of pavement performance associated with top-down cracking.

7.1.3 Combination of Temperature and Load Effect

A modified Energy Ratio (ERC) was introduced that incorporates the effect of both load and temperature-induced damage on top-down cracking. The parameter can be used

as a single criterion to evaluate top-down cracking performance of asphalt mixtures. Use of the modified Energy Ratio (ERC) resulted in better correlation between predicted and observed top-down cracking performance of pavement in Florid, indicating that the approach developed properly accounts for the effect of temperature on top-down cracking. Consequently, it may be concluded that the Energy Ratio Correction appears to be promising as a more accurate and reliable predictive tool for evaluating top-down cracking performance.

7.1.4 Increase of Performance Related to Mixture's Rheology

In understanding the nature of thermal cracking it is important to identify a fundamental parameters that most strongly to contribute the development of thermal cracking in asphalt pavement. According to HMA fracture model, it appears that a lower rate of creep and a higher DCSE limit play an important role to increase the top-down cracking performance. However, further analysis indicates that delayed elasticity, which is represented as short-term creep response of mixture's rheology, is an important factor that affects thermal cracking. Short-term creep response results in lower thermal stresses developed in asphalt pavement that help to mitigate the potential contribution of the thermal stresses on top-down cracking.

Although reduction of the rate of creep strain rate may reduce the thermal cracking performance, the effect of the creep strain was less significant than that of the delayed elasticity. In conclusion, an asphalt mixture that shows a lower rate of creep strain and higher short-term creep may be the best combination to effectively mitigate top-down cracking.

7.2 Conclusions

The findings of this study may be summarized as follows:

- The work performed in this study indicates that the dissipated energy determined as the area of the hysteresis loop appears to be composed of delayed elastic and viscous response. Consequently, it is not a good measure of the dissipated creep strain energy. Viscous response of mixtures should be obtained from static creep tests.

- An HMA thermal fracture model was developed based on the same principle and failure criteria used in the HMA fracture model. The performance evaluation of the model indicates that the HMA thermal fracture model developed has the potential to reliably evaluate the performance of asphalt mixtures subjected to thermally induced damage.

- Predicted performance using the HMA thermal fracture model with regional temperature effect indicated that although the top-down cracking performance in Florida was most strongly affected by traffic loading, thermal effects can also affect performance.

- A combined system (ERC) that incorporates the effect of both load- and temperature-induced damage on top-down cracking resulted in better correlation between predicted and observed top-down cracking performance. Consequently, the Energy Ratio Correction appears to be promising as a more accurate and reliable predictive tool for evaluating top-down cracking performance.

- Further analysis indicates that delayed elasticity strongly affects thermal cracking development. In conclusion, an asphalt mixture that shows a lower rate of creep strain and higher short-term creep may be the best combination to effectively mitigate top-down cracking.

7.3 Recommendations

The system developed in this study was only evaluated for a limited number of sections throughout the state of Florida. The system should be evaluated in more extended sections that gathered from a broad range in the nation, to include a broader range of environmental conditions.

Although the system based on modified Energy Ratio (ERC) is practical to pavement engineers, a more fundamental study should be performed to fully understand

pavement behavior. For example, a more mechanistic model needs to be developed to predict crack growth induced by traffic loading and thermal stresses.

APPENDIX A
SUMMARY OF NON-DESTRUCTIVE TESTING (FWD)

Table A-1. Location A

Distance (in)	I10 - 8C		I10 - 9U		SR 471C		SR 19C		SR 997U	
	Measured	Calculated	Measured	Calculated	Measured	Calculated	Measured	Calculated	Measured	Calculated
0	6.4	6.4	5.9	5.9	13.3	13.1	16.4	16.4	7.9	7.9
8	4.5	4.5	4.4	4.4	8.6	8.7	13.3	13.2	4.6	4.6
12	3.6	3.6	3.7	3.7	5.9	6	11	11.2	3	3
18	2.6	2.6	2.8	2.8	3.5	3.5	9.1	8.9	1.9	1.9
24	2	2	2.2	2.2	2.3	2.3	7.2	7.2	1.5	1.5
36	1.3	1.3	1.4	1.4	1.5	1.5	4.7	4.7	1.2	1.2
60	0.7	0.7	0.7	0.7	0.9	0.8	1.9	1.9	0.7	0.7

Table A-1. Location B

Distance (in)	I10 - 8C		I10 - 9U		SR 471C		SR 19C		SR 997U	
	Measured	Calculated	Measured	Calculated	Measured	Calculated	Measured	Calculated	Measured	Calculated
0	7.1	7.1	6.6	6.6	12.3	12.1	17.8	17.9	6.8	6.9
8	5.2	5.2	4.5	4.5	7.8	7.9	14.6	14.3	3.9	3.9
12	4.2	4.2	3.4	3.5	5.3	5.4	11.8	12.1	2.5	2.5
18	3.2	3.1	2.5	2.5	3.2	3.2	9.7	9.6	1.6	1.6
24	2.3	2.4	1.9	1.8	2.2	2.1	7.6	7.6	1.3	1.3
36	1.5	1.5	1.1	1.1	1.4	1.4	4.8	4.8	0.9	0.9
60	0.8	0.8	0.5	0.5	0.8	0.8	1.7	1.7	0.5	0.5

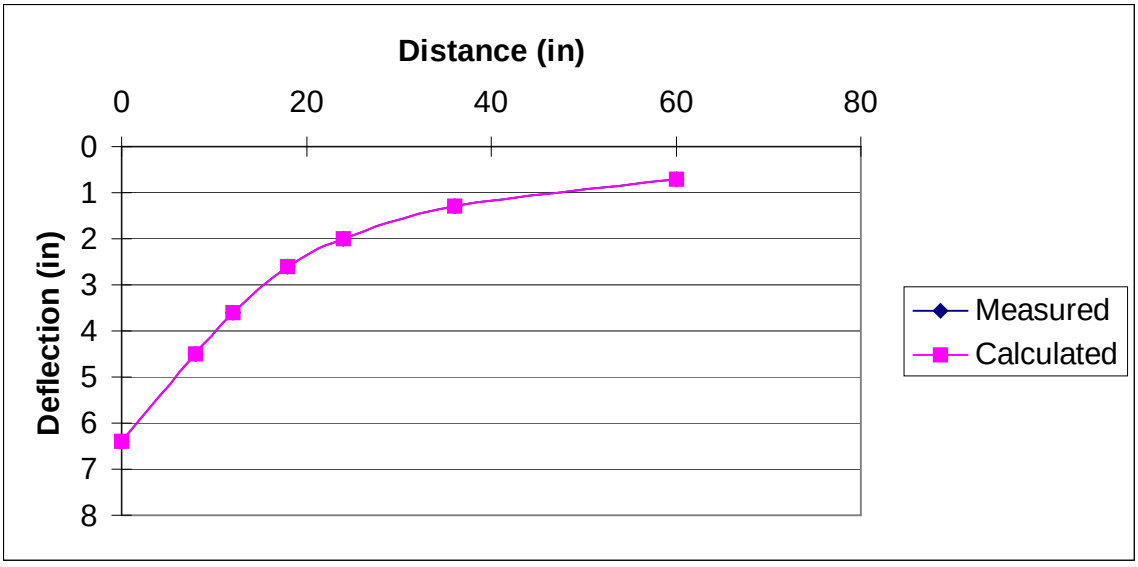

Figure A-1. Deflections of I 10-8C at Location A

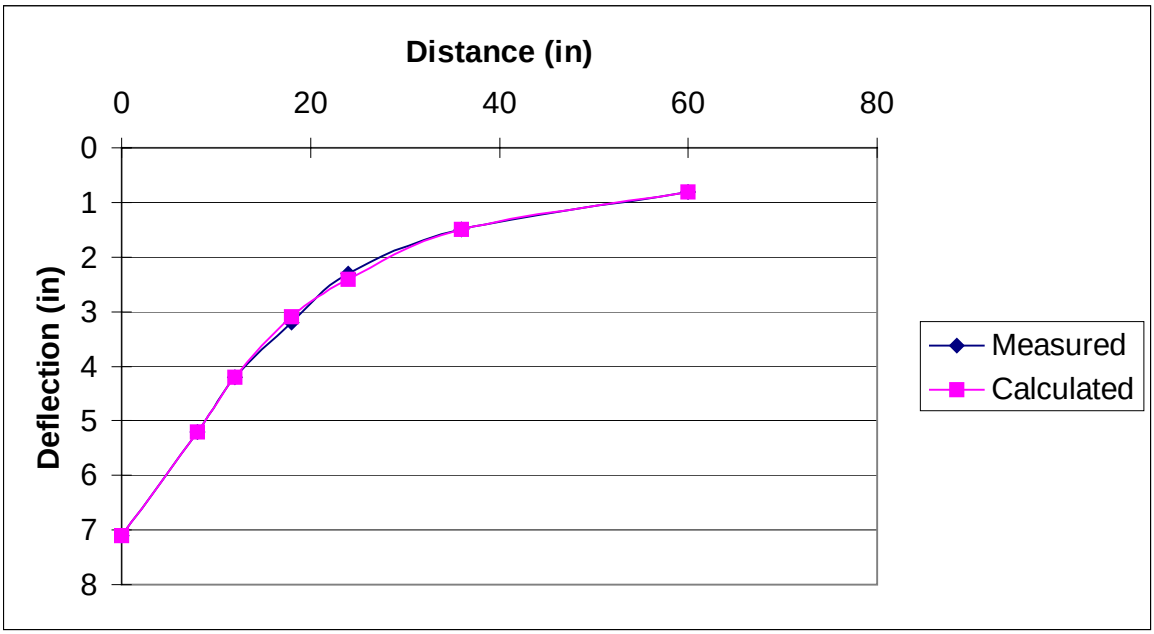

Figure A-2. Deflections of I 10-8C at Location B

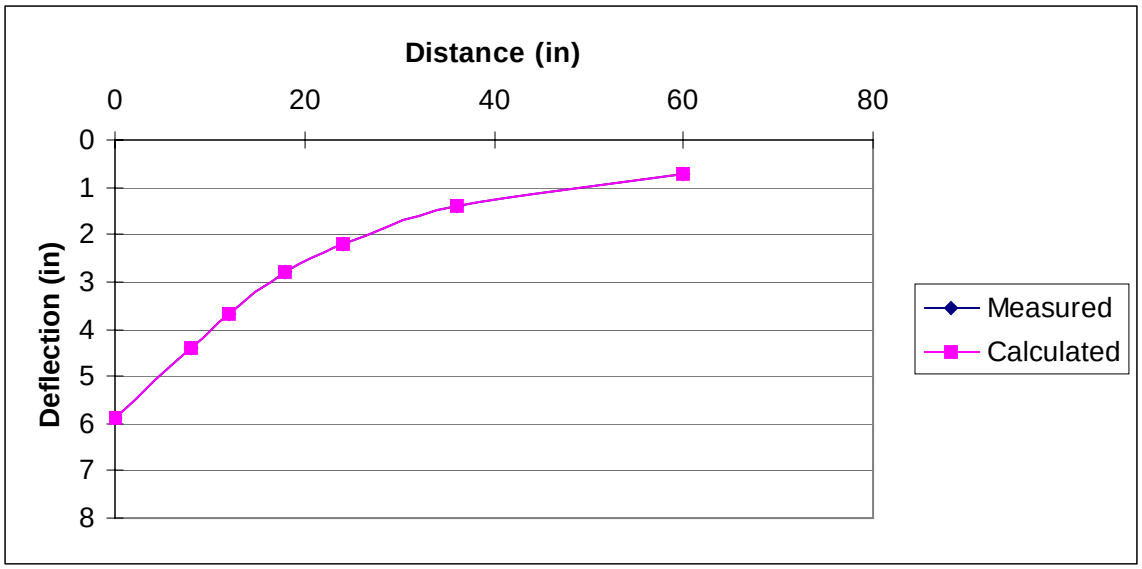

Figure A-3. Deflections of I 10-9U at Location A

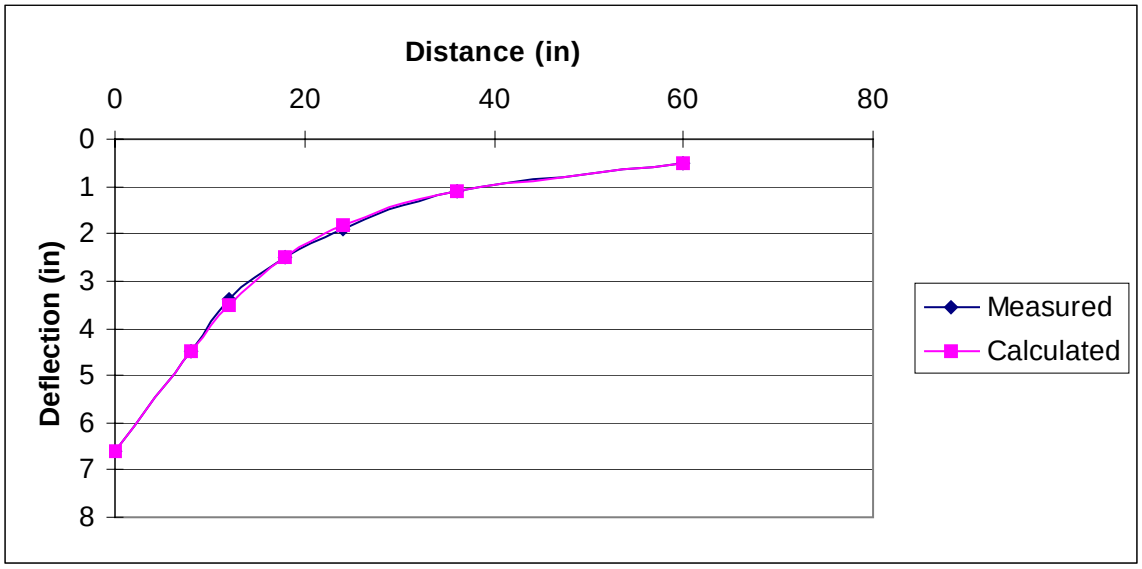

Figure A-4. Deflections of I 10-9U at Location B

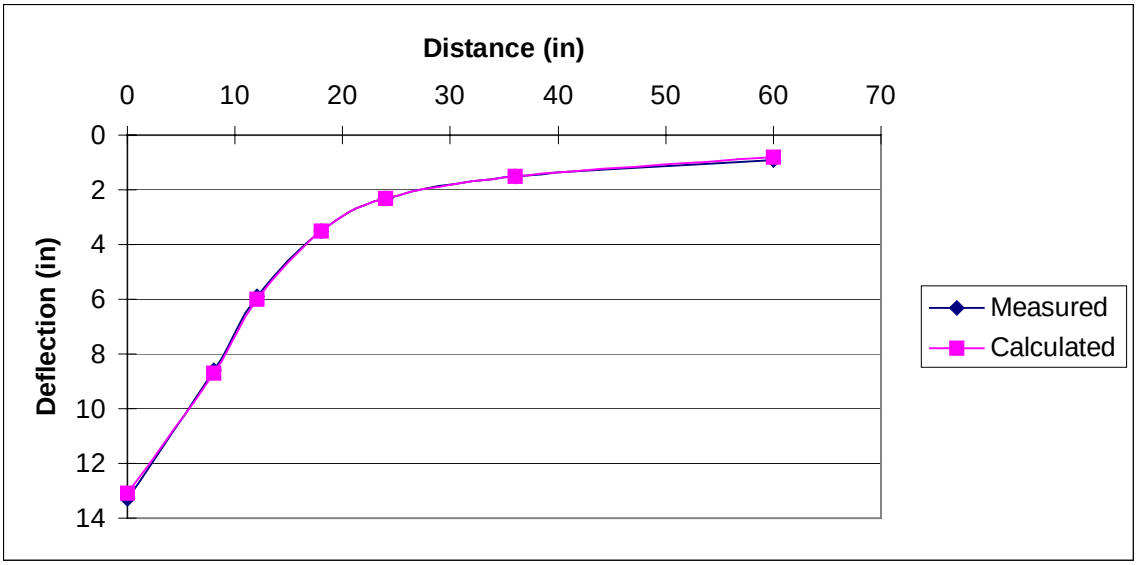

Figure A-5. Deflections of SR 471C at Location A

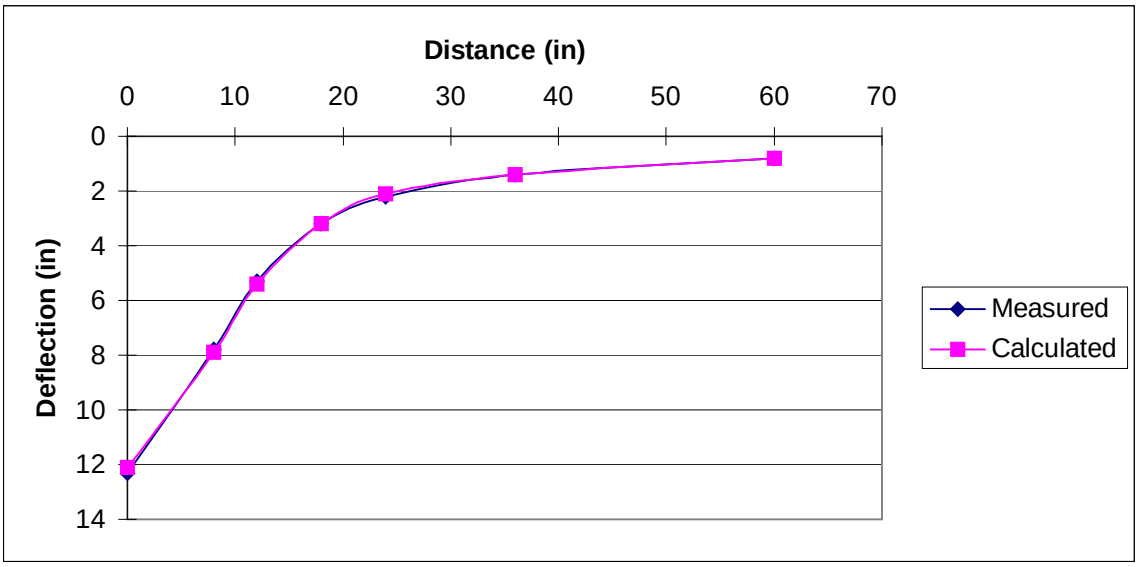

Figure A-6. Deflections of SR 471C at Location B

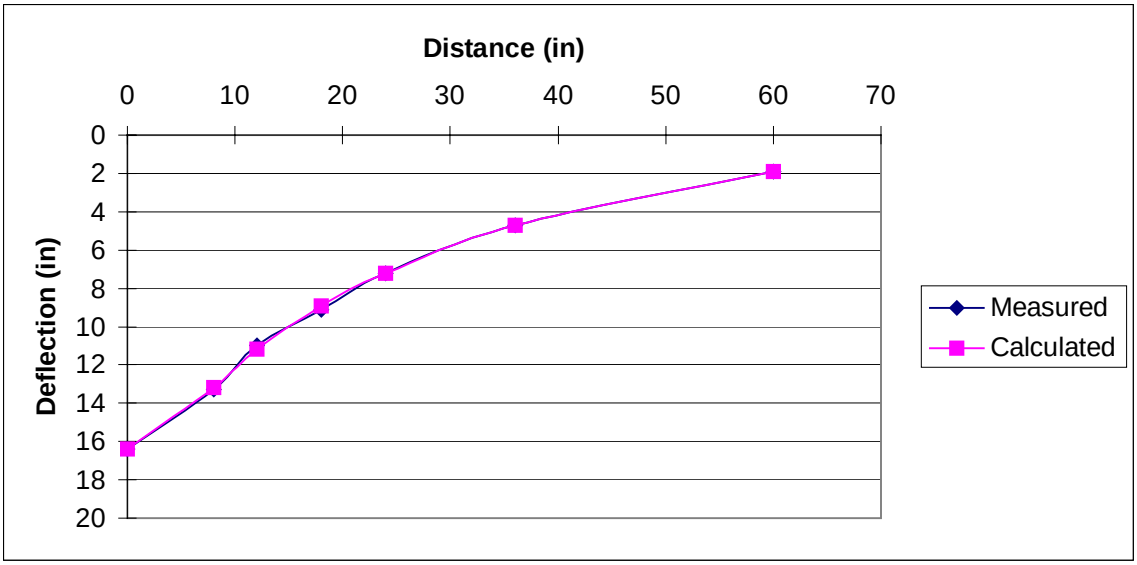

Figure A-7. Deflections of SR 19U at Location A

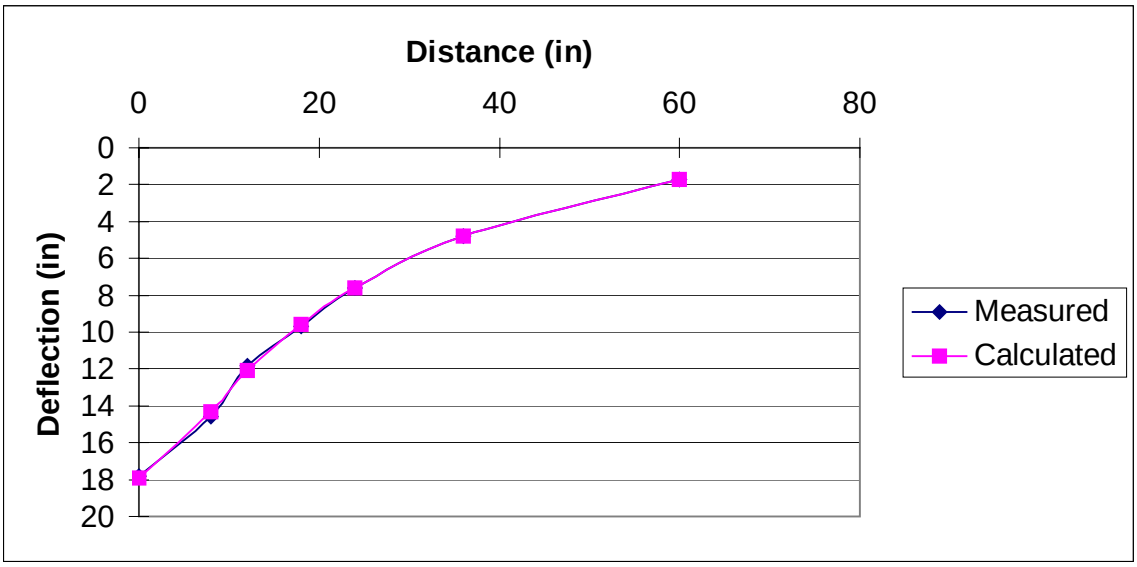

Figure A-8. Deflections of SR 19U at Location B

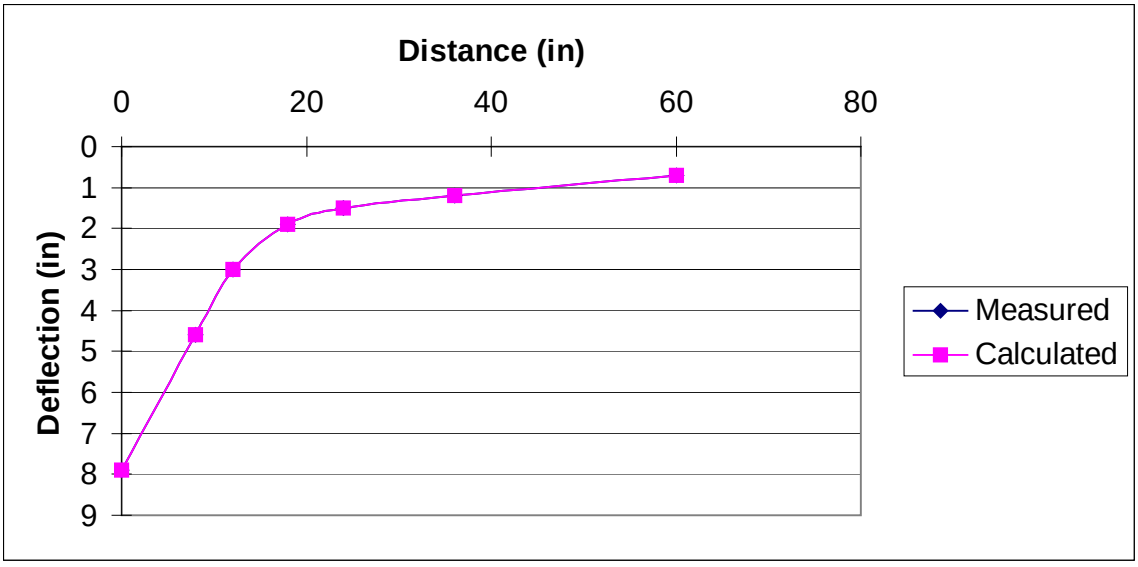

Figure A-9. Deflections of SR 997U at Location A

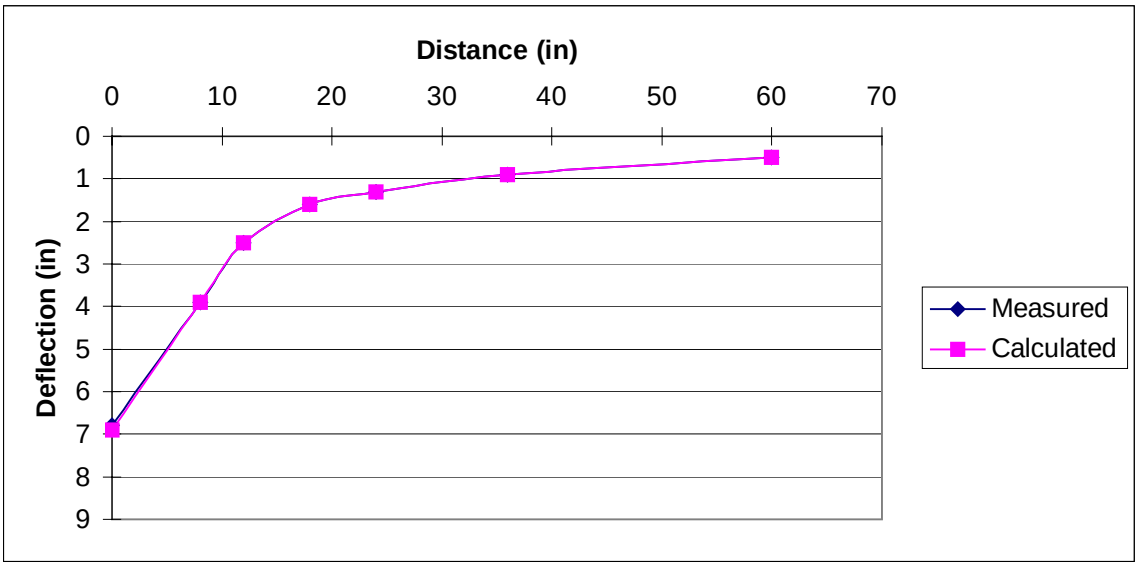

Figure A-10. Deflections of SR 997U at Location B

APPENDIX B
INDIRECT TENSILE TEST RESUTLS

Table B-1. Resilient Modulus Test Results at 0°C

	I10 - 8C	I10 - 9U	SR 471C	SR 19C	SR 997U
Modulus (Gpa)	10.12	10.26	12.70	13.02	14.44

Table B-2. Creep Compliance Test Results at 0°C

	I10 - 8C	I10 - 9U	SR 471C	SR 19C	SR 997U
D1 (1/Gpa)	4.699E-02	6.461E-03	1.377E-02	5.985E-02	5.350E-02
m	0.222	0.511	0.478	0.344	0.136
Rate of Creep Compliance	4.82E-05	1.13E-04	1.78E-04	2.21E-04	1.85E-05

Table B-3. Tensile Strength Test Results at 0°C

	I10 - 8C	I10 - 9U	SR 471C	SR 19C	SR 997U
Tensile Strength (psi)	207	213	329	380	374
Failure Strain (με)	219	227	569	782	397
Fracture Energy (KJ/m^3)	0.2	0.2	0.8	1.3	0.6
DCSE (KJ/m^3)	0.10	0.09	0.60	1.04	0.37

Table B-4. Resilient Modulus Test Results at 10°C

	I10 - 8C	I10 - 9U	SR 471C	SR 19C	SR 997U
Modulus (Gpa)	9.85	10.21	7.67	9.30	11.74

Table B-5. Creep Compliance Test Results at 10°C

	I10 - 8C	I10 - 9U	SR 471C	SR 19C	SR 997U
D1 (1/Gpa)	6.062E-02	4.939E-02	9.647E-02	1.038E-01	4.794E-02
m	0.326	0.337	0.501	0.426	0.256
Rate of Creep Compliance	1.88E-04	1.71E-04	1.54E-03	8.39E-04	7.22E-05

Table B-6. Tensile Strength Test Results at 10°C

	I10 - 8C	I10 - 9U	SR 471C	SR 19C	SR 997U
Tensile Strength (psi)	226	184	260	248	338
Failure Strain (με)	386	415	2040	1338	594
Fracture Energy (KJ/m^3)	0.4	0.4	2.5	1.6	0.9
DCSE (KJ/m^3)	0.28	0.32	2.29	1.44	0.67

Table B-7. Resilient Modulus Test Results at 20°C

	I10 - 8C	I10 - 9U	SR 471C	SR 19C	SR 997U
Modulus (Gpa)	8.05	6.64	5.17	5.28	9.21

Table B-8. Creep Compliance Test Results at 20°C

	I10 - 8C	I10 - 9U	SR 471C	SR 19C	SR 997U
D1 (1/Gpa)	1.078E-01	8.323E-02	8.806E-02	1.955E-01	8.253E-02
m	0.434	0.478	0.713	0.572	0.343
Rate of Creep Compliance	9.38E-04	1.08E-03	8.66E-03	5.80E-03	3.04E-04

Table B-9. Tensile Strength Test Results at 20°C

	I10 - 8C	I10 - 9U	SR 471C	SR 19C	SR 997U
Tensile Strength (psi)	161	148	122	177	238
Failure Strain (με)	500	607	1977	2472	750
Fracture Energy (KJ/m^3)	0.4	0.4	1.7	1.3	0.8
DCSE (KJ/m^3)	0.32	0.32	1.63	1.16	0.65

LIST OF REFERENCES

Birgisson, B., R. Roque, J. Kim, and L. V. Pham, 2004, *The Use of Complex Modulus to Characterize the Performance of Asphalt Mixtures and Pavements in Florida*, Final Report for FDOT BD-273 Contract, Gainesville, Florida, University of Florida.

Buttlar, W. G. and R. Roque, 1994, "Development and Evaluation of the Strategic Highway Research Program Measurement and Analysis System for Indirect Tensile Testing at Low Temperatures," *Transportation Research Record*, No. 1454, pp. 163-171.

Buttlar, W. G., R. Roque, and B. Reid, 1998, "Automated Procedure for Generation of Creep Compliance Master Curve for Asphalt Mixtures," *Transportation Research Record,* No. 1630, pp 28-36.

Daniel, J. S., W. Bisirri, and Y. R. Kim, 2004, "Fatigue Evaluation of Asphalt Mixtures Using Dissipated Energy and Viscoelastic Continuum Damage Approaches," *Journal of the Association of Asphalt Paving*, Vol. 73, pp. 557-583.

Dauzats, M. and A. Rampal, 1987, "Mechanism of Surface Cracking in Wearing Courses," *6th International Conference on Asphalt Pavements*, Vol. 1, No. 06020.

Findley, W. N., J. S. Lai, and K. Onaran, 1976, *Creep and Relaxation of Nonlinear Viscoelastic Materials,* New York, Dover Publications, Inc.

Ghuzlan, K. A. and S. H. Carpenter, 2000, "Energy-Derived, Damage-Based Failure Criterion for Fatigue Testing," *Transportation Research Record*, No. 1723, pp 141-149.

Hiltunen, D. R. and R. Roque, 1994, "A Mechanics-Based Prediction Model for Thermal Cracking of Asphaltic Concrete Pavements," *Journal of the Association of Asphalt Paving Technologists*, Vol. 63, pp. 81-117.

Huang, Y. H., 1993. *Pavement analysis and design*, New Jersey, Prentice Hall, Inc.

Jajliardo, A. P., 2003, *Development of Specification Criteria to Mitigate Top-Down Cracking*, Master's thesis. Gainesville, Florida, University of Florida.

Kim, B., 2003, Evaluation of the Effect of SBS Polymer Modifier on Cracking Resistance of Superpave, Ph.D. Dissertation, Gainesville, FL, University of Florida.

Kim, J., 2002, *Complex Modulus from Indirect Tension Testing*, Master's thesis. Gainesville, Florida, University of Florida.

Kim, J., R. Roque, and B. Birgisson, September 2005, "Obtaining Creep Compliance Parameters Accurately from Static or Cyclic Creep Tests," *Journal of ASTM International*, Vol. 2, No. 8.

Kim, Y. R., H. J. Lee, and D. N. Little, 1997, ''Fatigue Characterization of Asphalt Concrete Using Viscoelasticity and Continuum Damage Theory,'' *Journal of the Association of Asphalt Paving Technologists*, Vol. 66, pp. 520–569.

Kim, Y. R., Y. C. Lee, and H. J. Lee, 1995, ''Correspondence Principle for Characterization of Asphalt Concrete,'' *Journal of Materials in Civil Engineering*, ASCE, Vol. 7, pp. 59-68.

Lee, H. J., J. S. Daniel, and Y.R. Kim, 2000, "Continuum Damage Mechanics-Based Fatigue Model of Asphalt Concrete," *Journal of Materials in Civil Engineering*, ASCE, Vol. 12, pp. 105-112.

Lytton, R. L., U. Shaumugham, and B. D. Garrett, 1983, *Evaluation of SHRP indirect tension tester to mitigate cracking in asphalt concrete pavements and overlays*, Final Report for FHWA TX-83, Texas, Texas Transportation Institute.

Morland, L. W. and E. H. Lee, 1960, "Stress Analysis for Linear Viscoelastic Materials with Temperature Variation," *Transaction of the Society of Rheology*, Vol. 4, pp. 233-263.

Myers, L. A. and R. Roque, 2002, "Top-Down Crack Propagation in Bituminous Pavements and Implications for Pavement Management," *Journal of the Association of Asphalt Paving Technologists*, Vol. 71, pp. 651-670.

Myers, L. A., R. Roque, and B. Birgisson, 2001, "Propagation Mechanisms for Surface-Initiated Longitudinal Wheel Path Cracks," *Transportation Research Record*, No. 1778, pp. 113-122.

Myers, L. A., R. Roque, B. E. Ruth, and C. Drakos, 1999, "Measurement of Contact Stresses for Different Truck Tire Types to Evaluate Their Influence on Near-Surface Cracking And Rutting," *Transportation Research Record*, No. 1655, pp. 175-184.

Roque, R., B. Birgisson, C. Drakos, and B. Dietrich, 2004, "Development and Field Evaluation of Energy-Based Criteria for Top-down Cracking Performance of Hot Mix Asphalt," *Journal of the Association of Asphalt Paving Technologists*, Vol. 73, pp. 229-260.

Roque, R. and W. G. Buttlar, 1992, "The Development of a Measurement and Analysis System to Accurately Determine Asphalt Concrete Properties Using the Indirect Tensile Mode," *Journal of the Association of Asphalt Paving Technologists*, Vol. 61, pp. 304-332.

Roque, R., W. G. Buttlar, B. E. Ruth, M. Tia, S. W. Dickison, and B. Reid, 1997, *Evaluation of SHRP indirect tension tester to mitigate cracking in asphalt concrete pavements and overlays*, Final Report for FDOT B-9885 Contract, Gainesville, FL, University of Florida.

Roque, R., D. R. Hiltunen, and S. M. Stoffels, 1993, "Field Validation of SHRP Asphalt Binder and Mixture Specification Tests to Control Thermal Cracking through Performance Modeling," *Journal of the Association of Asphalt Paving Technologists*, Vol. 62, pp. 615-638.

Roque, R., P. Romero, and D. R. Hiltunen, 1992, "The Use of Linear Elastic Analysis to Predict the Nonlinear Response of Pavements," *7th International Conference on Asphalt Pavements*, Vol. 1, No. 07070.

Roque, R. and B. E. Ruth, 1987, "Materials Characterization and Response of Flexible Pavements at Low Temperatures," *Proceedings of the Association of Asphalt Paving Technologie*s, Vol. 56, pp. 130-167.

Roque, R. and B. E. Ruth, 1990, "Mechanisms and Modeling of Surface Cracking in Asphalt Pavements," *Proceedings of the Association of Asphalt Paving Technologie*s, Vol. 59, pp. 397-421.

Sangpetngam, B., 2003, *Development and Evaluation of a Viscoelastic Boundary Element Method to Predict Asphalt Pavement Cracking*, Ph.D. Dissertation, Gainesville, Florida, University of Florida.

Schapery, R.A., 1984, "Correspondence Principles and a Generalized J Integral for Large Deformation and Fracture Analysis of Viscoelatic Media," *International Journal of Fracture*, Vol. 25, pp. 195-223.

Soules, T. F., R. F. Busbey, S. M. Rekhson, A. Markovasky, and M. A. Burke, 1987, "Finite-Element Calculation of Stresses in Glass Parts Undergoing Viscous Relaxation," *Journal of the American Ceramic Society*, Vol. 70, No. 2, pp. 90-95.

Zhang, Z., R. Roque, B. Birgisson, and B. Sangpetngam, 2001, "Identification and Verification of a Suitable Crack Growth Law," *Journal of the Association of Asphalt Paving Technologists*, Vol. 70, pp. 206-241.

BIOGRAPHICAL SKETCH

Jaeseung Kim was born on March 3, 1974, in Seoul, South Korea. After graduating from Seoul High School, he enrolled in the Department of Civil Engineering at Myongji University. In the middle of his studies, he served as a soldier in the Korean military. He received a Bachelor of Engineering degree in February 1999.

His academic pursuit led him to attend the University of Florida in 2000. He received the master's degree in the Department of Civil and Coastal Engineering in Spring of 2002 from the University of Florida. Immediately after graduation, he joined the Ph.D. program of the materials group at the University of Florida and worked as a graduate research assistant with his doctoral advisor, Dr. Reynaldo Roque.

He was involved in many projects related to the experimental testing and analytical modeling of pavement materials and design. He is currently completing the Doctor of Philosophy Degree in civil engineering at the University of Florida.